Politecnico di Milano

School of Industrial and Information Engineering

Department of Aerospace Science and Technology

Master of Science in Space Engineering

*Academic year 2020/2021*

# Preliminary Studies on Damage Tolerance of CMC materials for hot structures in space vehicles

*Candidate*
Isabelle Honorato Diniz do Nascimento 10594290

*Supervisor*
Prof. Alessandro Airoldi

*October 2021*

*To Bianca, Thaís and Jorge.*
*You kept believing in me when I couldn't.*
*You pushed me, you kept me going.*

# Acknowledgements

The path to become an engineer is definitely not an easy one. Even less so if you decide to get two degrees, in two different countries. Those almost 8 years studying first aeronautical and then space engineering have been a journey. A crossing, I'd say. Sometimes it was beautiful and joyful, at others absurdly hard and nerve-wracking. And the thing I'm most certain of is that I would never have gotten as far as I did without the support of all the people that were by my side.

In that tone, I'd like to starting by thanking my supervisor, Alessandro Airoldi, for all the help, the immense patience and orientation that he provided during this thesis. This last step of the journey has been really trying and I couldn't have finished without his help.

I also want to thank my family for making my education a priority, they fought so I could have a good school, focus on university and finally come to a prestige university in Europe. They enabled me to go further then I had ever dreamed of. An special thanks to my brother Caius, for always being there for me, even when we're so far away from each other for so long.

I'd like to thank all the friends that crossed this path with me. I wouldn't have made through USP without Bacana, S.A., Jess and Bryan. You guys were my team, for projects, for studying, for parties, movies, travels, in the good days and specially in the bad ones. It was a pleasure and an honor to study with and befriend all of you. I must leave an special thanks to Bryan, my study partner and best friend during those university years. I told you many times, I couldn't do it without you, and I almost didn't when we weren't studying together anymore. You helped me much more then you think, and I'll be forever grateful.

I'd also like to thank João Betoni and Bruno Seviuc from USP for always helping to fix my problems with bureaucracy both in USP and on Politecnico. A lot of us students wouldn't ever graduate without your help.

I'd like to thank Anna, who helped me navigate Politecnico, Milano and Italy in general.

I'm also grateful to all my wonderful friends here in Milano, for making me feel like I had a piece of home away from home and for being my family overseas.

I'd like to thank all the amazing teachers that made me eager to learn during school, an special thanks for Marcos Benfica and Carlos Moreira, that were fundamental

in my decision to pursue engineering.

Finally, I'd like to thank the people to which I dedicated this thesis. Each of you marked a different period of my life and each one of you was by my side on the end of this journey, pushing me when I thought that I couldn't make it to the end. Thank you, immensely.

**Abstract**

Composites have always been widely used on the aeronautical and space industry. The combination of materials in order to achieve specific characteristics have been fundamental to advance those engineering fields that have such unique challenges.

Ceramic Matrix Composites are no exception. Ceramics have a wide use on high temperature applications but are very brittle. The incorporation of fibers into a ceramic matrix composite allows for utilization of the high temperature properties of ceramics and the strength of composites.

Ceramic Matrix Composites offer the highest specific strength at temperatures high temperatures among all engineering materials available. For this reason they are of special interest to aeronautical an space engineers. They have been used in aeronautical brake disks, rocket nozzle, Thermal Protection Systems and, more specifically in Hot Structures.

Hot Structures are structural components designed with materials that allow them to work under high temperature, eliminating or reducing the need for isolation/cooling strategies.

This thesis has as its main objective to perform a preliminary analysis on damage tolerance of a C/SiC ceramic matrix composite that is being studied for Hot Structure applications. This will be performed by simulating an Compact Tension Test on ABAQUS environment for both Translaminar Fracture Toughness and Interlaminar Fracture Toughness. The developed model used cohesive elements with Masx damage criterion in order to predict crack initiation and propagation.

This thesis will also use the stress fields obtained on the simulation to propose modifications in the design of the initial test specimen in order to make it able to withstand the test without undesirable failure modes.

A influence of strength in the results of Compact Tension tests was encountered, challenging the common simplification that only the fracture energy has impact on this test.

The development of a reliable model is the first step to being able to use the material for engineering projects. The ability to minimize the number of physical tests done by relying on simulations is essential in innovative fields such as aeronautical and space applications as the materials and manufacturing methods are highly specialized and can incur in very high costs for experimental campaigns.

**Sommario**

I materiali compositi sono da sempre ampiamente usati nell'industria aeronautica e spaziale. Possono essere ricombinati per ottenere caratteristiche specifiche, un aspetto fondamentale per l'avanzamento tecnologico in ambiti con requisiti particolari.

I compositi a matrice ceramica non sono un'eccezione. Le ceramiche sono principalmente usate per applicazioni ad alte temperature, ma hanno lo svantaggio di essere molto fragili. Tuttavia, incorporare delle fibre dentro una matrice ceramica permette di sfruttare sia le proprietà delle ceramiche ad alte temperature sia la resistenza dei compositi.

Questa specifica classe di compositi offre la più alta resistenza specifica alle alte temperature rispetto alle alternative disponibili e per questo è molto interessante in ambito aeronautico e spaziale. Materiali di questo tipo sono già stati utilizzati nei freni a disco aeronautici, negli ugelli dei razzi, nei sistemi di protezione termica e, più nello specifico, nelle Hot Structures.

Le Hot Structures sono componenti strutturali progettati con materiali che permettono delle alte temperature operative, eliminando o riducendo l'isolamento e i sistemi di raffreddamento necessari.

Questa tesi si pone come obiettivo principale di condurre un'analisi preliminare sulla tolleranza al danno di compositi a matrice ceramica in C/SiC che viene studiato per applicazioni Hot Structure. La ricerca è condotta tramite simulazioni di test a tensione compatta sul software ABAQUS, per la resistenza alla frattura translaminare e interlaminare. Il modello sviluppato adotta elementi coesivi con criterio di danno Masx, per predire l'inizio e la propagazione delle cricche.

Questa tesi utilizzerà anche i stress field ottenuti sulla simulazione per proporre modifiche nella progettazione del campione di prova al fine di renderlo in grado di resistere al test senza modalità di rottura indesiderate.

È stata riscontrata un'influenza della resistenza nei risultati dei test di trazione compatta, contraddicendo la comune semplificazione secondo cui solo l'energia di frattura ha un impatto su questo test.

Lo sviluppo di un modello affidabile è il primo passo per essere in grado di usare questo materiale nei progetti di ingegneria. Minimizzare il numero di test fisici, possibile grazie alle simulazioni, è essenziale in ambiti innovativi come le applicazioni aeronautiche e spaziali, poiché i materiali e i metodi di produzione sono altamente specializzati e i costi delle campagne sperimentali possono raggiungere valori molto elevati.

# Contents

# List of Figures

# List of Tables

# Acronyms

| | |
|---|---|
| **CMC** | Ceramic Matrix Composite |
| **PMC** | Polymer Matrix Composite |
| **MMC** | Polymer Matrix Composite |
| **FRP** | Fyber Reinforced Polymer |
| **TPS** | Thermal Protection Systems |
| **CEV** | Crew Exploration Vehicle |
| **LEO** | Low Earth Orbit |
| **SSTO** | Single Stage to Orbit |
| **NASA** | National Aeronautics and Space Administration |
| **HOST** | Multifunctional Hot Structure |
| **CRV** | Crew Return Vehicle |
| **ISS** | International Space Station |
| **ESA** | European Space Agency |
| **NGL** | Next Generation Launcher |
| **CT** | Compact Tension |
| **C/SiC** | Carbon Fibre Reinforced Silicon Carbide |
| **RP** | Reference Point |
| **CVI** | Chemical Vapor Infiltration |
| **PIP** | Polymer Infiltration and Pyrolysis |
| **MI** | Melt Infiltration |
| **LPI** | Liquidi Polymer Infiltration |
| **HT** | High Tenacity |
| **IM** | Intermediate Modulus |
| **HM** | High Modulus |

**UHM** Ultra High Modulus

**CFRP** Carbon Fiber Reinforced Plastic

**LSI** Liquid Silicon Infiltration

**RTM** Resin Trasfer Molding

**FMB** Fiber Matrix Bonding

**CIRA** Centro Italiano Ricerche Aerospaziali

**PRORA- SHS** National Aerospace Research Program - Sharp Hot Structures

# Introduction

## 0.1 Thesis objective

This thesis is part of a wider project funded by Italian Space Agency; Am3aC2a (Approccio Multiscala per la modellazione di materiali CMC e UHTCMC per compoenti riutilizzabili per l'aerospazio) . The project is aimed at the development of engineering approach for the design of hot structures in reusable space vehicles and is conducted by Politecnico di Milano in partnership with Centro Italiano Ricerche Aerospaziali, CIRA, Petroceramics and ISTEC . One of the project's objective is to characterize the mechanical properties of the IsiComp®, an CMC developed by the company and to develop a consistent computational model allowing for posterior use for engineering applications.

The material was developed by Petroceramics in partnership with Centro Italiano Ricerche Aerospaziali (CIRA) in the context of the project National Aerospace Research Program - Sharp Hot Structures (PRORA- SHS). The material has already been validated as re-usable in terms of conservation of mechanical properties after exposition to high temperatures into a experimental campaign in the CIRA's SCIROCCO Plasma Wind Tunnel. [8] [9] [30] [36].

The project will be divided into twoo main tasks:

1. CMC characterization study.

   The first objective of the project involved studying the state of the art of CMC in terms of mechanical properties, test campaigns and computational simulation.

2. Mechanical properties characterization.

   The second task includes designing a test campaign to fully characterize the material, proceeding to elaborate computational models of the tests to be performed and validate the computational models trough a experimental campaign, allowing not only for fully characterization of the material, but also for a consistent tool to use the material for project purposes.

This thesis focus on the first step of the project, also going in a partial manner on the third point. This work will expand in a precise collection of the state of the art information for CMC, proceeding into elaborating a experiment to characterize the material in terms of Translaminar fracture toughness and interlaminar fracture toughness and finally to simulate the experiment in ABAQUS, with the use of cohesive elements to explore and predict the non-linearity of the material.

## 0.2 Thesis outline

The thesis is structured as follows:

Section 1 is an accurate review of the state of the art related to CMC materials. The study is focused on the engineering applications with an special attention give to TPS and Hot Structures, as they're the main application for which the use of this material is being study.

Section 2 is a literature review about the the general mechanical properties of CMC materials. The first part of this section is dedicated to a characterization, including morphology, technologies and manufacturing of the material. The second part is dedicated to general damage, explaining in detail the in-plane behavior of the composites. The work proceed to explain the out of plane behaviour, presenting the delamination process. Finally, the mechanical tests that can be performed to evaluate the toughness of the composite are explained and the choice of the CT test is justified.

Section 3 describes the computational methods applied during this work, the parameters of the simulation performed, including computational parameters such as type of element and mechanical specifications such as material properties and geometry of the the body simulated. The results of the simulations are presented, proceeding to a discussion of their meaning and redesign propositions to the test specimen.

Finally, section 3.4.5 is the last part of the thesis. It sums up and comments the results obtained and points out the final considerations.

# 1 Problem statement and literature review

## 1.1 Ceramic Matrix Composite

Synthetic composites have been used in many areas of engineering since the 1930's with invention of glass fiber by Owens Corning in 1935 and the patent of unsaturated polyester resins in 1936 when the industry of Fyber Reinforced Polymer (FRP) as we know started to be developed [31] [19] [21] [35] , the technology was greatly improved during World War II, and made its way into the civil applications afterwards.

From the beginning of its utilization, those materials were rapidly adopted by the aeronautic industry, mostly for its great strength-to-weight ratio when compared with the materials previously available. In the 1950's the composite industry continued to develop new technologies and manufacturing methods resulting in its utilization in the Space Race [31] [19] [21].

The main composite types for aerospace utilization can be seen on Figure 1

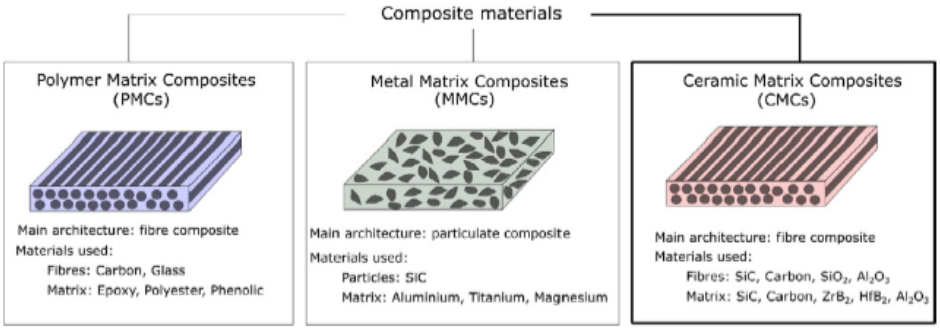


**Figure 1:** Summary of types of composite materials [2]

While polymer matrix composites are the most popular on the aeronautic industry, being widely used in structural components in commercial aviation, ceramic matrix composites are also being used, specially in the engine "hot zone" [16] or in thermal structural applications [3], where the use of CMC avoid the necessity of air cooling.

## 1.2 Applications

Composites are widely spread materials in several industries. The increased utilization comes mainly from the outstanding mechanical properties. With a higher strength-to-weight ratio when compared with non reinforced materials [2].

Ceramic materials posses high strength and modulus under high temperatures. Their usage for structural purposes is limited, though, as they're very brittle. By incorporating fibers on ceramic matrices is possible to reduce their tendency to catastrophic failure while taking advantage of it's attractive high-temperature strength behaviour [24].

The amount of research being done in the field of CMC, such as this thesis,has been increasing doing to the interest in using this class of materials for high temperature applications for which comprehensive data about not only its properties, but also on how to machine the material in order to be usable, is needed.

An important part of using those materials is machining them in order to achieve the needed form . While for Polymer Matrix Composite (PMC) and Polymer Matrix Composite (MMC) there is a large amount of research concerning it's machining [32], the amount of research available when it comes to CMC is much more limited. Some reviews of literature have been performed [33] but mostly for particulate ceramics, not fiber reinforced ones.

Still from [2] we can observe a list of applications of CMC materials, depicted on figure 2. The type of matrix and reinforcement influence greatly on the performance of the material, being, therefore, very important to choose properly the combination of those factors for each individual application.

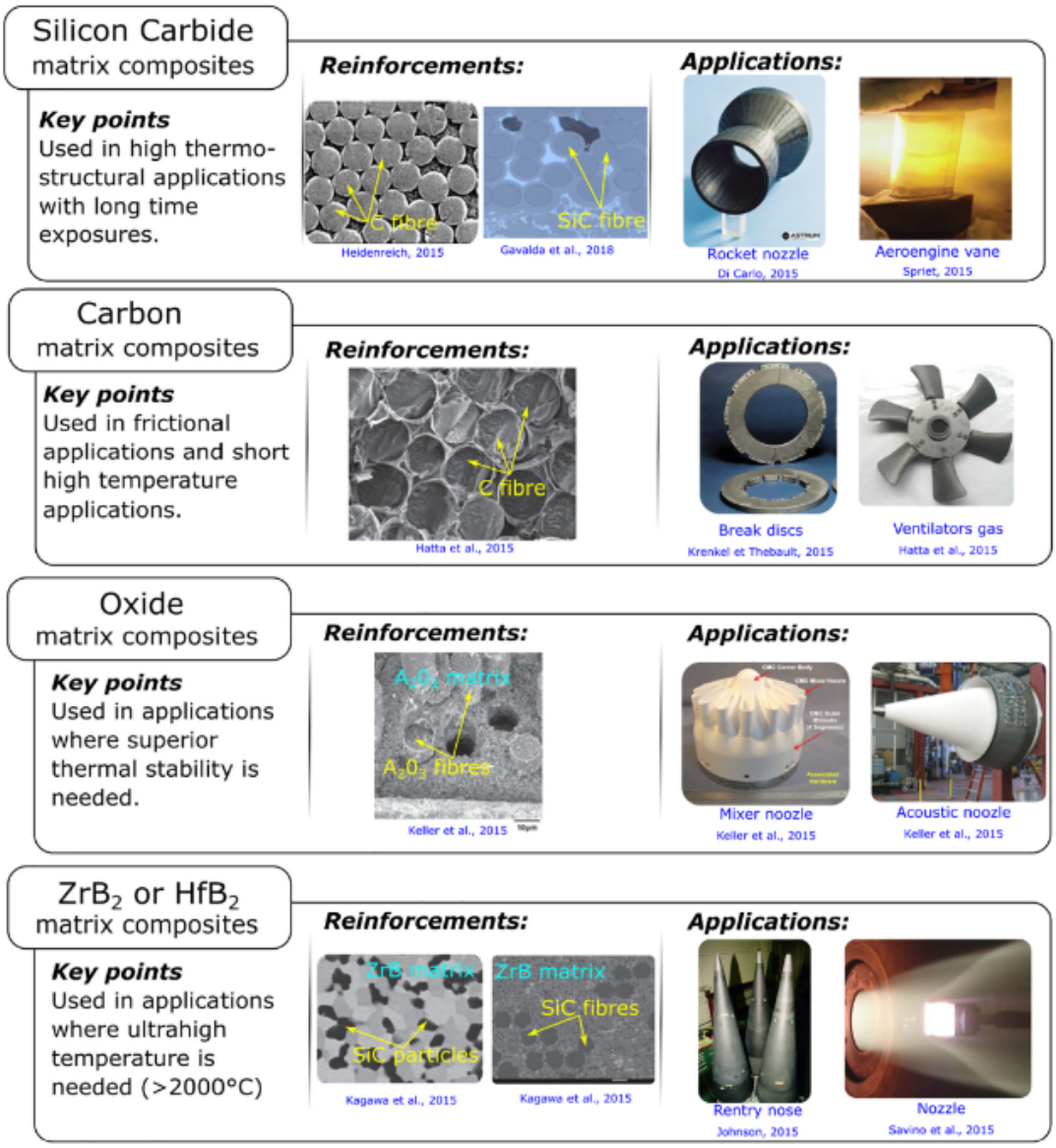


**Figure 2:** Summary of CMC and its applications [2]

The common characteristic behind all CMCs are the good thermal properties, hence the increased interest of the aerospace industry is them. Nozzles, re-entry noses, aeronautic engines are all applications that require the materials which are designed to sustain very high temperatures for extended period of times. That is also true for new technologies such as re-usable rockets in which the outer layer of the rockets must survive the re-entry and retain their mechanical properties for the next utilization.

### 1.2.1 Thermal-Structural Challenges

One example of aerospace application of CMC are hypersonic vehicles, in which the outer surface is subjected to high heat fluxes causing extreme temperatures to arise. Two strategies can be used in systems to deal with this extreme heating environment. The structure must either have a TPS to protect it from the high heat and keep temperature on the adequate threshold, or it must be able to work under extreme temperatures. The later is what we call a Hot Structure.

For a better understanding of the thermal aspect of hypersonic missions, we can consider three representative cases. A Crew Exploration Vehicle (CEV) capsule during it´s reentry from Low Earth Orbit (LEO), a Single Stage to Orbit (SSTO) air breather in its descent and the Space Shuttle Orbiter during descent. Those different missions have different heat flux profiles and therefore different needs in terms of TPS. The heat flux profile of a sphere of 1 $ft^2$ for each mission is shown in 3 and the heat load, that is, the heat flux integrated over time is shown on figure 4.

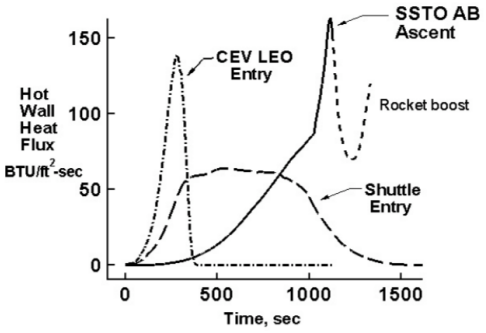


**Figure 3:** Heating on a reference one-foot diameter sphere for three different trajectories. [17]

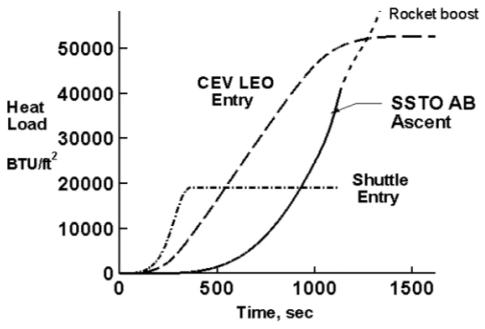


**Figure 4:** Heat load on a reference one-foot diameter sphere for three different trajectories. [17]

The first thermal-structural challenge is large thermal gradients. Taking cryo-

genic tanks as an representative example, the temperature difference can be as much as -423$^{o}$F internally to 3000$^{o}$F on the outer surface [17]. With this temperature range, the different materials can suffer severe stress due to unmatched expansion rates.

Another critical thermal-structural challenge is thin cross sections with high mechanical loads that operate at high temperatures. An example is sharp node leading edges, that must operate on those conditions and be able to maintain their shape, as it's fundamental for the correct operation of the vehicles.

Gaps and steps on aerodynamic surfaces are also a point of interest, as they can create severe thermal problems.

Finally, affordability is a fundamental point of any engineering project. As such, as TPS systems become more complex and expensive due to the need of fulfill more challenging conditions, the use of new materials become the factor that enables new vehicles. On figure 5 we can see how new materials, with improved thermal properties enabled new missions, historically.

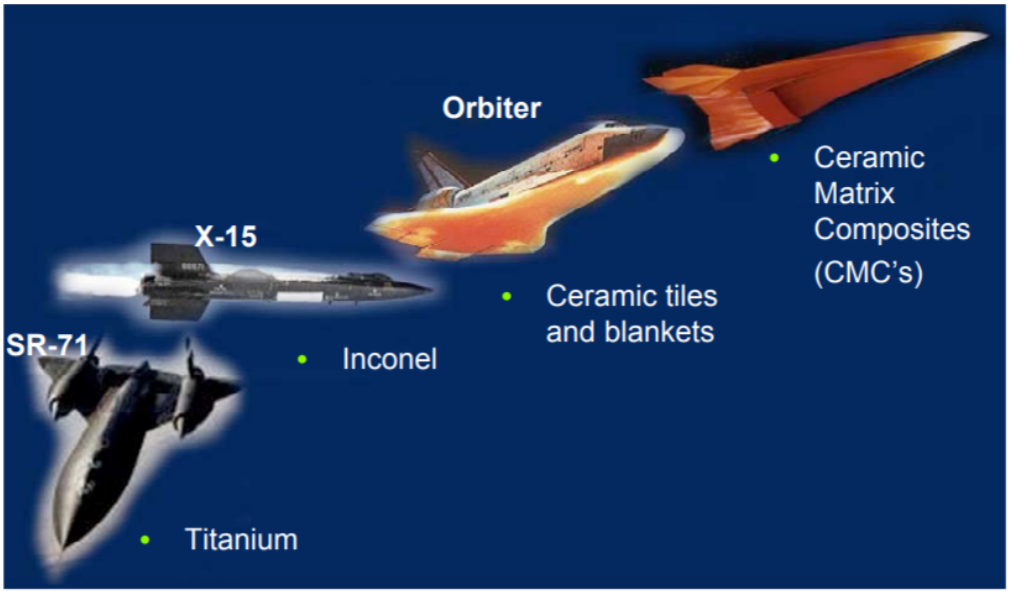


**Figure 5:** Examples of where new material systems have helped enable new vehicles. [17]

On figure 6 the specific strength of different materials in function of temperature can be seen. With this information is possible to understand why CMC materials are important for high temperature applications. With a high specific strength at high temperatures, those materials enable applications as hypersonic air-breathing vehicles.

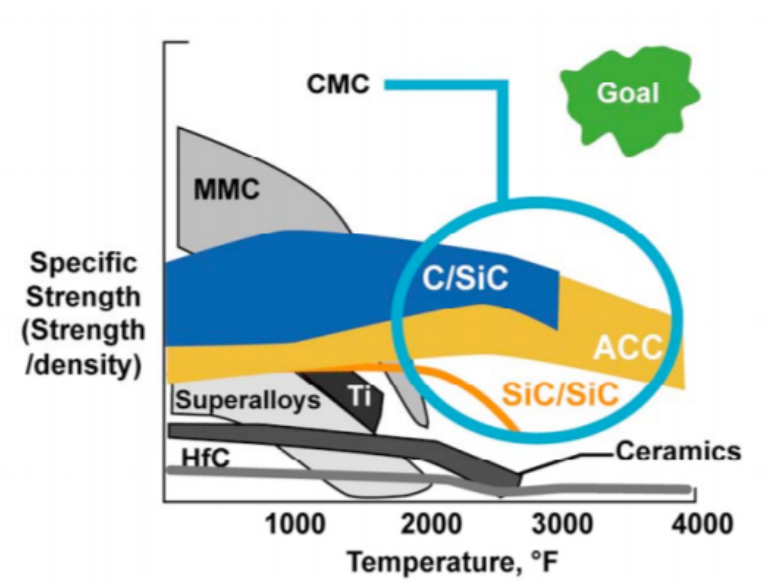


**Figure 6:** Material specific strength as a function of temperature for several material classes. [17]

Figure 7 shows an scheme of a CMC. Their structure reflects some of their positive thermal-mechanic characteristics. The environmental barrier coating is fundamental for proper functioning in extreme temperatures, as it will prevent or delay oxidation, a process that is very detrimental to the mechanical properties of the composite.

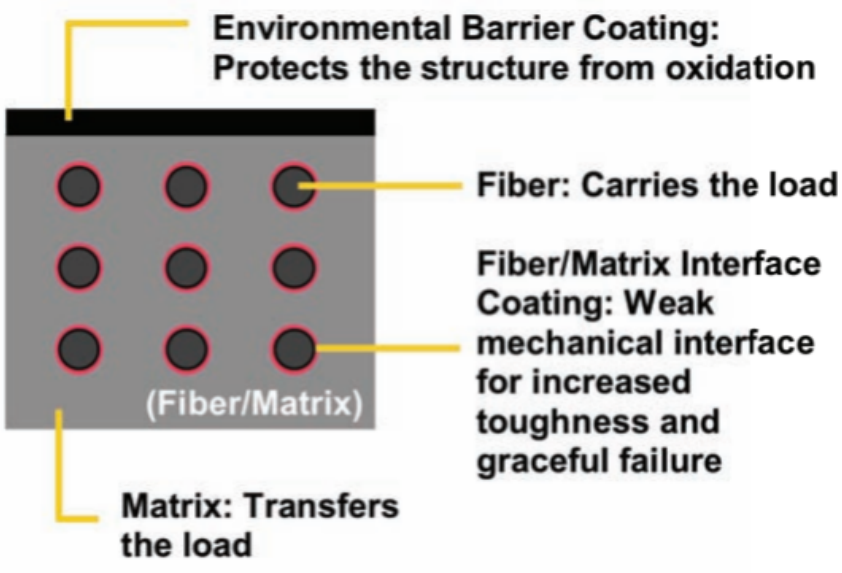


**Figure 7:** Schematic of a ceramic matrix composite with fibers inside of a matrix. [17]

On Figure 8 we can see the chemical equations for the oxidation process of SiC for both passive and active oxidation.

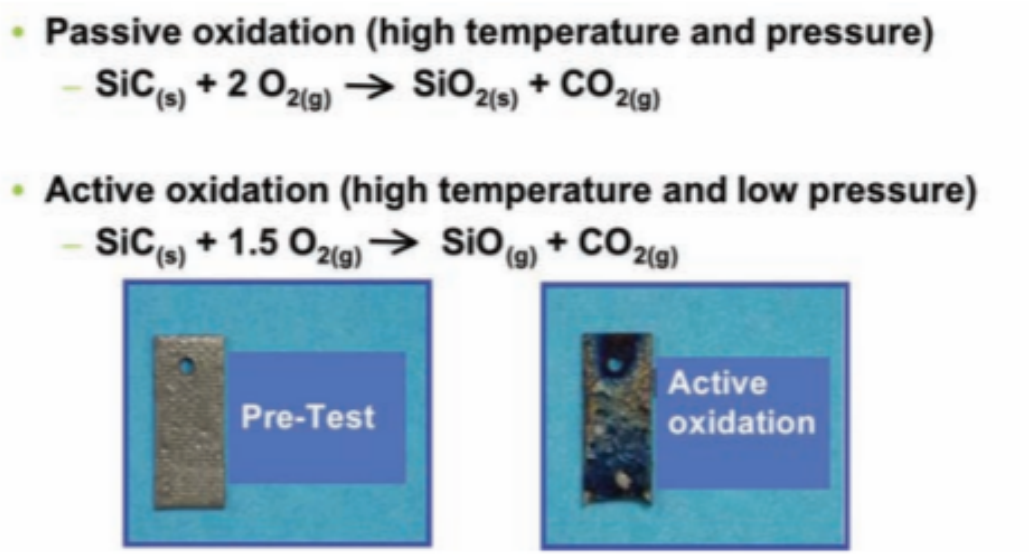


**Figure 8:** Comparison of active and passive oxidation. [17]

### 1.2.2 Thermal Protection Systems

TPS are needed for several aeronautical and space applications. For vehicles that travel at hypersonic speed within the atmosphere,as in a ballistic re-entrys or hypersonic cruise, the aerodynamic heating can generate very severe thermal conditions that need to be addressed by the usage of TPS [17]. In propulsion systems, the energy dissipation in form of heat also creates the need for TPS.

The temperatures and time of exposure to which the system is exposed will strongly influence the type of TPS chosen for its protection.

On Figure 9 some TPS strategies are showed, according to the temperatures and exposure time of the missions.

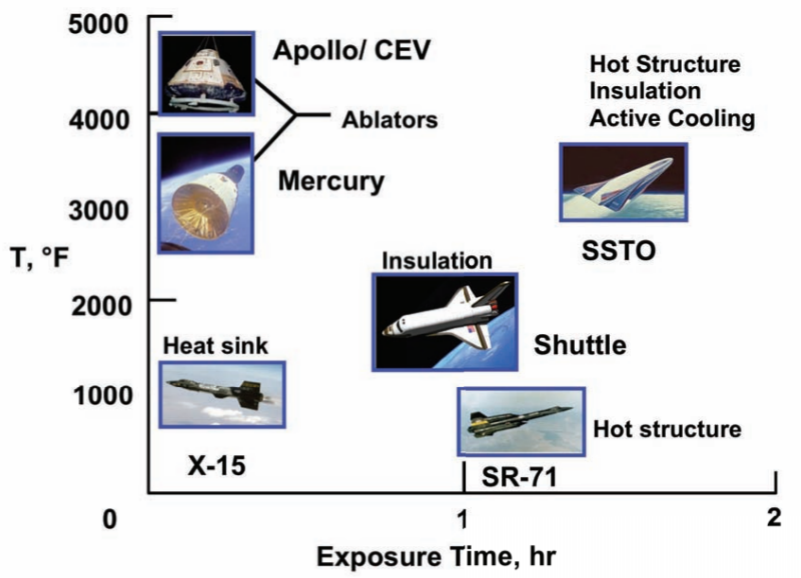


**Figure 9:** management approach for several vehicles as a function of temperature and exposure time. [17]

#### 1.2.2.1 Passive TPS

For moderate heat-fluxes and short exposition times, insulation can be used. Insulation, showed on Figure 10, aims to minimize heat reach to the structure, maintaining it cooled.

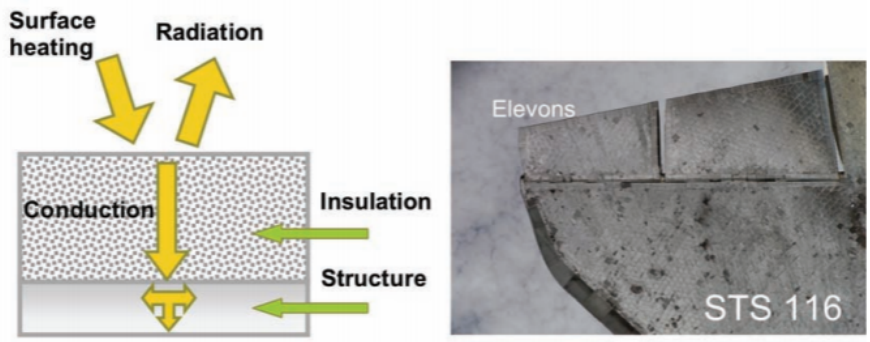


**Figure 10:** Schematic and photograph (Space Shuttle Orbiter elevons) of an insulated structure. [17]

A heat-sink is another passive strategy, it is showed on Figure 11. For moderate fluxes, in transient situations, the strategy, that relies in absorbing part of the heat and radiate away another part. The strategy only works for short periods of time as for long periods, the continuous absorption of heat eventually will result in over heating of the structure.

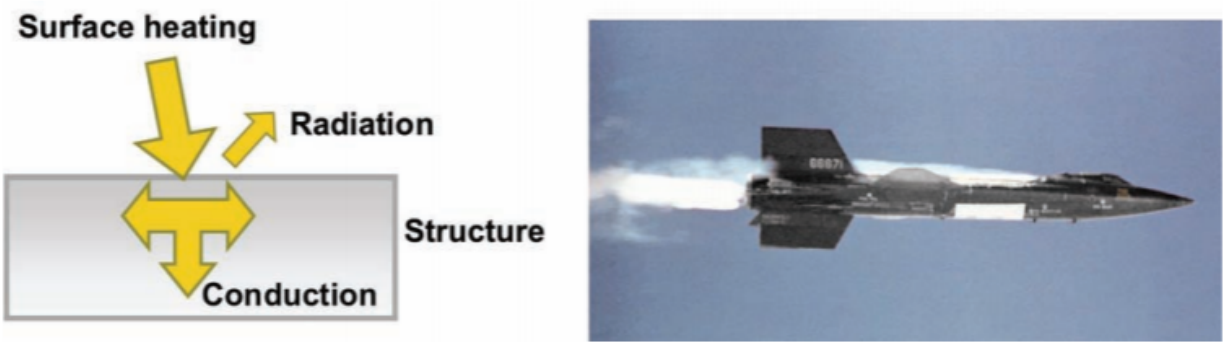


**Figure 11:** Schematic and photograph (X-15) of a heat sink structure. [17]

Hot structure, showed in Figure 12 is also a passive strategy. In this variety of TPS is similar to the heat sink idea, but does not have the limitation of operate in short spans of time. As the materials used can sustain loads at high temperatures, they can be operated for long periods of time without over heating.

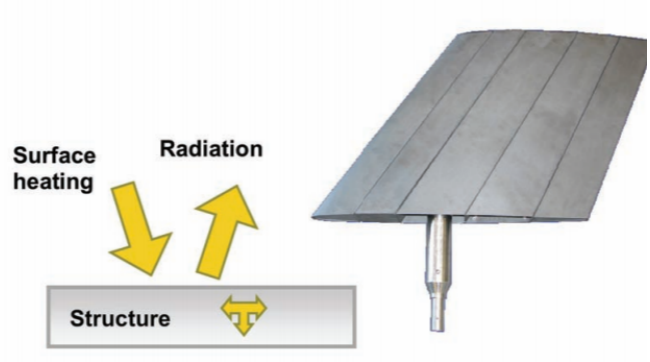


**Figure 12:** Schematic and photograph of a hot structure. [17]

#### 1.2.2.2 Semi-Passive TPS

For high heat fluxes that are applied for long times, semi-passive approach may be needed. The first example of this kind of strategy heat pipes (Figure 13 ). It relies on a working fluid that absorbs heat and transports it to be radiated on another region of the tubes.

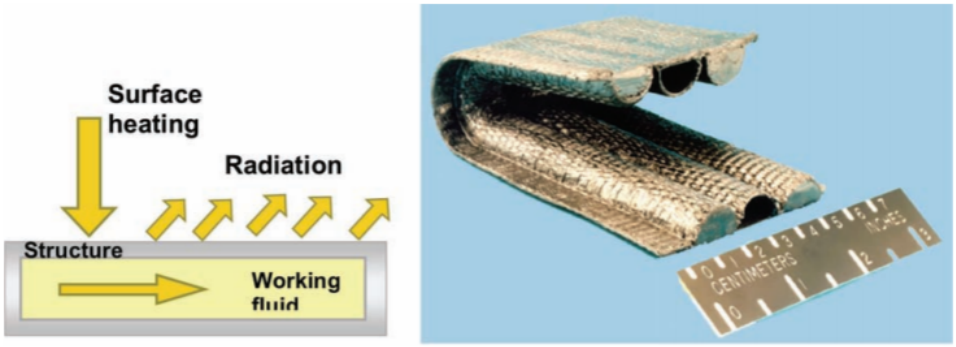


**Figure 13:** Schematic and photograph illustrating a heat-pipe-cooled leading edge. [17]

Another very important semi passive strategy for space applications is ablation (Figure 14). This thermal management approach is able to deal with very high heat fluxes for short times relies in using a material that will be ablated in order to dissipate energy and avoid heating of the structures. The ablator is consumed in the process.

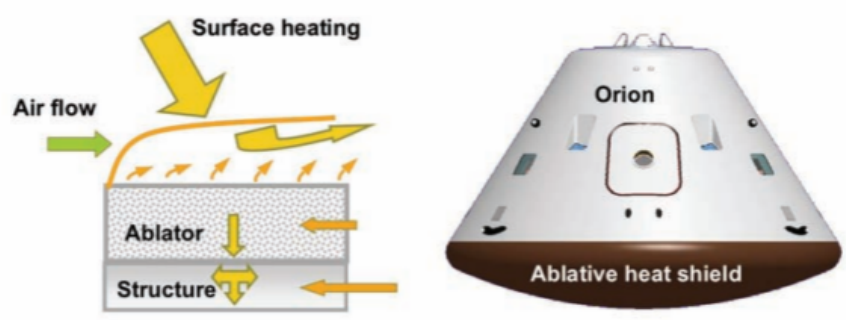


**Figure 14:** Schematic and illustration of an ablative heat shield. [17]

#### 1.2.2.3 Active TPS

When higher heat fluxes are used for long periods of time, active cooling is needed. Convective cooling (Figure 15) is one of the strategies that can be used and consists in transferring heat to a coolant and then carrying it away .

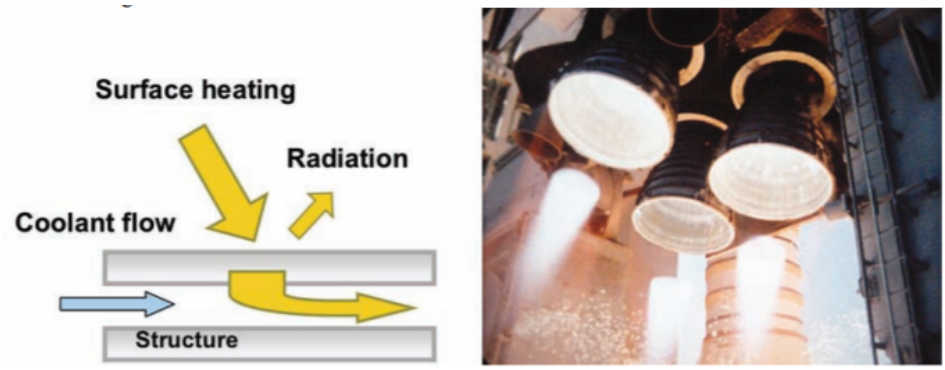


**Figure 15:** Schematic and photograph of actively cooled structure (SSME). [17]

Another strategy that can be used is film cooling. It consists in having a thin cool insulating blanket. The structure will heat and operate hot.

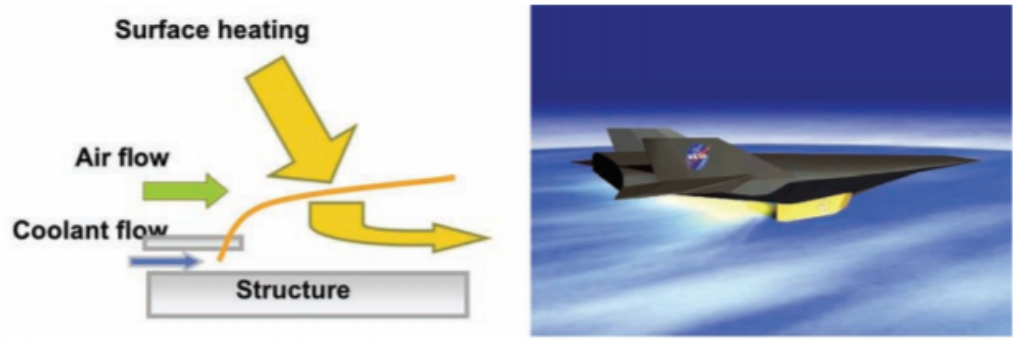


**Figure 16:** Schematic of film cooling and drawing of a hypersonic vehicle. [17]

Finally, transpiration cooling is the method used for high heat fluxes and long times. It is used, for example, for protection of combustion chambers. A coolant is continuously injected through a porous structure over large areas.

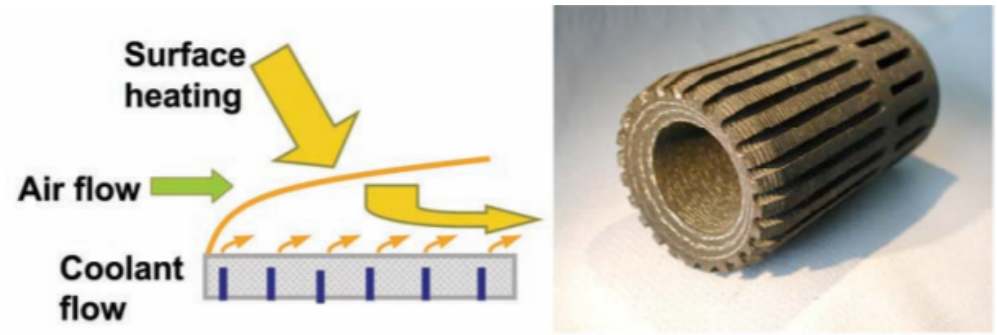


**Figure 17:** Schematic of transpiration cooling and a C/C cooled combustion chamber test article. [17]

#### 1.2.2.4 CMC TPS

On leading edges of hypersonic vehicles, a specially critical situation in terms of heating management, some TPS strategies can be observed as shown in Figure 18. CMC's are used in many of those systems, both passive and active. For passive TPS a C/C composite leading-edge can be used. C/C are also used in some implementations of heat pipes.

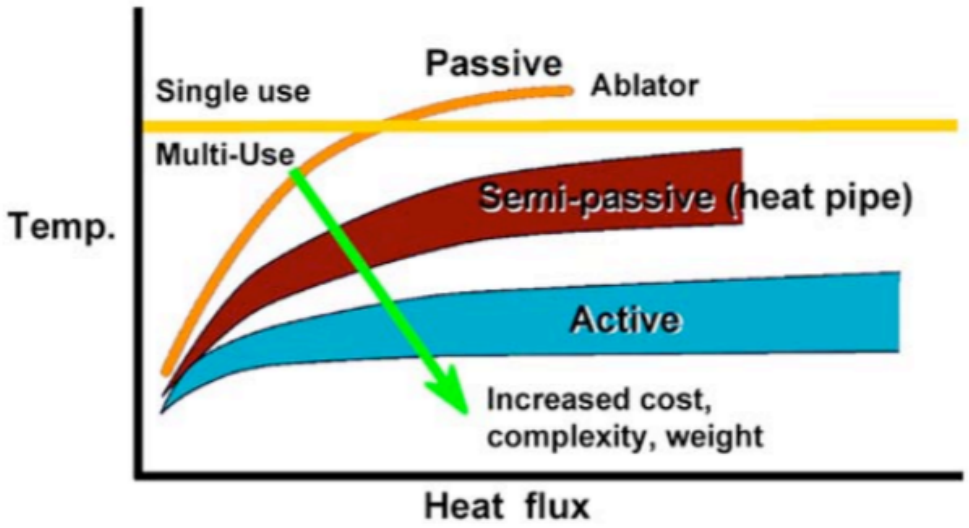


**Figure 18:** Leading-edge thermal management options [17]

For the highest heat fluxes, for which active cooling is needed, strategies involving CMCs are also used in combination with metallic actively cooled leading edges as seen in Figures 20 and 19. All composite active structures would provide the best temperature capabilities, with lightest weights, but still encounter multiple challenges such as oxidation protection, long life and cooling containment.

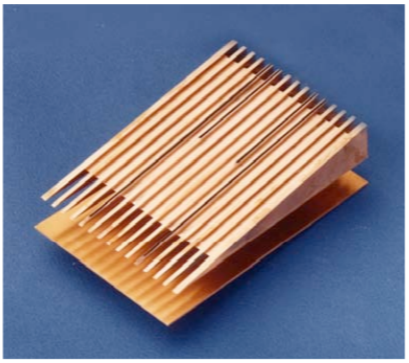

**Figure 19:** Photograph of the internal portion of an actively cooled leading edge [17]

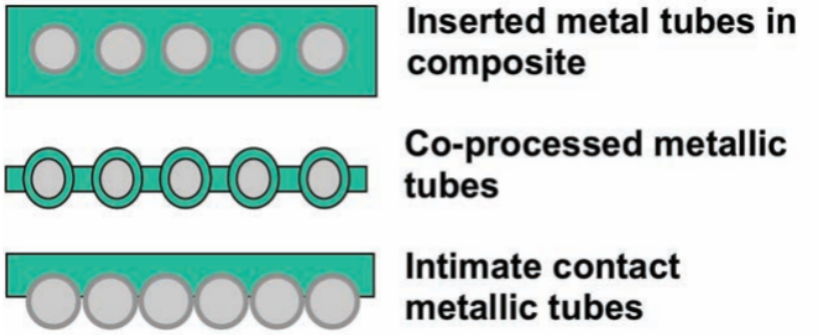


**Figure 20:** Approaches for actively cooled composites [17]

Insulated structures, Stand-Off TPS, internal insulation, load bearing aeroshell and structurally integrated TPS are some different strategies for acreage of hypersonic vehicles. Both Stand-Off TPS and Load Bearing AeroShell take advantage of CMC materials to operate under high temperatures.

Stand-Off strategies rely on transmitting to the structure only the aero loads, without transmitting the thermal loads. This strategy can be seen on Figure 21

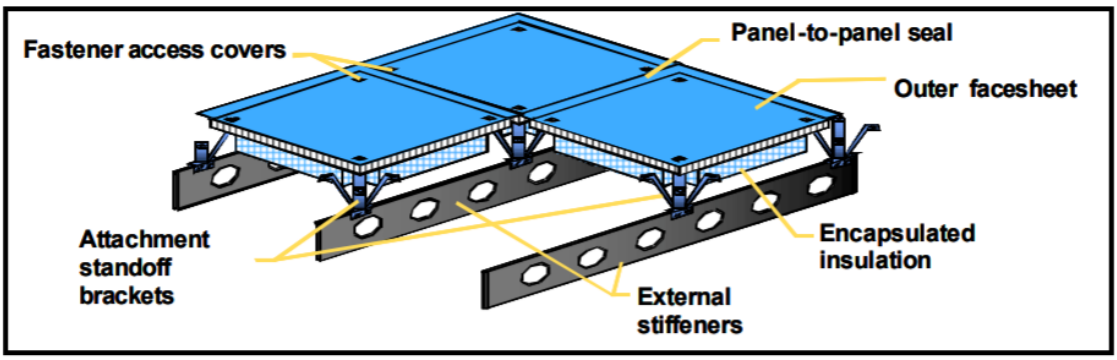


**Figure 21:** Schematic drawing of X-33 metallic TPS illustrating stand-off TPS attachment to sub-structure [17]

### 1.2.3 CMC Hot Structures for Space Vehicles

Hot structures are designed to sustain high temperatures while still performing their structural role. This means that the materials of which they're done should be capable of retaining its mechanical properties in elevated temperatures.

Two examples of applications of hot structures and their general 1D profile can be been on Figure 22.

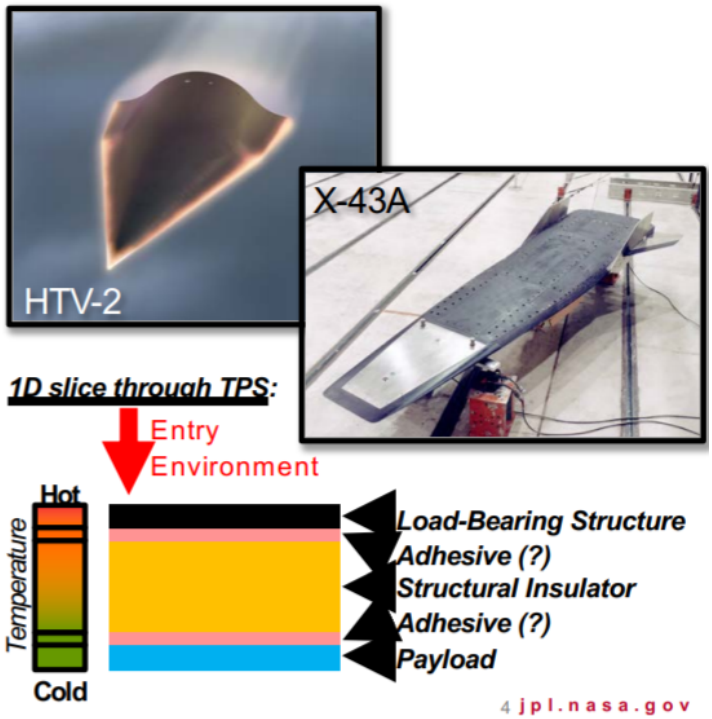


**Figure 22:** Schematic drawing of a hot structure and two application examples [26]

The advantages of using a Hot Structure together or to replace a TPS are reduced mass, re-usability, improved aerodynamic, improved structural efficiency and increased inspectability. Those advantages motivated the proposition of a Hot Structure based Re-Entry capsule for the Mars Sample Return mission, developed by California Institute of technology [26], the capsule, seen in Figure 23, uses multiple components made of the a C/C CMC working as Hot Structures.

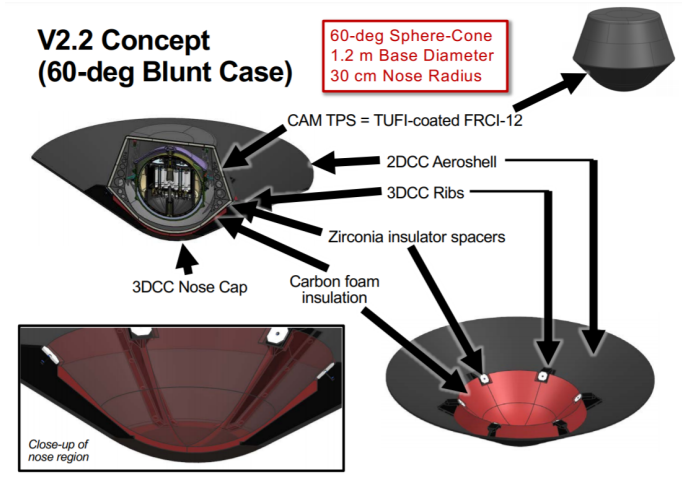


**Figure 23:** Drawing of a proposed re-entry capsule for the Mars Return Mission [26]

The IsiComp material itself is also an example of those advantages, it was used

to develop a Hot Structure for the Space Rider. The material was implemented into the creation the first flap made of ceramic material [7], shown in Figure 25. With the CMC material the structure is capable of enduring temperatures up to 1650$^{o}$C, while sustaining loads of 1200 Kg and weighting only 10 Kg. An detail of the structure with its mechanisms can be seen also on Figure [6].

**Figure 24:** Flap made of IsiComp material [7]

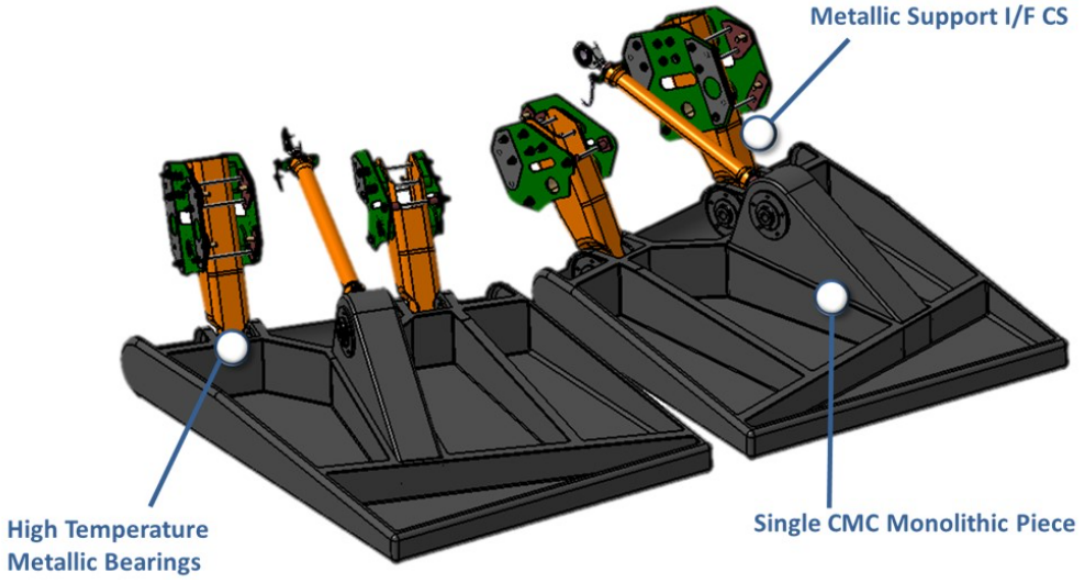


**Figure 25:** Model of flap made of IsiComp material [6]

Hot Structures are enablers of reusable components and has been used previously on National Aeronautics and Space Administration (NASA) programs such as the Space Shuttle, Hyper-X and X-37 [34]. The development of Hot Structures for usage in liquid rocket engine propulsion system is also a great point of interest for today's development.

One of the main types of materials of interest for further development of this kinda of system are the CMCs. The development needed includes not only new technologies and material compositions, but also better manufacturing methods, optimization in

oxidation protection, improving the time of production and improving the design process, being specially important to develop a consistent and reliable test and design process that allows for the properties from test coupons to be scalable to prototypes [34].

Re-Usable CMC elements have already been validated by European Space Agency (ESA) for such purposes in the concept studies for the Next Generation Launcher (NGL) system [13] in realistic environments such as dynamic flow or simulated in plasma arcjet facilities.

The main technological gap that CMCs could help to fill is Hot Structures for temperatures above the $1600^{o}$C range.

The fact that CMC materials retain great mechanical properties even when working under very high temperatures has made it the material of choice for hot structures for space vehicles in some recent studies and missions.

Heatshields are a critical component for planetary entry vehicles. When a vehicle enters the atmosphere of a planet severe aerodynamic heating occurs. Traditional systems for this purpose include the use of TPS. Typically a material with the capacity to ablate is used on the downward surface of the vehicle to dissipate energy.

An innovative approach for heatshields is proposed by NASA researchers on the paper "A Multifunctional Hot Structure Heatshield Concept for Planetary Entry" [39] with the objective of enabling future planetary missions.

The Multifunctional Hot Structure (HOST) heatshield concept differs from the traditional approach by using the TPS also as a structural component while on the traditional systems the ablative materials have very low load carrying capability and therefore, are isolated from the structural loads. The CMC material allows the TPS to also act as a structural component, as it can resist extreme temperatures while carrying significant structural loads. With this, it's possible to reduce size and mass of the re-entry systems. The concept of HOST can be seen in Figure 26

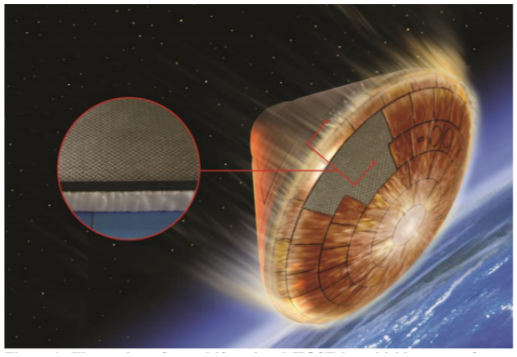

**Figure 26:** Illustration of a multi functional HOST heatshield concept for an Earth entry application and a close-up of the carbon-carbon outer layer with a blanket insulation underneath. [39]

Another take into the use of CMC on re-entry vehicles is the X-38 prototypes Crew Return Vehicle (CRV) designed by NASA [28]. The objective of the project, that included 5 prototypes, was to research and develop technology to develop an emergency vehicle for return of astronauts of the International Space Station (ISS). The X-38 vehicles uses a lifted re-entry approach, as in opposition to a ballistic re-entry but they endure the same challenge of sustaining the aerodynamic heating during the descent. For this reason the vehicles also rely in TPS and hot structures [18]. CMC materials are used to endure the extreme temperatures on the nose cap system that was fully flight qualified in 2001 [18] (Figure 27).

**Figure 27:** The X-38 prototype of the Crew Return Vehicle for the International Space Station drops away from its launch pylon on the wing of NASA's NB-52B mothership as it begins its eighth free flight on Thursday, Dec. 13, 2001. [NASA] [28]

CMC materials are also being used to develop nozzles that act as hot structures supporting mechanical loads while under extreme temperatures. An example of CMC nozzle extensions tested by NASA can be seen on Figure 28 ,the tests performed to access mechanical and thermal properties demonstrated great potential for the use of CMC nozzles as a resource to save mass, when compared with the current metallic state

of the art technology, without losing performance [29].

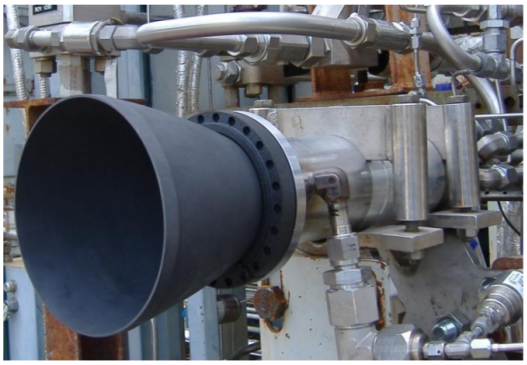

**Figure 28:** [28]

NASA is currently investigating several possible usages for Hot Structures with an special interest in CMC materials [34]. The possible usages of CMC Hot Structures for Space applications [34] are:

- Upper Stage Engine Systems
- In-Space Propulsion Systems
- Lunar/Mars descent/ascent Propulsion Systems
- Solid Motor Systems
- Propulsion Systems for Commercial Space Industry
- Improved Re-Entry Vehicles
- Re-usable space systems and components

# 2 Material Characterization and Failure Modes CMC

## 2.1 Material Characterization

In this section the general characterization of Carbon Fibre Reinforced Silicon Carbide (C/SiC) CMCs will be discussed.

As discussed on the previous section, CMC materials are widely used as thermal structural materials in aeronautic and space fields. For this reason, is important to describe both thermal and mechanical characteristics of such composites.

When a structure is heated thermal stresses can be induced if some of its parts are not free to expand or contract. Nonuniform temperature distribution can also create those kind of internal stresses.

The effect of those stresses can be serious and result into failure of components. Therefore is important to properly understand and describe such phenomena to prevent failures. CMCs are often also exposed to harsh oxidation environment for its exposition to high temperatures and harsh atmosphere.

C and SiC fiber-reinforced ceramics offer the highest specific strength at temperatures above 900ºC in all available engineering materials. For this reason they are specially interesting for aeronautical and space industry.

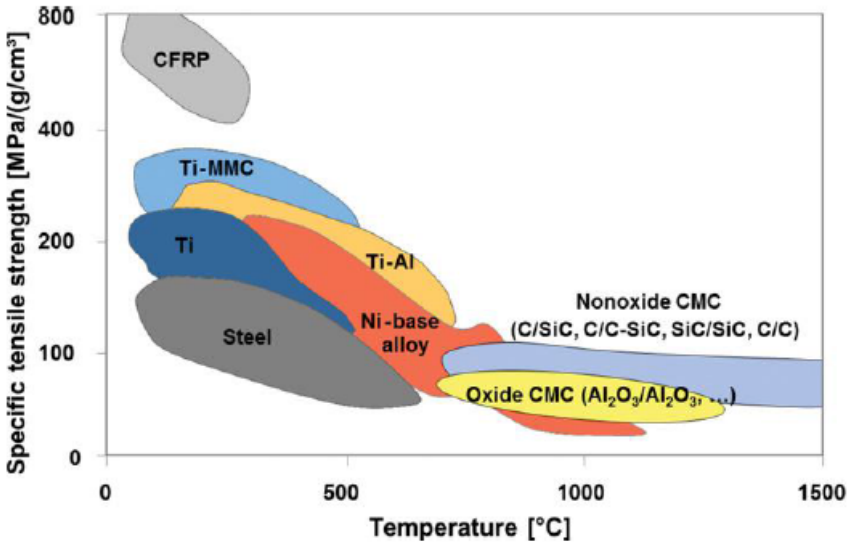


**Figure 29:** Weight-specific strength of materials as a function of temperature (DLR). [22]

While ceramics are well know for its high thermal and chemical stability, hardness and abrasive wear resistance, being used in aeronautical applications such as coating of of engine blades, for example, they have the important drawback of brittleness and low damage tolerance. Cracks propagate rapidly leading to catastrophic failure.

Imperfections such as porosity, cracks and microcracks will determinate the strength of the ceramics and are governed, in terms of quantity, distribution and size, by Weibull statistics, meaning that there is no universal strength value for design for monolithic ceramics.

Embedding fibers in the ceramics provides the most promising method to improve the reliability and fracture behaviours of those materials. These CMC combine the positive properties of ceramics with the advantages from the fibers, resulting in general properties of:

- Quasi-ductile fracture behaviour
- high fracture toughness
- low Young's modulus
- very low CTE
- extreme thermal shock stability
- low density

The energy dissipating mechanisms introduced by the fibers, such as crack deflection, crack splitting and crack stopping, as well as crack bridging increases toughness and reliability.

To achieve those benefits, a weak embedding of the fibers on the matrix is essential. In case of strong embedding, crack bridging is not achieved, leading to brittle fracture behaviorus.

Strength values of C/SiC structures are mainly determined by fiber content, orientation and are independent on size and volume, resulting in thin-walled, lightweigth structures that can be dimensioned by deterministic approaches.

The final properties of a C/SiC composite is very dependent on the process and specifications with which it was produced. Therefore is important to understand its manufacturing processes and technologies.

### 2.1.1 Manufacturing

For production of a C/SiC material the C fibers must be embedded in a SiC matrix. This is done, usually, by building up the matrix inside a fiber preform. Three main methods are used nowadays, which were derived from the industrial manufacture of SiC components. They differ on the strategy used to build up the SiC matrices [22].

Those manufacturing methods are [22]:

- Chemical Vapor Infiltration (CVI) - Deposition of gaseous SiC precursors
- Polymer Infiltration and Pyrolysis (PIP) or Liquidi Polymer Infiltration (LPI) - Pyrolysis of Si polymers
- Melt Infiltration (MI) - Reaction of molten Si with C

A simplified scheme of the processes can be seen on Figure 30

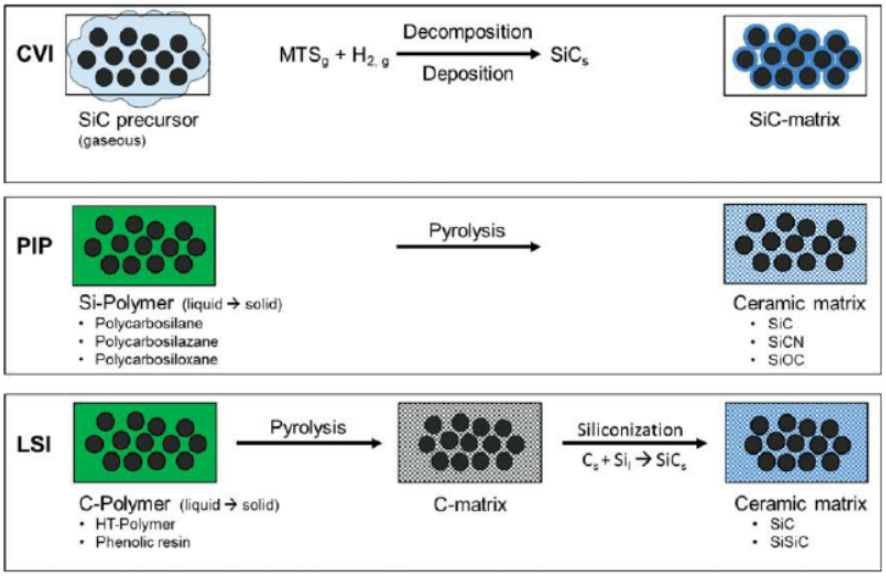


**Figure 30:** Schematic overview of the different methods used for the buildup of SiC matrix in C/SiC materials (DLR). [22]

All methods rely on 3 steps [22]:

- CVI - Manufacture of a C fiber preform or **CRFP!** (**CRFP!**) preform
- PIP or LPI - Pyrolysis of Si polymers

- MI - Reaction of molten Si with C

All types of carbon fibers can be used for the fiber preform. For economic reasons, High Tenacity (HT) fibers are more common for the Liquid Silicon Infiltration (LSI) process. As C/SiC composites are fiber-dominant, improved material properties can be obtained using Intermediate Modulus (IM) and High Modulus (HM) fibers, offering highest tensile strength and Young modulus [22]. For this reason IM are widely used in PIP and CVI C/SiC composites. While Ultra High Modulus (UHM) fibers do exist, their price is too elevated and is not generally used. They're also not adequate for LSI processes as fiber embedding and protection is insufficient [22].

For homogeneous distribution of the SiC and to take advantage of the properties of the C fibers, fine rovings based on 1000-6000 single filaments are preferred.

On the CVI process the SiC matrix is built up directly in the fiber preform. For PIP and LSI Carbon Fiber Reinforced Plastic (CFRP) preforms have to be manufactured. They can be prepared either by dry fiber preforms infiltrated with the polymer, as for the transfer molding method, or polymer infiltrated fibers can be used in autoclave technique, warm pressing and wet filament winding.

Dry fiber preform are usually manufactured by stacking cut layers of two-dimensional (2D) woven fabrics resulting in orthrotropic ($0^{o}/90^{o}$) or quasi-isotropic ($0^{o}/90^{o}$, $\pm\ 45^{o}$) fiber architectures. 1D fiber layers can be used as cross-ply laminates is combined with fabric. Multiaxial fibre architectures are achieved by filament winding or braiding. They can be combined with 3D weaving, stitching or needling leading to 2.5D and 3D preforms. 2.5D and 3D preforms have increased interlaminar shear strength when compared with 2D fabrics. Short fibers can be used to achieve randomly oriented fiber reinforcement [22].

To take advantage of the the high strength of the C fibers and obtain high fracture toughness and damage tolerance, a weak embedding of the C fibers in the SiC matrix is fundamental. The fibers are usually separated from the matrix by coating the fibers with an interphase material, providing low shear strength regions between the matrix and the fibers. Usually the coating is made of pyrolitic carbon (pyC).

#### 2.1.1.1 Chemical Vapor Infiltration

The CVI process consists in the deposition of a ceramic matrix out of a gaseous precursor. It is used for simple plates as well for very large and complex structures. The process has 3 main phases:

1. Manufacture and stabilizing of a carbon fiber preform - A porous preform is made on near net shape geometry.

2. Deposition of fiber coating (interphase) A thin layer of coating is applied by cracking methane in a first CVI process step

3. Deposition of the SiC matrix The porous fibers preform is set inside an infiltration chamber and heated to temperatures between 800ºC and 1000ºC. The gaseous precursor passes through the infiltration chamber and penetrates in the porous fiber preform. A chemical reaction is activate on the hot surface of the porous fiber preform and SiC is deposited.

One of the greatest advantages to this method is that the SiC obtained is highly pure and fine grained leading to excellent mechanical properties of the final composite, especially at high temperatures. Another important advantage is the low process temperature, uncritical for the carbon fibers. The method also offers great flexibility in terms of which kind of components can be manufacturing using it.

The main drawbacks are high investment cost for the facilities, demanding process control and long process times. A limited fiber content and remaining open porosity are other drawbacks. 2D fabric materials made with this process can experience sensitivity to delaminations. This drawback can be avoided with the usage of 3D-woven fiber preforms.

#### 2.1.1.2 Polymer Infiltration and Pyrolysis

The PIP is characterized by the buildup of the SiC matrix via thermal decomposition of preceramic polymers in multiple densification cycles. The fibers preform are are infiltrated by the liquid precursor in the initial step. After the polymer is cured, the thermoset matrix obtained is then converted in ceramic using heat in a non-oxidizing atmosphere. SiC matrices are usually obtained from polycarbosilanes with high yields of SiC, such as polymethylsilane. The main disavantage of polycarbosilanes is the high cost, up of 1300 \$/Kg up to 1800 \$/Kg caused by expensive raw materials, elaborate synthesis processes and low volume of prodcution. For his reason, polycarbosilanes are typically limited to aerospace and military application. Polysilzane precursors can be used as alternative for cost critical applications, with costs of 50-200 €/kg but they support only lower temperatures of service, up to 1200ºC. [22] [20]

The PIP technique is one of the most advanced methods for manufacturing of large complex-shaped C/SiC structures in the aerospace industry. It can be divided in 4

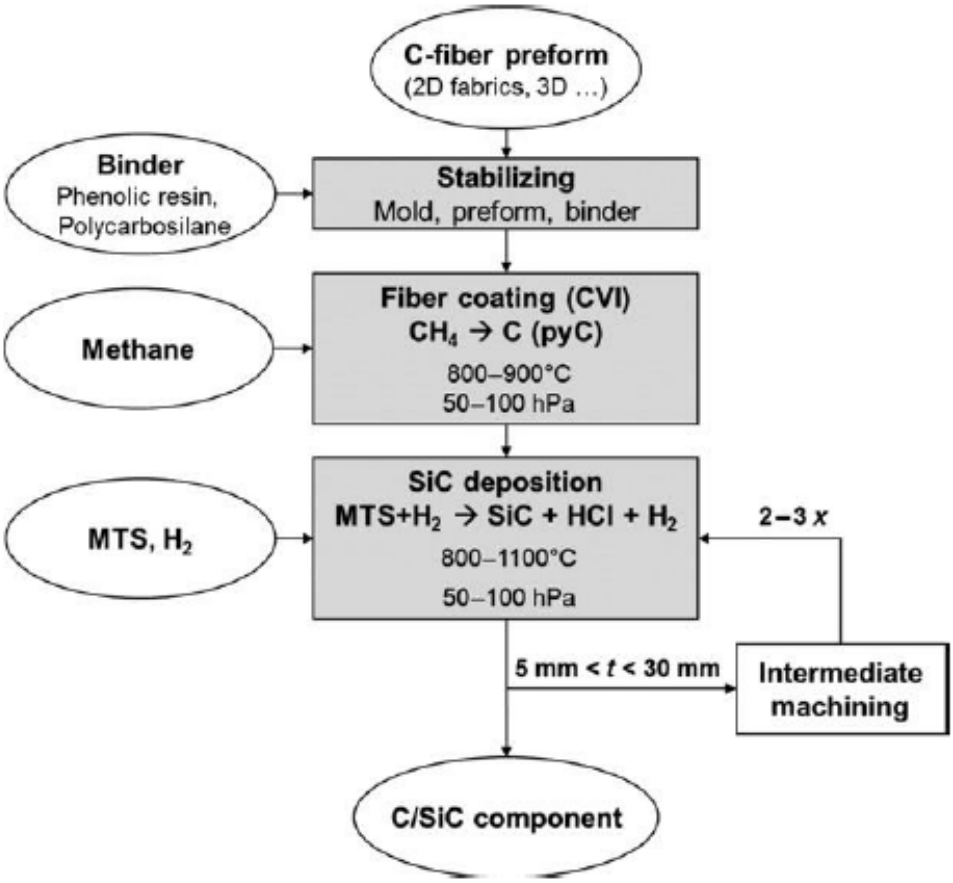


**Figure 31:** Schematic overview of the manufacture of C/SiC materials via I-CVI (DLR). [22]

steps:

- Deposition of fiber coating (interphase).

  The first phase consists in coating the fibers in an interphase layer. Typically this thin layer is made of pyC and serves to the proposite of guaranteeing weak embedding of the fibers in the SiC matrix.

- Manufacture of a CFRP preform.

  For the manufacture of the CFRP preforms many strategies can be used such as wet filament winding and fiber placement, vacuum-assisted polymer (VAP) infiltration (developed by Astrium ST/EADS IW) or RTM as well as autoclave technique and warm pressing.

- Pyrolysis of the CFRP preform.

  In the third step the CFRP preform is pyrolized in inert gas atmosphere or vacuum. The chemical bonds of the polymer breaks, the organic side chains separate and the polymer matrix is converted into the ceramic matrix resulting also in a considerable mass loss. The morphology of the matrix is strongly influenced by the temperature of the process. Low heating rates result in dense SiC with low porosity while low max temperature results is porous amorphous SiC matrices. Low porous, crystalline matrices are obtained for high maximum process temperatures (up to 1600$^{o}$C).

- Densification via repeated polymer infiltration an pyrolysis.

  Due to the high mass loss and porosity obtained in the third step, a densification process is needed in order to achieve sufficient mechanical properties, this is performed with multiple densifying cycles consisting of polymer infiltration and pyrolysis. To obtain porosities under 10% it's necessary to perform those steps for 5 to 8 cycles.

The main advantage of PIP is controllable matrix buildup enabling stoichiometric SiC and avoiding free silicon. Fibers are not influenced or damage by the temperatures used during the processing of the material. High mechanical properties can be achieved. Unidirectional (1D) fiber reinforcement can be achieved. Wall thickness is not limited as the matrix buildup is homogeneous [22].

The main disadvantages are high costs for the preceramic precursos, long manufacturing times of several weeks up to months and low interlaminar shear strength due to relatively high porosity. This is specially critical for 2D fiber-reinforced materials. Multi-axial fiber preforms can be used to mitigate this point in order to produce high performance components.

On the PIP process the

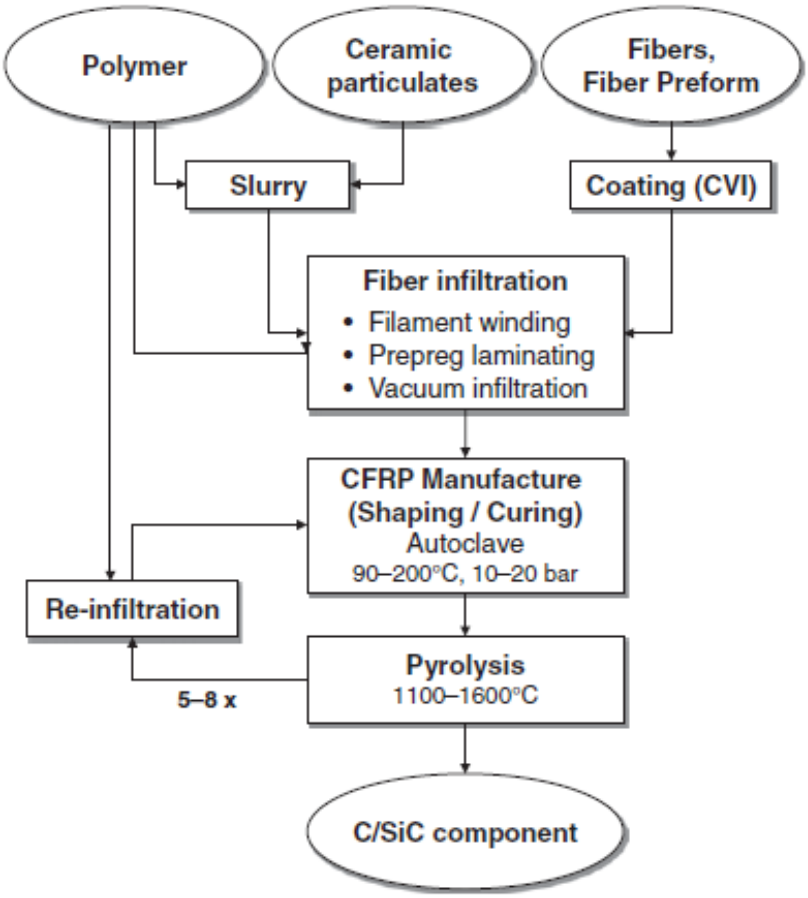


**Figure 32:** Schematic overview of the manufacture of C/SiC materials via PIP (DLR). [22]

#### 2.1.1.3 Melt Infiltration

The MI method consists in the infiltration of a porous C/C preform with molten Si and buildup of the SiC matrix using an exothermic chemical reaction of the liquid silicon with the solid carbon.

This technique is used for manufacturing C/C-SiC as well as C/SiC materials. Flat plates as well as complex shaped structures are possible to be manufacture utilizing this method. Due to economical and technical advantages as high thermal conductivity, this method is preferred for brake disks and other friction components.

This manufacturing process can be divided in 4 steps:

- Buildup of fiber/matrix interphase, for example, by fiber coating.

- Manufacture of a CFRP preform.
- Pyrolysis of the CFRP preform to a C/C preform.
- Siliconization of the C/C preform.

  The most common process for the siliconization is the LSI process, a capillary infiltration of molten Si. Other methods used are pack cementation and capillary infiltration (CPI) and pressurized melt infiltration (PMI).

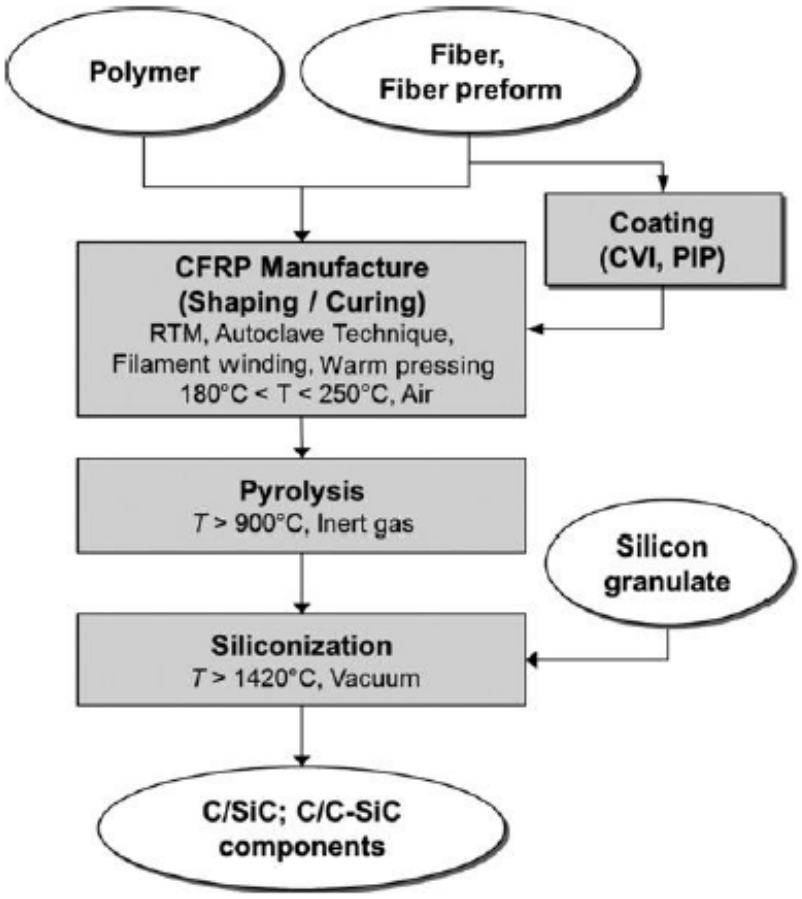


**Figure 33:** Schematic overview of the manufacture of C/SiC materials via MI (DLR). [22]

While on the CVI and PIP processes the SiC matrix buildup does not influence or damage the carbon fibers, on the MI process, due to the molten silicon being highly reactive to the C matrix ans well as to the C fibers, the direct contact of the Si melt and C fibers must be avoided. Is important to also preserve the weak embedding of the brittle fibers in the brittle matrix to obtain the beneficial CMC properties such as high strength, fracture toughness and thermal shock resistance.

To guarantee fiber protection and weak fiber-matrix interface three methods are used for the production of MI Si/C composite (Figure 34. They are:

- Fiber coating with pyrolitic cabon (pyC) via CVI/CVD

  A thin layer or pyC is deposited on each fiber filament, resulting in C/SiC with individually embedded filaments.

- Fiber embedding in carbon matrix via multiple PIP

  Is widely used to manufacture short fiber-reinforced C/SiC break disks. The fiber bundles are impregnated with phenolic resin, that is then cured and pyrolized. After a number of repetitions of this cycle the fiber filaments are embedded in a dense carbon matrix resulting in a C/C like material. The coated fiber budles are then cut to defined lengths and mixed to phenolic resin and the CFRP preform. The resulting CMC has C/C bundles inbedded in the SiSiC matrix, but is still usually called C/SiC by manufacturers.

- In-situ fiber embedding in carbon matrix

  The manufacture of C/C-SiC materials and components will following.

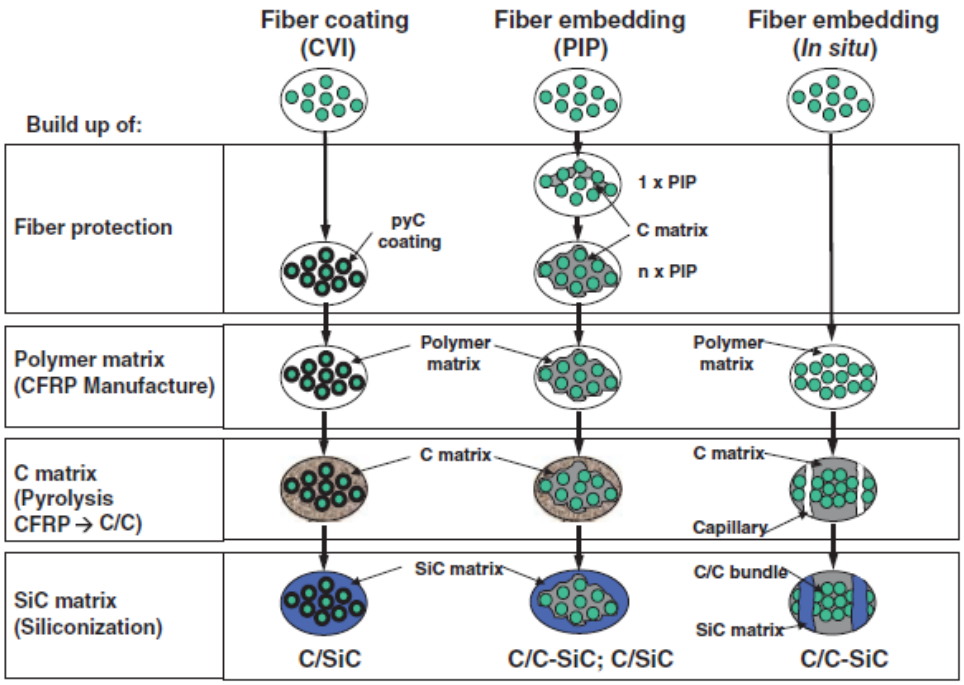


**Figure 34:** Schematic overview of industrially used methods for providing fiber protection and weak fiber–matrix interfaces in the MI process (DLR). Fiber coating with pyC interphase via CVI (left). Embedding C fibers in C matrix by multiple PIP (middle). In situ fiber embedding in C matrix (right). [22]

#### 2.1.1.3.1 Manufacture of CFRP Preforms

Commercially available C-fibers and polymer are used to manufacture CFRP preforms. The carbon yield of the polymer precursor has to be high, to ensure low mass loss and volume shrinkage during pyrolysis. Typically high temperature resins are used. Almost all C fibers can be used. For high performance, light structures typically 3 K and 6 K fibers. 1D layers or 2D fabrics are favored, but low cost 12 K, 24 K, up to 360 K fibers can be used for short fiber materials. For near net shape manufacture the common technologies are listed bellow and their main characteristics are described on Figure 35 [22]:

- Resin Trasfer Molding (RTM)
- Autoclave technique
- Warm technique
- Wet filament widing

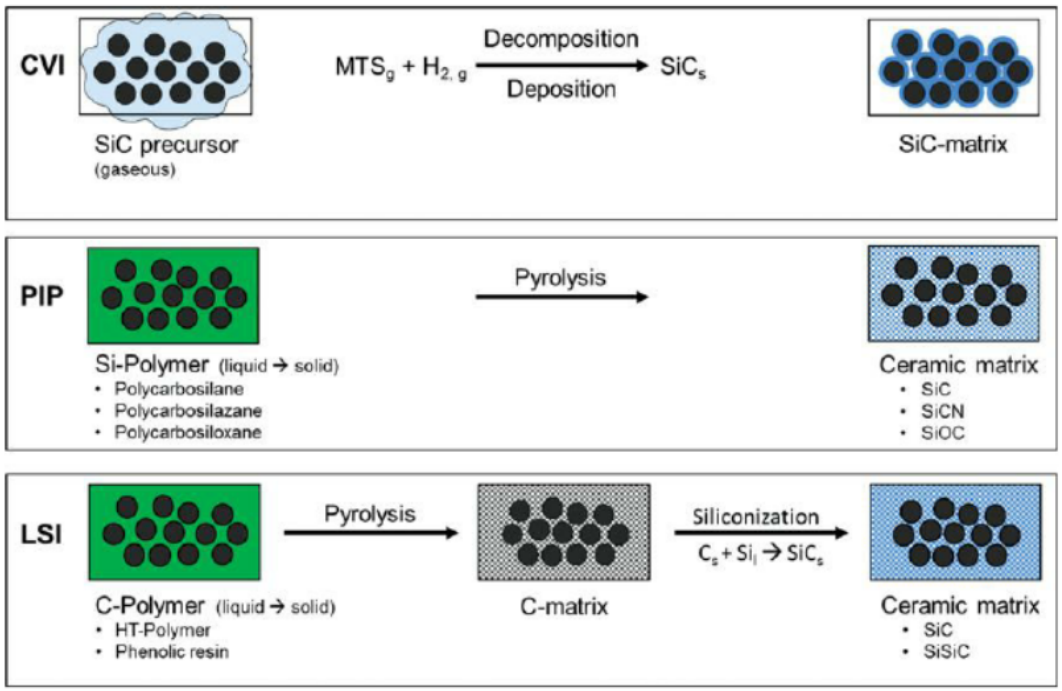


**Figure 35:** Manufacturing Methods for CFRP Preforms Used in the LSI Process [22]

#### 2.1.1.3.2 Pyrolysis of CFRP

On the second step, the CFRP is pyrolyzed at temperatures ranging from 900$^o$C to 2000$^o$C in non oxidazing atmosphere. A glassy C matrix is obtained as result. The mass

loss and volume contraction are, therefore, high. Up to 40 and% 60% respectively. The geometry of the carbon fibers remains mostly unchanged, as the material is thermally stable. This leads to the development of internal stresses, resulting in the formation of cracks.

The resulting C/C preform has open porosity from 10 to 30% characterized by a system of interconnected microcracks. Even then, they're safe to handling and machining.

The C/C microstructure will greatly influence the silicon infiltration and the properties of the CMC obtained. It is influenced by the fiber preform and fiber orientations, but the main factor is the strength of the Fiber Matrix Bonding (FMB). Materials with low FMB tend to suffer total peel off of the fiber filaments, resulting in the whole fiber bundle being infiltrated with Si during siliconization. The CMC will then have brittle behavior, close to those of monolithic ceramics.

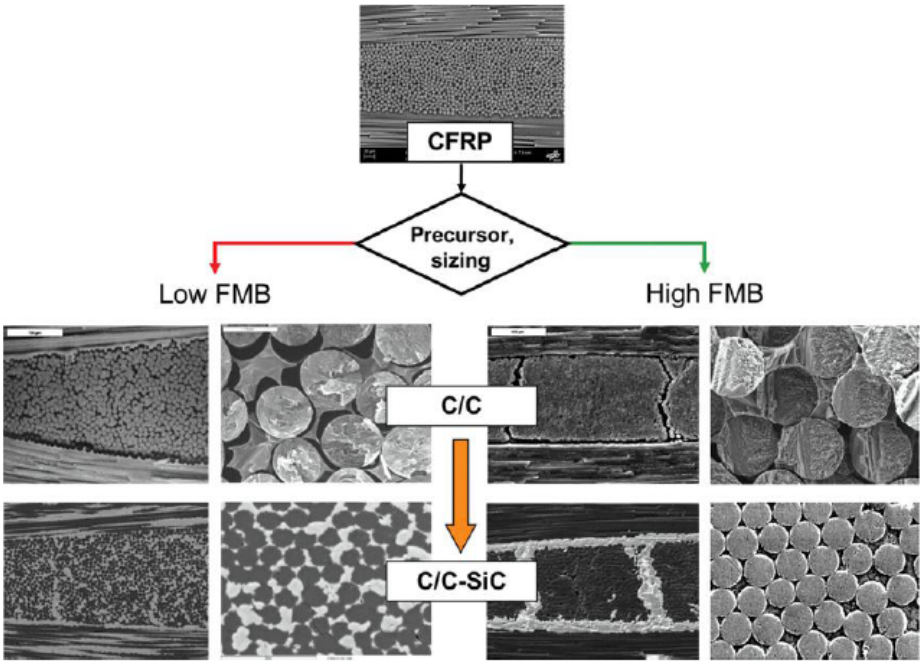


**Figure 36:** SEM figures showing the influence of the FMB strength in the CFRP preform on the microstructure of the C/C preform and the final C/C-SiC material. Low FMB with the matrix peeled off from the single fibers in the C/C preform and completely infiltrated fiber bundle after siliconization, with C fibers partially converted to SiC (left from top to bottom, DLR). High FMB, leading to a segmentation of the fiber bundle by microcracks, forming dense C/C bundles with the fibers embedded in C matrix, and C/C-SiC microstructure showing the microcracks filled with SiSiC matrix, but no infiltration of Si into the C/C bundle (right from top to bottom, DLR). [22]

The pyrolisis is the most crytical step of the LSI process. If the gases generated are not safely released, delaminations will occur due to the build up pressure, the damage

can be serious enough to result in total destruction of the component.

#### 2.1.1.3.3 Siliconization

In the last step the Si is infiltrated on the C/C preform by capillary forces. This step is performed used vacuum, such as to fill almost all open porosity with Si.

In in-situ fiber embedding a small amount of the carbon matrix and fibers are converted in SiC instead of only the C matrix.

### 2.1.1.4 Comparison of Manufacturing Methods

All methods here discussed are feasible for producing simple components as well as large, complex-shaped structures. Integral structures can be built up by manufacture of sub-components and in situ joining. In CVI no contraction of the matrix takes place during processing. Internal stresses and microcracks are induced only by the mismatch in thermal expansion between the C fiber and the SiC matrix. For this reason the manufacture of curved structures is less critical for CVI when compared with PIP and LSI. CVI also frequently usds 3D-woven fabrics, that reduces the risk of delamination.

LSI is specially critical when it comes to delamination, as the matrix contraction during pyrolysis results in anisotropic geometry changes and interlaminar stresses, with increased risk of delamination.

For CVI wall thickness is limited to around 30 mm, while for the PIP and LSI methods, there is no process related restriction to the component wall thickness.

Manufacturing time is highly dependent on size , geometry and complexity of the component produces for all methods. Large complex structures can have process times up to months.

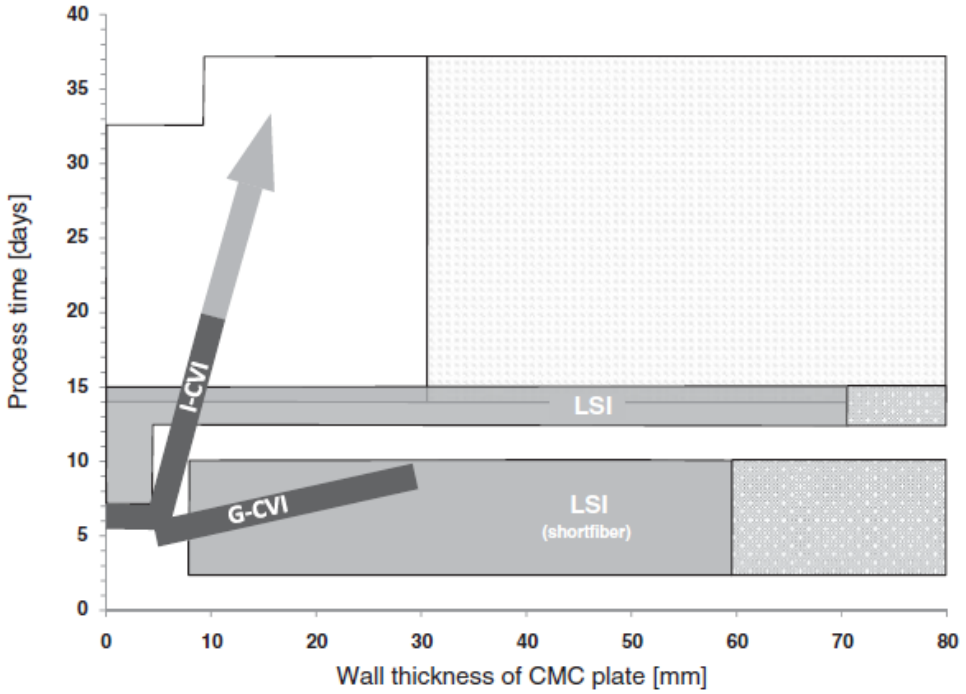


**Figure 37:** Typical process times for the manufacture of 2D fabric-based C/SiC plates (about 300 mm × 300 mm) dependent on the manufacturing method and wall thickness (DLR). The diagram is based on net process times, excluding dead times between the process steps and final machining. Maximum wall thicknesses manufactured to date are shown in dark color, whereas light color areas indicate prognosticated feasibilities. [22]

Using CVI a high temperature stable, stoichiometric and dense SiC matrix is achieved. PIP matrices are less stable due to inner porosity. SiSiC matrices, typical of LSI materials, are critical in long-terms applications and service temperatures above 1400°C due to melting of free Si.

### 2.1.2 Morphology

C/SiC and C-C/SiC CMCs are multiphase materials. They consist of C fibers, C fiber coating and $\beta$-SiC matrix. In case of LSI derived materials, there is also a C matrix and residual Si. For CVI in general a stoichiometric SiC matrix can be obtained. For PIP‘the matrix composition is dependent on the precursor chosen.

The morphology of the CMC material is defined by its manufacturing processes, including not only the method chosen, but also the conditions applied during manufacture, such as temperature and pressure, fiber orientations, precursors composition, between other factors.

The fiber architecture chosen for the material will influence not only it’s micro

structure, but also it's properties as the fiber positioning have a great influence on load resistance. On Figure 38 the most common fiber placements for C/SiC composites are presented.

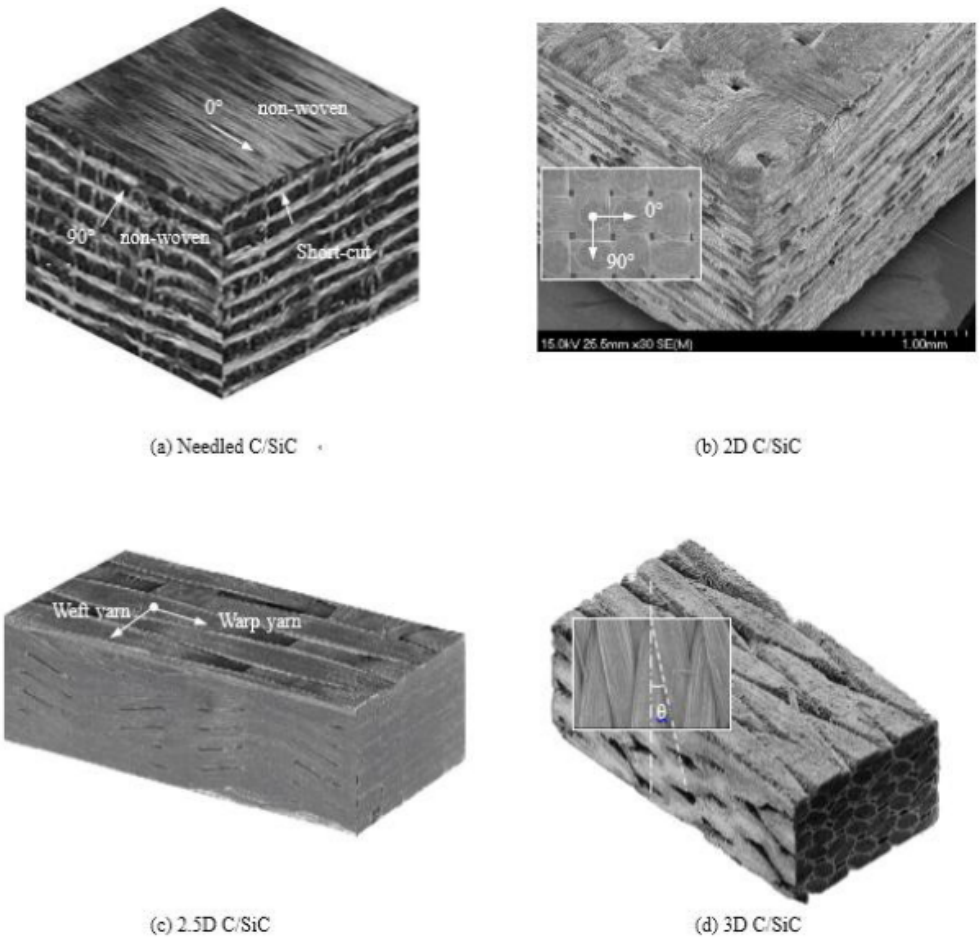


**Figure 38:** Three-dimensional presentations of fiber architectures in (a) needled C/SiC, (b) 2D C/SiC, (c) 2.5D C/SiC, and (d) 3D C/SiC composite specimens. [3]

Between the fiber and the matrix a interface is formed. This interface has also a important role on the mechanical behaviour of the composite. The crack of the interface and the separation between the interface and the fiber itself are important phenomena linked to the non-linear mechanical properties of the material, collaborating to delay the final failure by dissipating energy and making new paths for the load to be carried as the matrix progressively cracks and therefore loses rigidity. Crack deflection, fiber bridging and pull out of fibers are responsible for the quasi-ductile behaviour of CMC composites, the micrography of such phenomena are presented on Figure **??**

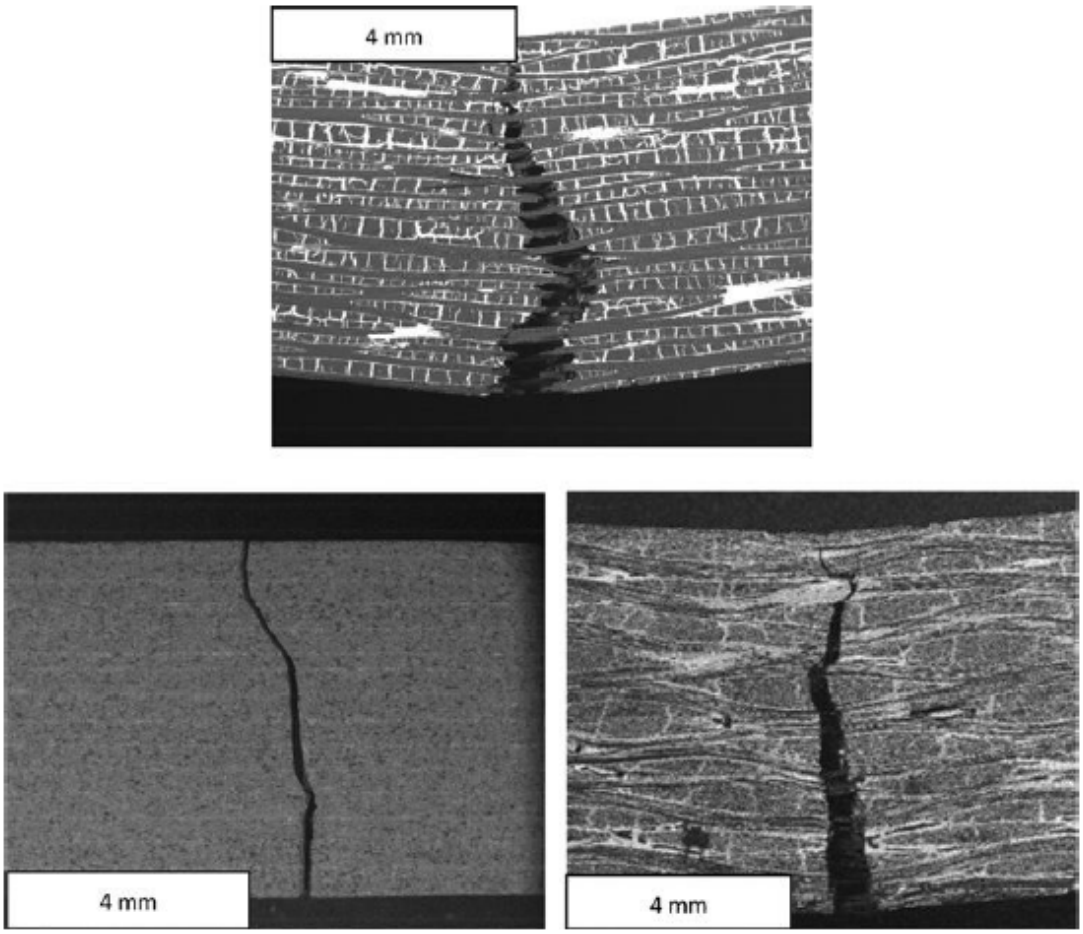


**Figure 39:** SEM of bending samples, showing the typical, quasi-ductile fracture behavior of C/C-SiC XB (top), characterized by crack deflection, fiber bridging and pull out of fibers and C/C bundles. Catastrophic failure of bulk SiSiC (bottom left) and C/C-SiC XD with high SiC content and almost all the C fibers converted to SiC (bottom right, all figures DLR). [22]

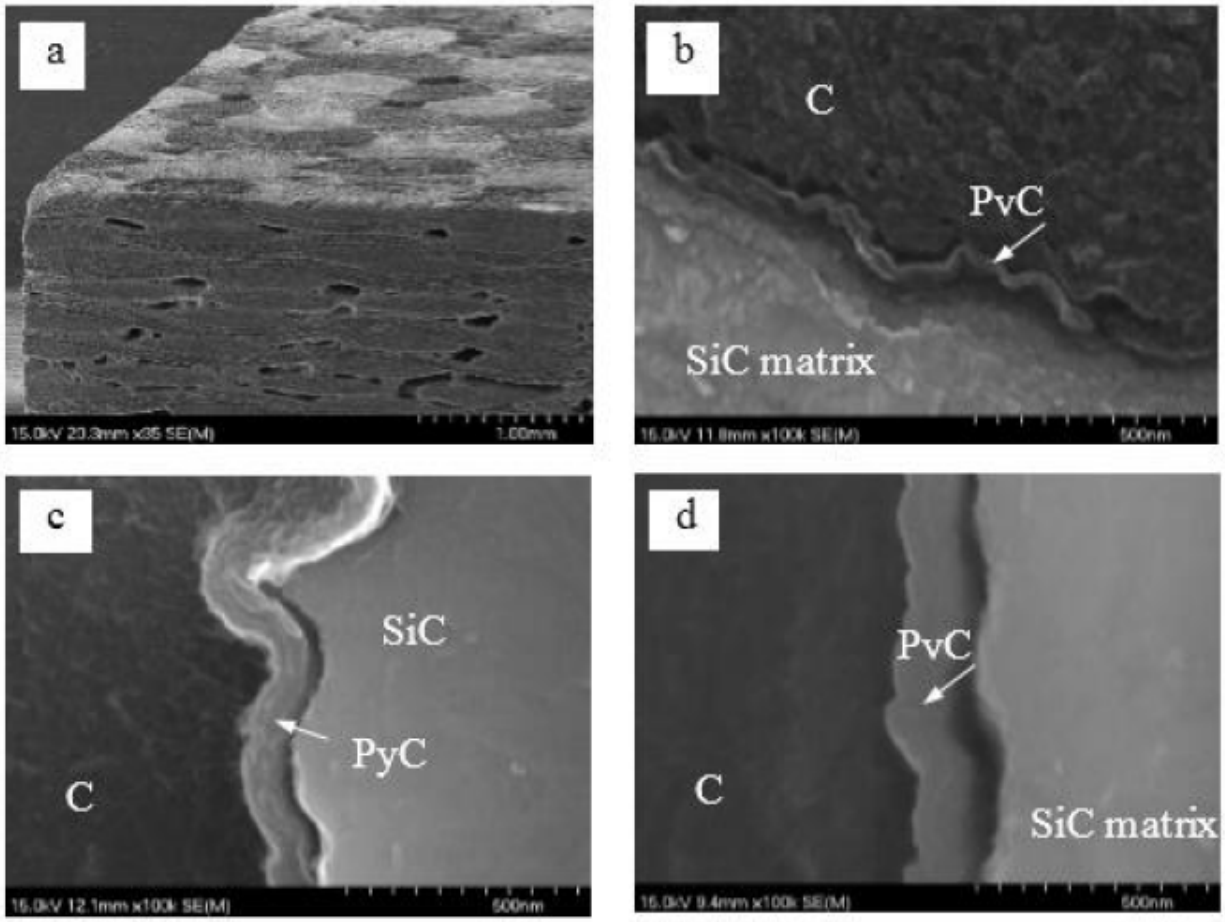


**Figure 40:** Micrographs showing (a) the fiber architectures in the uncoated 2D C/SiC composites and the thickness of PyC interphase between carbon fiber and SiC matrix, (b) 40 nm in S1, (c) 90 nm in S2 and (d) 140 nm in S3. [3]

In terms of C content, CVI and PIP offer moderate C (C fiber and pyC fiber coating) content and high SiC percentage (42 to 58% volume of C 35 to 50% volume of SiC). On the other side, LSI based materials and high fiber contents are characterized by higher C content of about 75 % volume and low SiC content, 15 to 20 %. This difference comes from the build up process of the SiC matrix. On the MI process, as the C matrix is built up in a first step in order to embed and protect the fibers, whith only part of the C matrix being converted to SiC, large amounts of residual C matrix remains on the C/C-SiC or C/SiC material (15 to 30 % in volume) [22].

Another relevant factor about the microstructure of those materials is the existence of porosity. Residual open porosity depends on the manufacturing process. For CVI derived C/SiC materials, residual open porosity is 8-12% in general, but can go up to 15 %, due to the competition between surface deposition and in-depth infiltration mechanisms. Matrix build up on PIP process is stopped at residual open porosity of 6-10% due to economical reasons. The MI process in other hard can achieve porosities

of 1-4%, presenting a relatively dense C/SiC and C/C-SiC material.

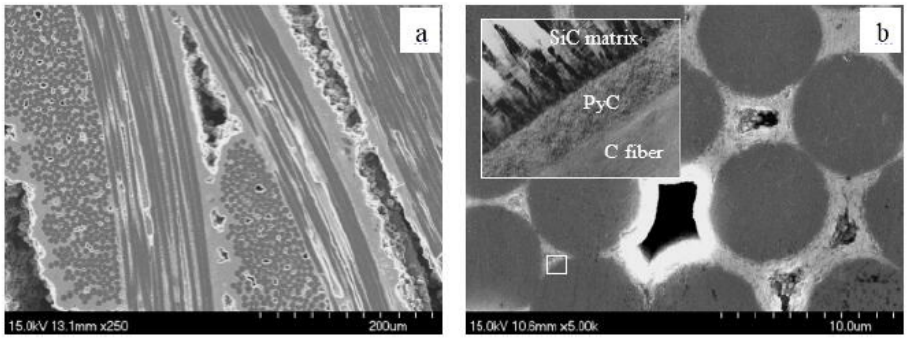


**Figure 41:** Micrographs showing porosity present in the virgin 2D C/SiC, (a) inter-bundle pores and (b) inter-filament pores. The TEM observation indicating the constituent microstructures of carbon fiber, PyC interphase and CVI-SiC matrix. [3]

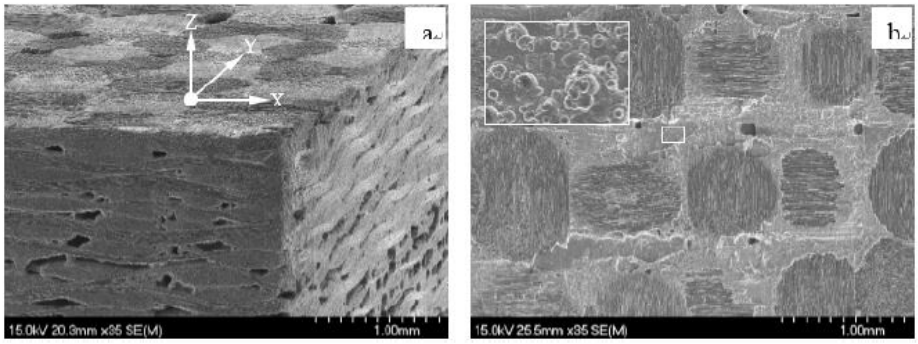


**Figure 42:** SEM micrographs showing the fiber architectures of the 2D C/SiC composite prepared by CVI, (a) 3D view and (b) top view. The magnified observation indicating the morphology of the CVI-SiC matrix. [3]

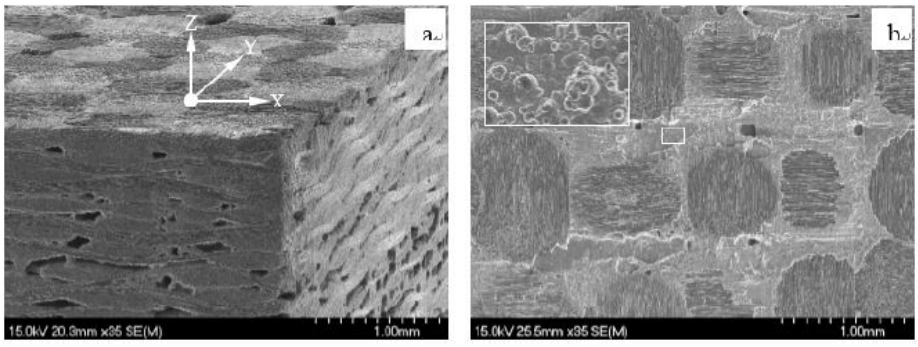


**Figure 43:** SEM figures of typical fracture surfaces of MI-based C/C-SiC XB, showing pull out of C/C bundles (top, DLR) and PIP-based C/SiC materials (bottom left, COIC) with single fiber pull out (bottom right, COIC). [22]

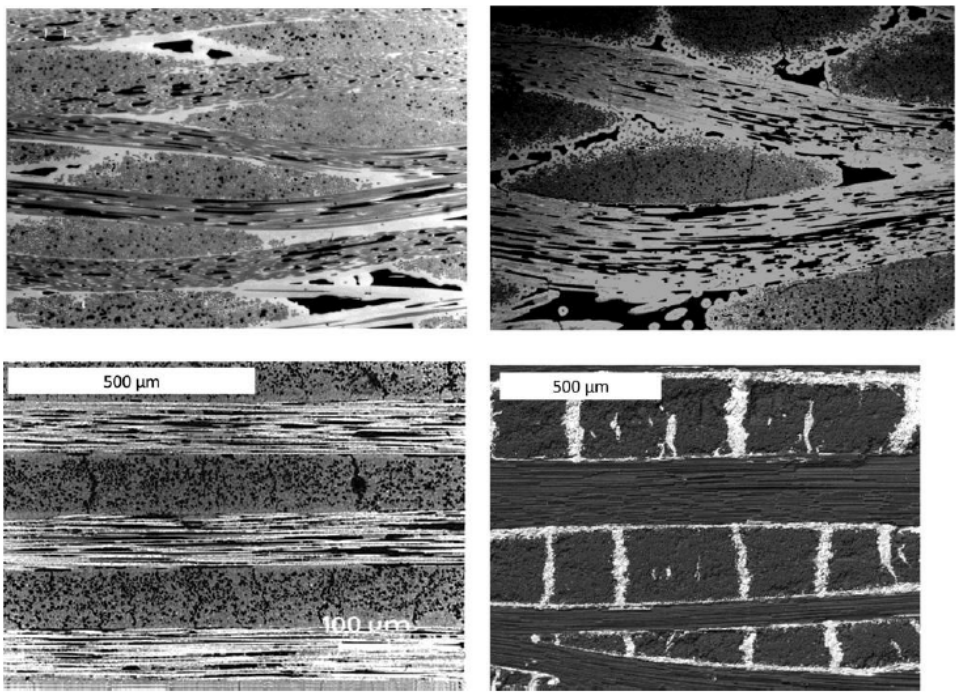


**Figure 44:** Typical microstructures of C fiber-reinforced SiC based on 2D fiber preforms. C/SiC materials manufactured via CVI (Keraman®, top left, MT; Sepcarbinox®, top right, Herakles) with C fiber filaments (dark gray) embedded in the SiC matrix (light gray). Porosity is shown in black. C/SiC material based on PIP and 0∘/90∘ cross-ply laminate (SICARBON®, bottom left, Astrium ST/EADS IW), showing single C fibers (dark gray) embedded in SiC matrix (light gray). LSI-based C/C-SiC XB (bottom right, DLR) showing dense C/C bundles (dark gray) embedded in SiSiC matrix (light gray).. [22]

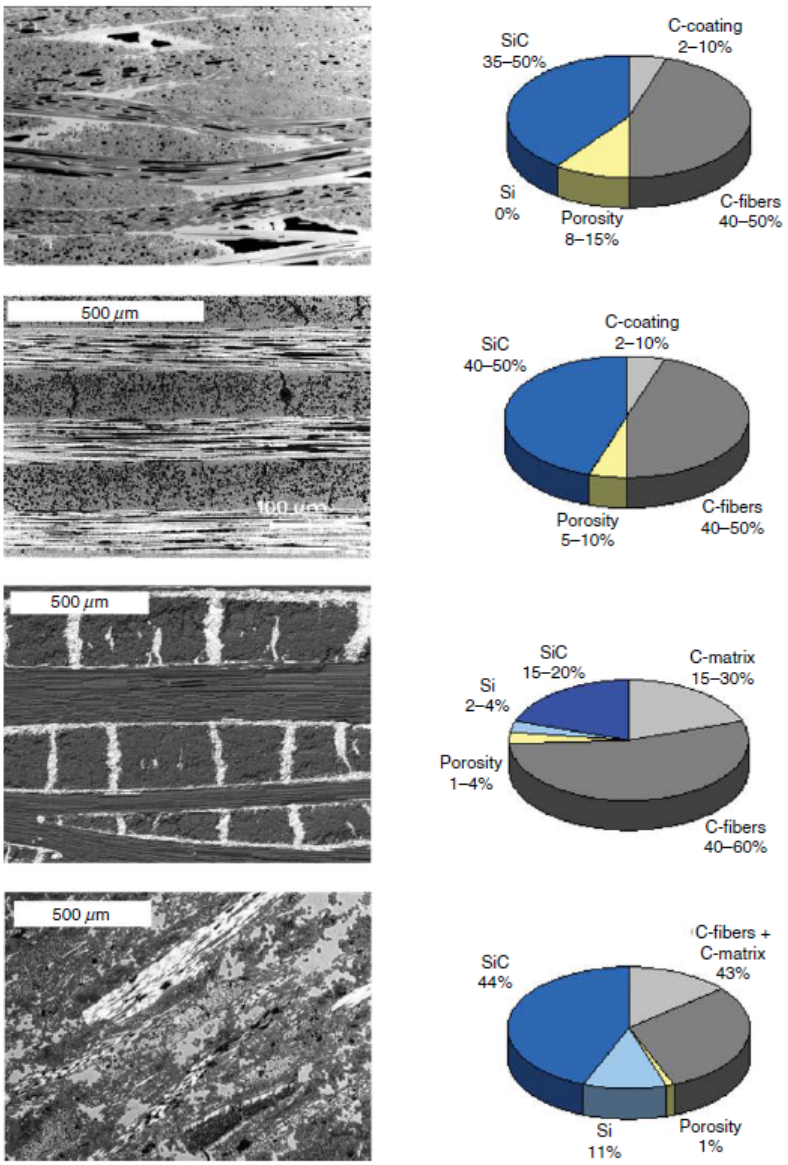


**Figure 45:** Typical microstructures and phase compositions (in vol.%) of C/SiC materials based on different manufacturing methods. From top to bottom: CVI-derived C/SiC materials based on 2D fiber fabrics (Keraman®, MT), PIP-derived SICARBON® (Astrium ST/EADS IW) based on UD cross-ply laminate, LSI-derived C/C-SiC based on 2D fiber fabrics (C/C-SiC XB, DLR) and typical LSI-derived C/SiC (SIGRASIC® 6010 GNJ, SGL) based on randomly oriented, short fibers. [22]

## 2.2 General Damage Mechanisms and Failure Modes

### 2.2.1 In-plane load damage behaviour

The in-plane failure of composites is characterized by the 3 failure modes represented in Figure 46.

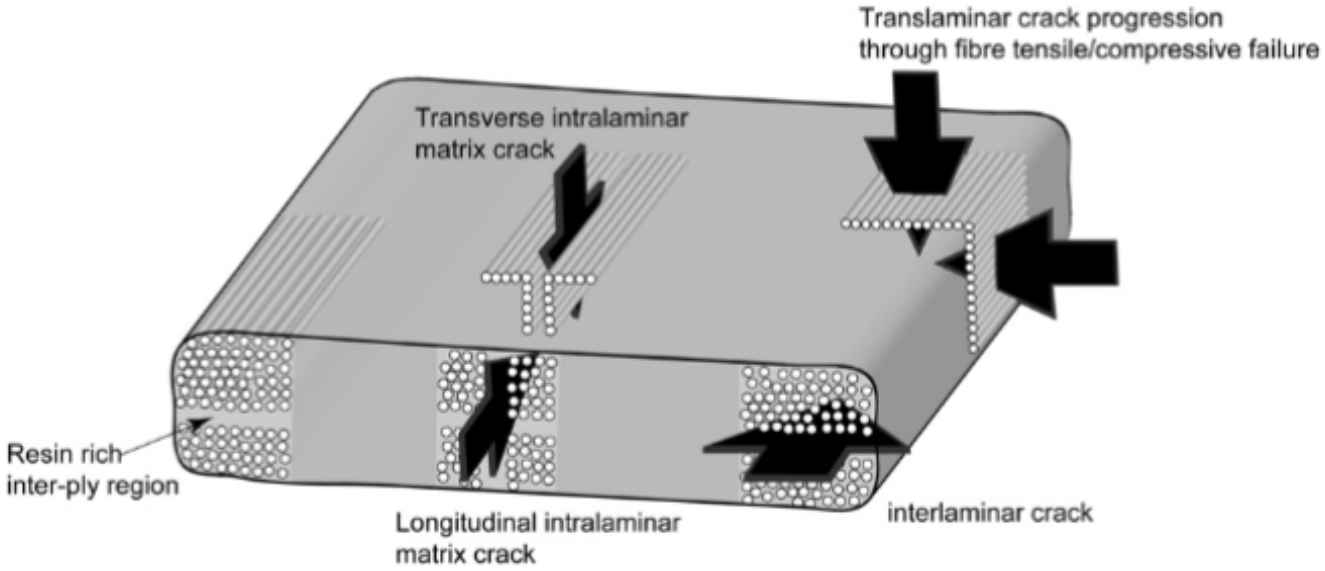


**Figure 46:** Overview of ply-level failure modes [27]

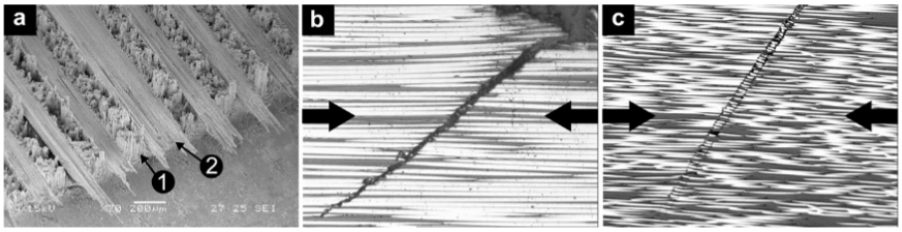


**Figure 47:** Failure mechanisms in FRP: (a) fracture surface including (1) translaminar fibre tensile failure and (2) longitudinal matrix failure, (b) shear driven fibre compressive failure (the arrows indicate the loading direction), (c)fibre kinking (the arrows indicate the loading direction) [27]

Those failure modes are:

- Translaminar fiber tensile failure

  This failure mode is characterized by great energy dissipation as is the main interest of this thesis. As the tension in applied on the material, micro-mechanisms

such as fiber de-bonding and pull-out will prevent brittle failure and give to the CMC composite the mechanical behaviour needed for it to be used in structural components.

- Translaminar fiber compressive failure

  Under compressive loads the fibers can fail either by shear driven fibre failure or fibre kinking. The mechanism will depend on the presence of shear stresses. As the damage progresses, the relative motion of the crack faces will always transition to the development of fibre kinking.

- Intralaminar matrix failure

  This failure mode consists in failure of the matrix parallel to the fiber. The toughness of this mode is equivalent to the one of interlaminar matrix failure, as it also does not experiment the energy dissipation of the micro-mechanisms related to the fibers.

For the purpose of this thesis, the tensile behaviour will be analyzed. Meaning that the predominant failure mode will be Translaminar fiber tensile failure.

When subjected to tensile strains the macroscopic behaviour of CMC materials is highly non-linear. That behaviour is linked to the microscopic mechanisms of failure.

On Figure 48 we can see a representation of different damage mechanisms that can occur on CMC around a notch when traction is imposed [1]. The way that it propagates after the start of the crack depends on the microscopic damage that are occurring on the material. The behaviour of the composites under tension is highly non-linear.

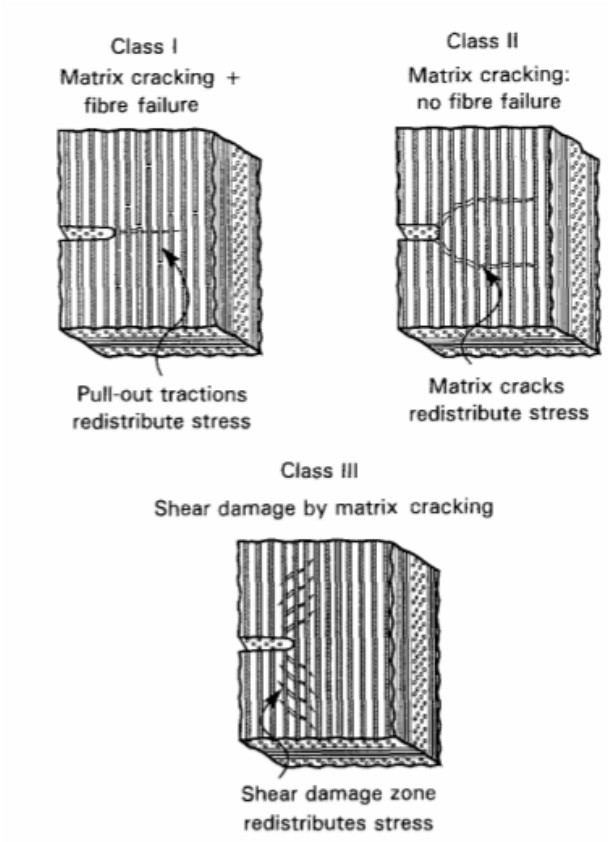


**Figure 48:** Three prevalent damage mechanisms occurring around notches in CMCs. Each mechanism allows stress redistribution by a combination of matrix cracking and fibre pull-out. [1]

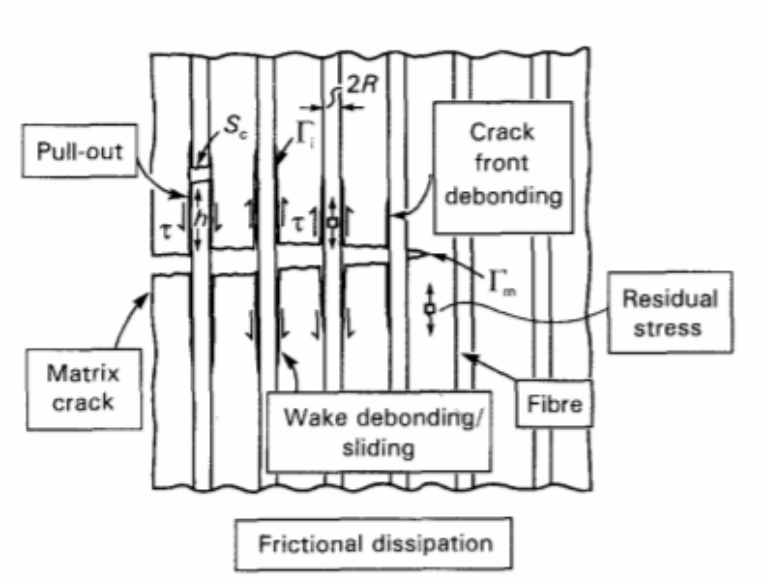


**Figure 49:** The fundamental mechanisms that operate in CMCs as a crack extends through the matrix. [1]

The main mechanisms that create the inelastic strains, and therefore, the non-

linear behaviour on CMCs are matrix cracks, interface cracking, fibre de-bonding, sliding and pull out [1] [27] [22].

Those microscopic phenomena can be seen on Figure 49

Those mechanisms can combine in different failure modes. For 2D woven SiC/Sic composite, for example, 5 modes can be obseved [24]:

- Mode 1: transverse cracking in the transverse tow, with debonding at the tow boundary;
- Mode 2: transverse cracking and matrix cracking with perfect fiber/matrix bonding and fracture
- Mode 3: transverse cracking and matrix cracking with fiber/matrix debonding and sliding in the longitudinal tow;
- Mode 4: matrix cracking with perfect fiber/matrix bonding and fracture of fibers occurs in the longitudinal tow;
- Mode 5: matrix cracking and fiber/matrix interface debonding and sliding in the longitudinal tow.

The micro-cracking of the matrix generates a loss of stiffness [4]. If the interface between the fiber and the matrix is weak enough, crack propagation will occur between the matrix and the fiber, this mechanisms avoids early failure of the composite as the debonding allows fibre-matrix sliding with friction to occur, absorbing energy. The failure is further delayed by other mechanisms that absorb energy such as the fibre pull-out and out of matrix crack-plane fibre fracture [4]. All those mechanisms combined are responsible for the non-linear behaviour that can be observed on CMC materials.

The progression of the damage Class I of Figure 48 can be observed on Figure 50. As the figure shows, the damage starts with a few matrix cracking, evolving with more cracks, then cracking on the interface between the fiber and the matrix, causing fiber sliding, then the fibers start to suffer rupture, a process called fiber pull-out. Eventually all those micro damages will result into the final rupture of the material.

On Figure 51 we can see an schematic of the stress x strain curve of a generic CMC material with its evolution in function of the microscopic damage mechanisms that are actuating [4].

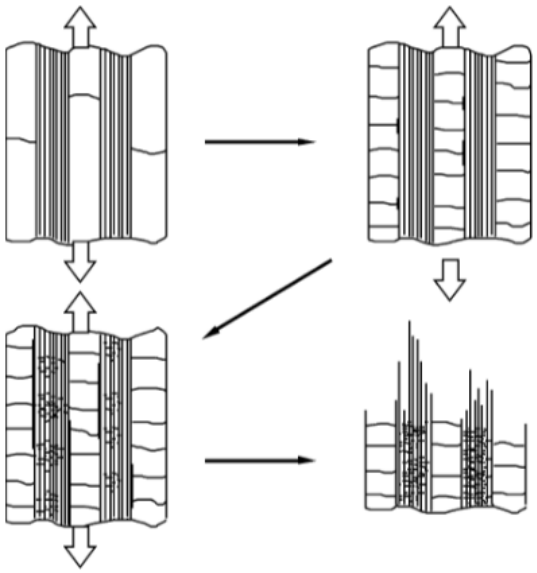

**Figure 50:** Damage mechanisms in CMCs [4]

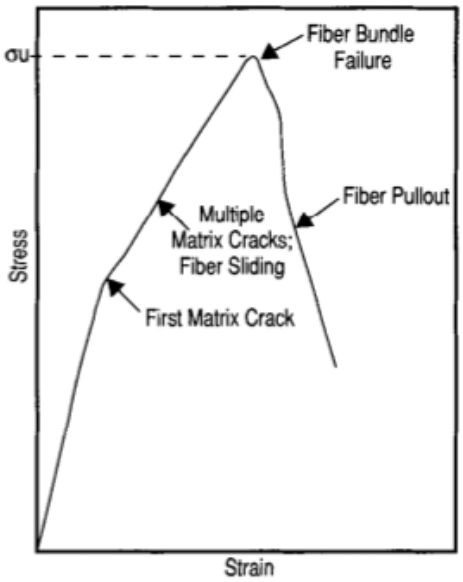


**Figure 51:** A schematic diagram of fiber-reinforced composite stress-strain response and associated damage processes. [23]

## 2.3 Out of Plane Behaviour

Ceramic matrix composites are frequently used in aerospace applications, being specially advantageous for applications that involve working under high temperatures.

In this kind of utilization, substantial shear stresses can arise, specially around stress concentrators such as notchs and holes, even if the load applied is tensile or com-

pressive.

In oxidizing environment, such as the ones encountered by hot structures while working under high temperatures, early shear failure may happen, as oxidation can degrade shear properties by damaging the carbon fibers or the interfaces between the fibers and the matrix. [40].

It is important, therefore, to understand out of plane behaviour of those composites, investigating its interlaminar shear strength and the mechanisms that can lead to delamination on CMC.

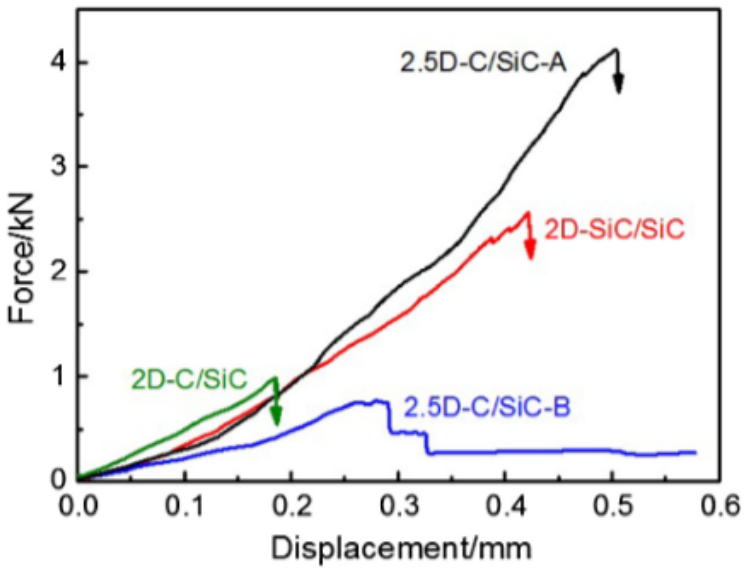


**Figure 52:** Displacement–load curves for the three kinds of composites

An example of the behaviour for interlaminar shear strength can be seen on Figure 52 [40]. It can be observed that the curve demonstrates a brittle behaviour of the CMC when resisting this kind of loading.

In fact, micro images of the surface of delaminated specimens (figure 53) shows that the failure occurs by matrix cracking and debonding of the matrix/fiber interfaces.

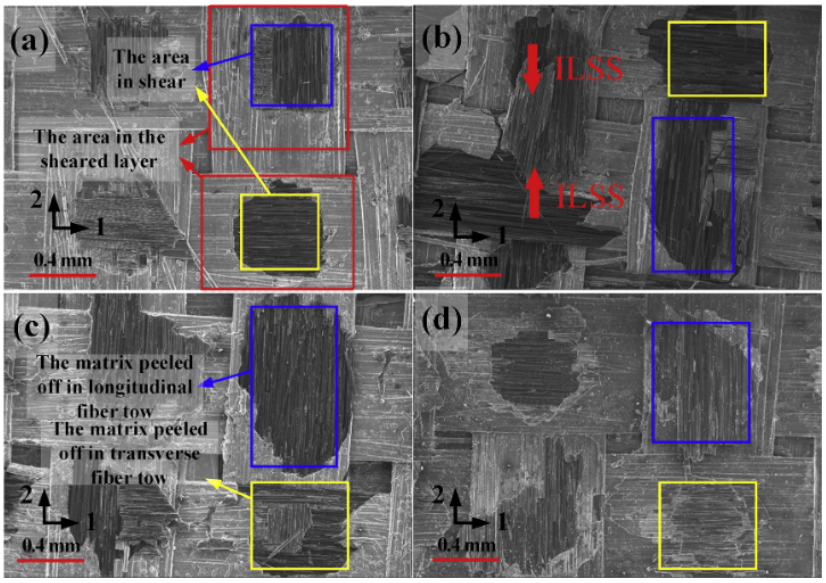


**Figure 53:** Failure morphologies of Double Notch Shear samples. (a) S-RT, (b) S-7, (c) S-10, (d) S-13. [5]

The evolution of the damage, with propagation of the matrix cracking and the interface cracking can be seen on Figure 54. This will be one of the loading/failure conditions to be simulated in this thesis.

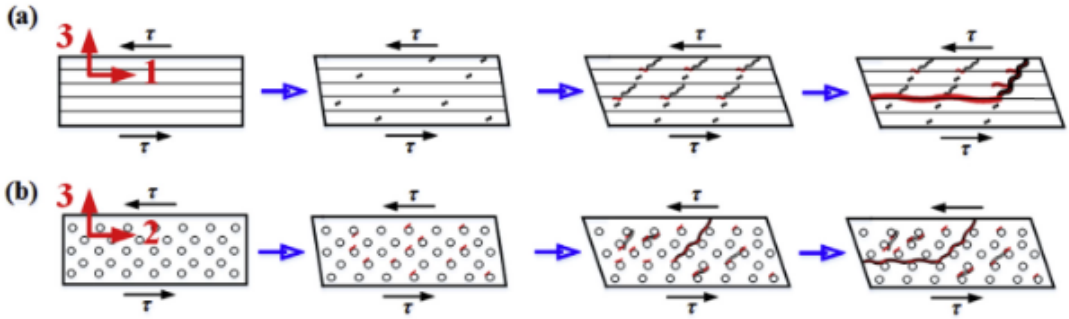


**Figure 54:** Matrix cracking evolution under interlaminar shear stress with respect to (a) longitudinal fiber tow, (b) transverse fiber tow. Red color denotes interface cracking and black color denotes matrix cracking. [5]

## 2.4 Translaminar Fracture Toughness Characterization

The main focus of this series is the simulation of a test to determinate the Translaminar Fracture Toughness of the C/SiC CMC. For this reason, it is important to understand why the compact tension test was chosen between the tests that are available in the literature for this purpose.

On Figure 55 some specimens found in the literature can be seen, they are:

- Compact tension

  The Compact Tension test is probably the most widely used for determination of translaminar fracture toughness in composites. It has been used on carbon/epoxy, C/C, carbon/PEEK and boron/aluminum laminates [27].

  The most frequent approach is to use the critical stress intensity factor, as determined by the ASTM E399 for metallic materials [15].

  The crack growth in this test is stable. This stability is important to determinate the changes in critical strain release rate with the evolution of the damage.

- Extended compact tension

  The extend compact tension test also originates from metallic material characterization procedures. It was used to avoid undesirable failure modes encountered during some 3 points bending and compact tension tests [27]. On the CT case, cracks growth perpendicular to the desirable direction.

  ASTM E1922-04, an extension of ASTM E1922, is used, as it includes pultruded thick-section composites, but has the limitation of covering fracture toughness only for damage initiation.

  The crack growth in this type of test is also stable.

- Centre notched tension/compression

  This type of experiment has been used to derive fracture toughness for carbon/epoxy, carbon/bismaleimide and boron/aluminum [27]. I has also been used for compressive fracture toughness determination by reverting the load configuration [27].

  The crack growth in this experiments are not stable.

- Four/Three point bend

  The four/three point bend is the last test with stable crack growth.

  It has been used to characterize translaminar toughness of composites. It also originates from an ASTM standard for metals.

- Single edge notched tension

  Single edge notched tension has been used to characterise carbon/epoxy systems as well as e-glass, Kevlar and boron/epoxy.

  The crack growth is not stable.

- Double edge notched tension

  Double edge notched tension has been used to characterise carbon/epoxy systems as well as e-glass, Kevlar and boron/epoxy and glass/epoxy systems.

  The crack growth is not stable.

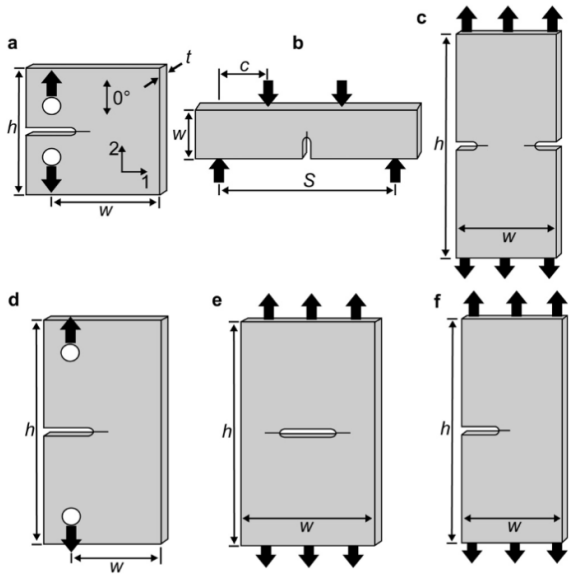


**Figure 55:** Specimen configurations used for translaminar fracture toughness measurement: (a) compact tension (has also been used for compressive tests), (b) four-point bend (three point bend configuration also possible but not shown), (c) double edge notched tension, (d) extended compact tension, (e) centre notched tension (has also been used for compressive tests), (f) single edge notched tension.M.J. Laffan et al. [27]

### 2.4.1 The CT test

The interlaminar fracture toughness of CMC materials in the Am3ac2a project is currently being performed by using End Notched Flexure and Double Cantilever Beam, but this thesis wants to find a test suitable for translaminar fracture toughness.

We want:

1. Controlled crack growth to study fracture mechanisms
2. Possibility to perform the test on thin laminates and small amount of materials

The choice goes towards CT specimens.

The CT test is the most widely spread test for composite materials, has been used in ceramic matrix composites before with success and has stable crack growth. It does not have limitations of providing the fracture toughness just for crack initiation.

There are a number of studies published on fracture toughness of S/SiC materials using the CT test and [25] [38] [37].

Furthermore, CT tests were recently utilized on Politecnico di Milano to characterize C/C CMC materials [14], meaning that the existing know-how of the manufacturing and machining of CMC specimen for the other CT exists. Furthermore, the knowledge gathered about the modelling and simulation of CMC materials behaviour under tension is an important starting point to develop a reliable model for characterization of the C/SiC composite.

For the CT test, Translaminar Fracture Toughness can be derived by first calculating the critical stress intensity factor ($K_{Ic}$) as recommended by ASTM E399 [15] where $P_c$ is the critical load causing crack extension,$t$ and $w$ are defined on Figure 55, $a$ is the crack length and *f(a/w)* is a correction factor. It is not always totally accurate for composites, as it was designed for isotropic metallic materials. The critical strain $G_{Ic}$ can be derived from the critical stress intensity factor. Equations 1, 3 and 2 show the expressions for such calculations.

$$K_{Ic} = \frac{P_c}{t\sqrt{w}} f(\frac{a}{w}) \tag{1}$$

$$G_{Ic} = \frac{K_{Ic}^2}{\sqrt{2E_{11}E_{22}}} \sqrt{\sqrt{\frac{E_{11}}{E_{22}}} + \frac{E_{11}}{2G_{12}} - \nu_{12}} \tag{2}$$

$$f(a/w) = \frac{2 + a/w}{(1 - a/w)^{1}.5} [0.886 + 4.64(a/w) - 13.32(a/w)^2 + 14.72(a/w)^3 - 5.6(a/w)^4] \tag{3}$$

# 3 Design of CT test for toughness characterization

## 3.1 CT Test

In order to study damage tolerance and the evolution of failure modes for the CMC composite utilized in this project, a CT test was chosen. The results of the simulation will be compared with experimental results. The project aims to develop a reliable model of the material, allowing for later scaling of the properties for engineering use.

There is no standard for CT tests for composites, therefore the standardized specimen for fracture toughness tests determined by ASTM E399 for metallic materials [15] was used as reference for this project, but not fully respected. For this work, the CT specimen presented on Figure 56 was used, as the presented geometry was used previously for simulation of a C/C CMC with success [14].

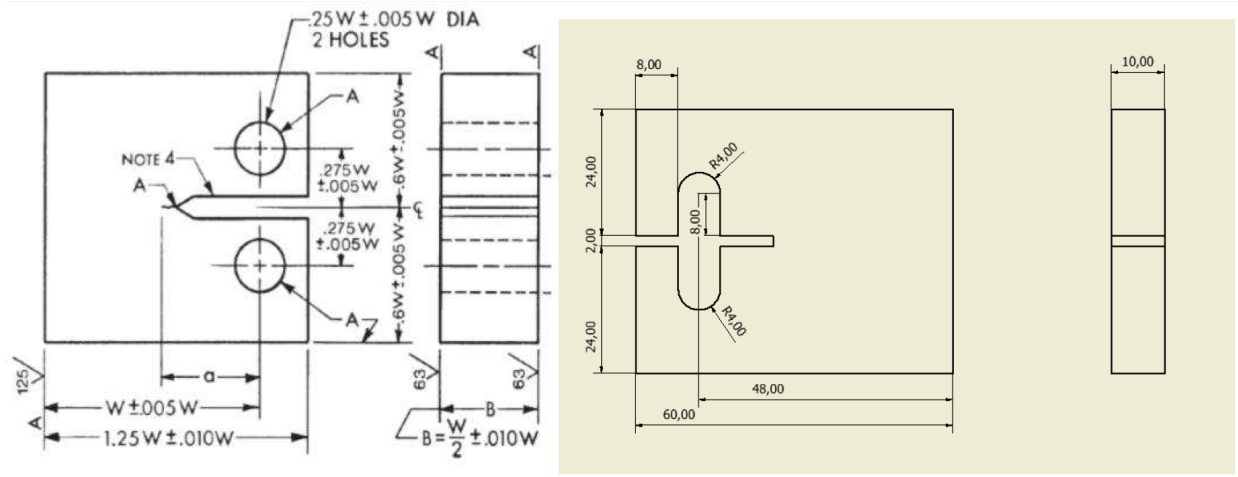


**Figure 56:** CT Specimen according to ASTM E399 standard (left) and chosen specimen [14] (right)

## 3.2 Modelling

The modelling of this work was fully performed using ABAQUS simulation environment.

The first step of the simulation procedure was to model the CT specimen geometry on ABAQUS. This was achieved by modelling two different parts; one for the body of the CT specimen ("TOP_AND_BOTTOM") and a second part for the cohesive elements ("COHESIVE"). The cohesive elements are specially important in this simulation and they are what allows the determination of the crack initiation and propagation with the highly nonlinear behaviour observed in CMC composites.

It must be noted that ABAQUS does not impose units or have unit options, its left to the user to apply consistent units throughout the work. In this thesis [mm], [N], [MPa] were used.

| Quantity | SI | SI (mm) | US Unit (ft) | US Unit (inch) |
|---|---|---|---|---|
| Length | m | mm | ft | in |
| Force | N | N | lbf | lbf |
| Mass | kg | tonne ($10^3$ kg) | slug | lbf $s^2$/in |
| Time | s | s | s | s |
| Stress | Pa ($N/m^2$) | MPa ($N/mm^2$) | $lbf/ft^2$ | psi ($lbf/in^2$) |
| Energy | J | mJ ($10^{-3}$ J) | ft lbf | in lbf |
| Density | $kg/m^3$ | $tonne/mm^3$ | $slug/ft^3$ | lbf $s^2/in^4$ |

**Figure 57:** Consistent ABAQUS units

### 3.2.1 Cohesive elements

The cohesive elements were used to determinate where the crack would start during the CT test. The type of cohesive element chosen was traction separation, as it was the adequate for a Fracture Strength test such as the one simulated From the ABAQUS documentation we have:

> "You may use the cohesive elements in areas of the model where you expect cracks to develop. However, the model need not have any crack to begin with. In fact, the precise locations (among all areas modeled with cohesive elements) where cracks initiate, as well as the evolution characteristics of such cracks, are determined as part of the solution. The cracks are restricted to propagate along the layer of cohesive elements and will not deflect into the surrounding material.
>
> In three-dimensional problems the traction-separation-based model assumes three components of separation—one normal to the interface and two parallel to it; and the corresponding stress components are assumed to be active at a material point. In two-dimensional problems the traction-separation-based model assumes two components of separation—one normal to the interface and the other parallel to it; and the corresponding stress components are assumed to be active at a material point." [10]

We can see a representation of a cohesive element on Figure 58

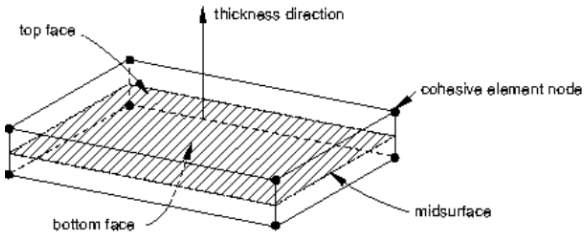


**Figure 58:** Spatial representation of a three-dimensional cohesive element [14] (right)

The type of cohesive element used was COH3D8.

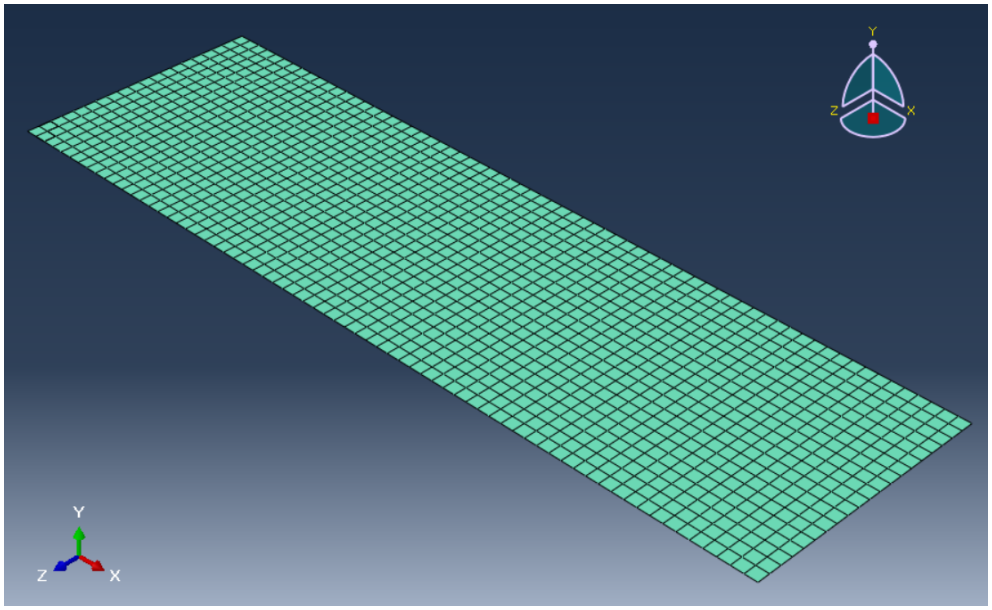


**Figure 59:** Cohesive part ("COHESIVE")

### 3.2.2 Solid elements

For the body of the CT specimen solid elements of the type C3D8 were utilized. A initial attempt was made with C3D8R (reduced integration) elements to decrease simulation time, but was abandoned as the simulation would crash, most probably for hourglass problems to which this kind of element is very prone [11].

Using the C3D8 all simulations were able to continue until the end of the imposed displacement conditions.

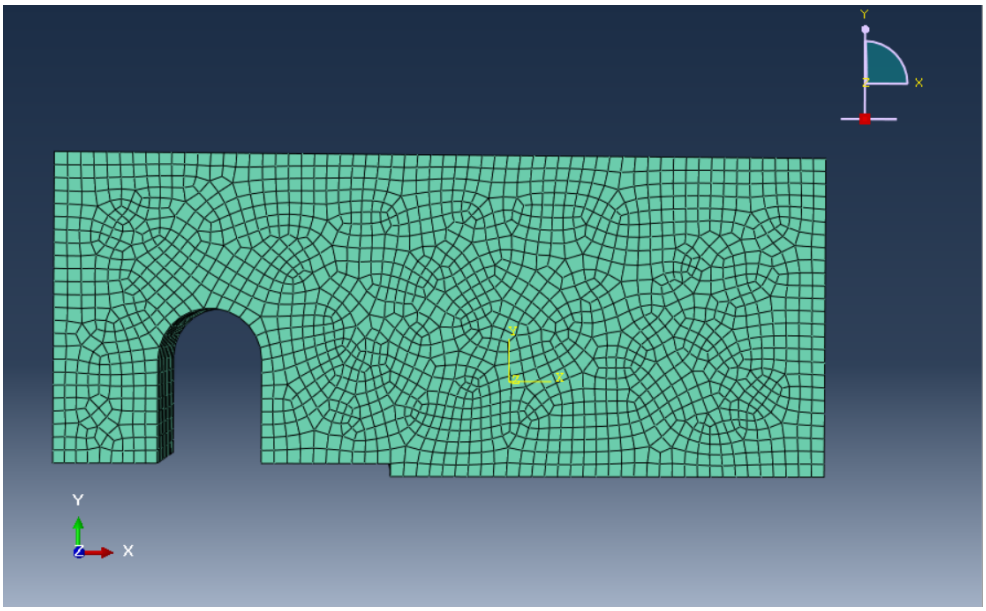


**Figure 60:** Solid elements Part("TOP_AND_BOTTOM")

### 3.2.3 Axis Orientation

On the Figure 61 the orientation of the Axis on the model can be seen. Direction 1 is referent to the X Axis displayed on the image, Direction 2 to the Y axis and Direction 3 to the Z Axis. It's important to have this information in mind in order to correctly read the results of the simulation.

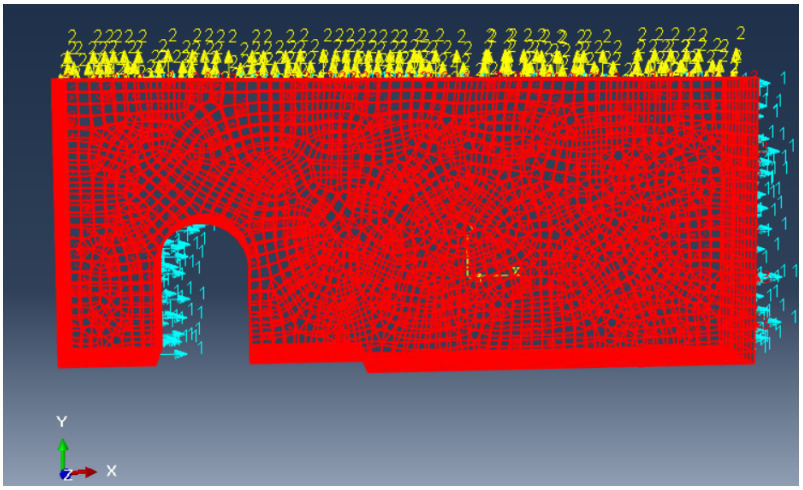


**Figure 61:** Axis Orientation

### 3.2.4 Constraints

The two types of constraints utilized were Tie Constraints and Rigid Body.

A Tie constraint ties two separate surfaces together imposing no movement between them [12].

A rigid body constraint contrains the motion of regions of the assembly to the motion of a reference point, they are used in this simulation to impose boundary conditions in a later step [12] .

The constraints imposed to the parts were:

- Tie Constraint 1 ("BOT TO COH") (Figure 62) - connects the top surface of the bottom part to the bottom surface of the cohesive part

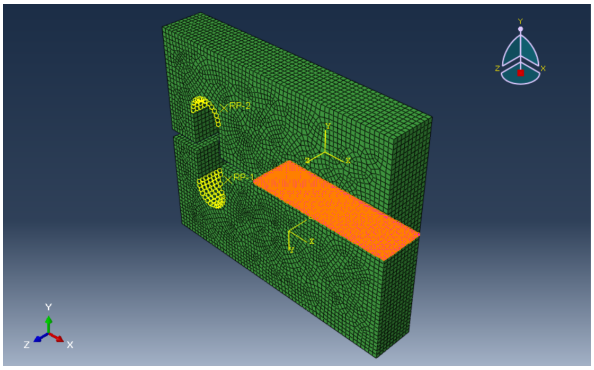

**Figure 62:** Tie Constraint 1 ("BOT TO COH")

- Tie Constraint 2 ("TOP TO COH") (Figure 63) - connects the bottom surface of the top part to the top surface of the cohesive part

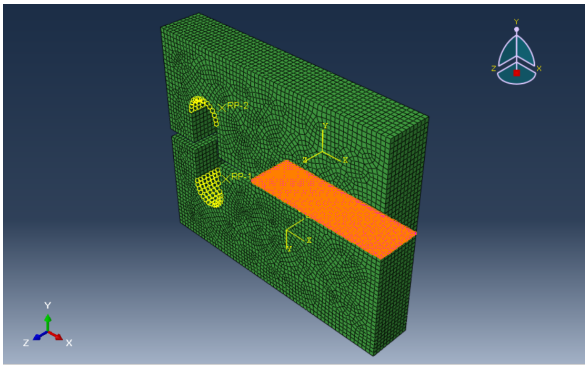

**Figure 63:** Tie Constraint 2 ("TOP TO COH")

- Rigid Body 1 (Figure 64) - creates a rigid body in the bottom part, for posterior application of boundary conditions. It's reference point is on the center of the circular section (Reference Point (RP) 1), in the mid point of the Z length of the body.

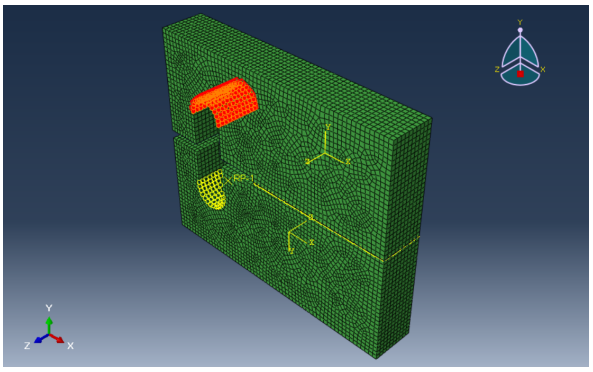

**Figure 64:** Rigid Body 1

- Rigid Body 2 (Figure 65) - creates a rigid body in the top part, for posterior application of boundary conditions. It's reference point is on the center of the circular section (RP 2) , in the mid point of the Z length of the body.

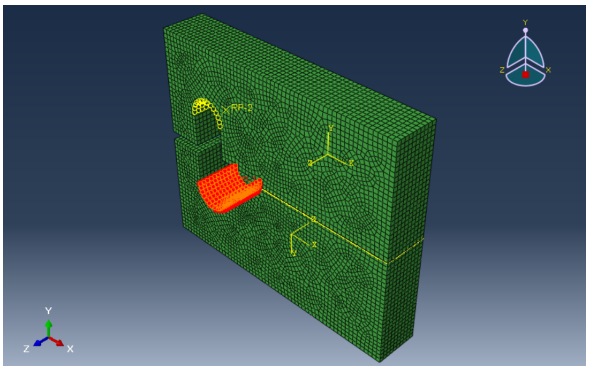

**Figure 65:** Rigid Body 2

### 3.2.5 Boundary Conditions

The boundary conditions of this model were all applied to the Reference Points defined in the constraints.

- Pinned in RP 1
- No Spin around Y Axis in RP 1
- Displacement of 1 [ mm ] in Y applied in RP 2
- Zero displacement in X and Z axis applied in RP 2

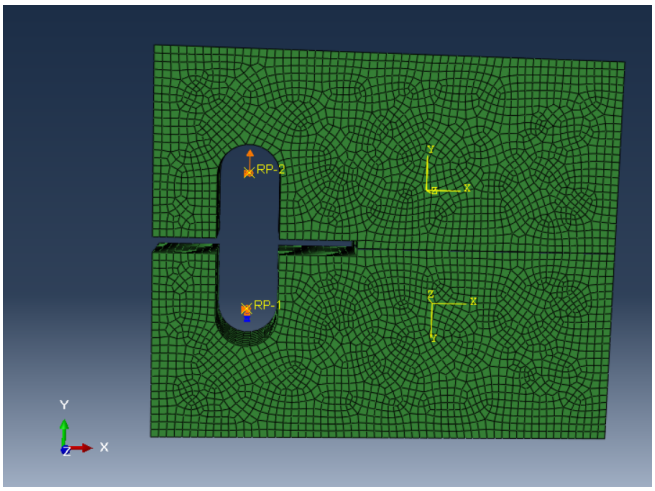


**Figure 66:** Boundary Conditions and it's points of application

### 3.2.6 Material Properties

The material utilized in this project is IsiComp®, an CMC of Carbon fiber plain weave fabric embedded in a Silicon Carbide matrix.The composite is produced by a PIP process.

The material was developed by Petroceramics in partnership with CIRA as a part of the project PRORA- SHS. It has already been validated as re-usable in terms of conservation of mechanical properties after exposition to high temperatures into a experimental campaign in the CIRA's SCIROCCO Plasma Wind Tunnel. [8] [9] [30] [36].

Two cases were the focus of this work. In the first one, Case A, the fabrics were disposed in the plane XZ. This orientations causes the CT test to break the specimen without needing to break the fibers. In other words, case A will test the Interlaminar Fracture Toughness of the material.

The effect of this loading condition is that its behaviour is dictated by the matrix properties, assuming a brittle-like curve for Force x Displacement without the main benefits of the fiber reinforcement and with a higher risk of catastrophic failure.

Furthermore, in practical terms, Case A would be very difficult to manufacture, as it would require a layup of several laminae of the composite and present machining difficulties.

On the other hand, in the main case of this thesis, Case B, the fabrics are oriented on the XY plane. Therefore the test will test the Translaminar Fracture Toughness. In this case the material is oriented in a more favorable way and the energy dissipation mechanisms discussed in Section 2. That translates greatly in the Force x Displacement

**Table 1:** Cohesive element Material properties per case

| Case | Nominal Stress Normal Only Mode | Nominal Stress - First Direction | Nominal Stress - Second Direction | Fracture Energy |
|---|---|---|---|---|
| A | 30 | 30 | 30 | 0.5 |
| A 2 | 30 | 30 | 30 | 0.5 |
| B | 140 | 80 | 80 | 9.0 |
| C | 30 | 30 | 30 | 4.75 |
| C 2 | 30 | 30 | 30 | 4.75 |
| D | 85 | 55 | 55 | 4.75 |
| D 2 | 85 | 55 | 55 | 4.75 |
| E | 85 | 55 | 55 | 9.0 |
| E 2 | 85 | 55 | 55 | 9.0 |
| F | 140 | 80 | 80 | 9.0 |
| F 2 | 140 | 80 | 80 | 9.0 |
| G 2 | 140 | 80 | 80 | 18.0 |
| H 2 | 140 | 80 | 80 | 9.0 |
| I 2 | 140 | 80 | 80 | 9.0 |

behaviour of the specimen.

The other cases are auxiliary cases used to understand the isolated influence of strength, toughness and modulus on the behaviour of the specimens under tension.

The method used to predict failure on the cohesive elements was Maxs Damage, with the properties shown on Table 1. For damage evolution, a energy criteria was used. The fracture energy can also be seen of Table 1 .

For fully understanding the results of the simulations is also important to know the maximum stresses that can be sustained by the material.

**Table 3:** Maximum forces and time of maximum force per case

| | Maximum Stress [MPa] |
|---|---|
| Tension | 140 |
| Compression | 120 |
| Shear | 70 |

**Table 2:** Solid Elements Material properties per case

| Case | $E/E_{nn}$ | $G_1/E_{ss}$ | $G_2/E_{tt}$ | $E_1$ | $E_2$ | $E_3$ | $\nu_1$ | $\nu_2$ | $\nu_3$ | $G_{12}$ | $G_{13}$ | $G_{23}$ |
|---|---|---|---|---|---|---|---|---|---|---|---|---|
| A | 6000 | 6000 | 6000 | 75000 | 25000 | 75000 | 0.011 | 0.2 | 0.2 | 11000 | 5500 | 5500 |
| A 2 | 6000 | 6000 | 6000 | 75000 | 75000 | 25000 | 0.011 | 0.2 | 0.2 | 5500 | 11000 | 5500 |
| B | 6000 | 6000 | 6000 | 75000 | 75000 | 25000 | 0.011 | 0.2 | 0.2 | 5500 | 11000 | 5500 |
| C | 6000 | 6000 | 6000 | 75000 | 25000 | 75000 | 0.011 | 0.2 | 0.2 | 11000 | 5500 | 5500 |
| C 2 | 6000 | 6000 | 6000 | 75000 | 75000 | 25000 | 0.011 | 0.2 | 0.2 | 5500 | 11000 | 5500 |
| D | 6000 | 6000 | 6000 | 75000 | 25000 | 75000 | 0.011 | 0.2 | 0.2 | 11000 | 5500 | 5500 |
| D 2 | 6000 | 6000 | 6000 | 75000 | 75000 | 25000 | 0.011 | 0.2 | 0.2 | 5500 | 11000 | 5500 |
| E | 6000 | 6000 | 6000 | 75000 | 25000 | 75000 | 0.011 | 0.2 | 0.2 | 11000 | 5500 | 5500 |
| E 2 | 6000 | 6000 | 6000 | 75000 | 75000 | 25000 | 0.011 | 0.2 | 0.2 | 5500 | 11000 | 5500 |
| F | 6000 | 6000 | 6000 | 75000 | 25000 | 75000 | 0.011 | 0.2 | 0.2 | 11000 | 5500 | 5500 |
| F 2 | 6000 | 6000 | 6000 | 75000 | 75000 | 25000 | 0.011 | 0.2 | 0.2 | 5500 | 11000 | 5500 |
| G 2 | 6000 | 6000 | 6000 | 75000 | 75000 | 25000 | 0.011 | 0.2 | 0.2 | 5500 | 11000 | 5500 |
| H 2 | 30000 | 30000 | 30000 | 75000 | 25000 | 75000 | 0.011 | 0.2 | 0.2 | 5500 | 11000 | 5500 |
| I 2 | 70000 | 70000 | 70000 | 75000 | 25000 | 75000 | 0.011 | 0.2 | 0.2 | 5500 | 11000 | 5500 |

## 3.3 CT Test Design

### 3.3.1 Simulation Results

#### 3.3.1.1 Maximum Force and instant of Maximum Force by case

**Table 4:** Maximum forces and time of maximum force per case

| Case | $F_{max}$ | t ($F_{max}$) |
|---|---|---|
| A | 1.201 E+03 | 8.460 E-02 |
| A 2 | 1.139 E+03 | 8.960 E-02 |
| B | 4.948 E+03 | 3.746 E-01 |
| C 2 | 2.247 E+03 | 3.046 E-01 |
| D 2 | 3.439 E+03 | 2.796 E-01 |
| E 2 | 4.303 E+03 | 4.046 E-01 |
| F 2 | 4.948 E+03 | 3.746 E-01 |
| G 2 | 6.391 E+03 | 5.546 E-01 |
| H 2 | 5.030 E+03 | 3.746 E-01 |
| I 2 | 5.048 E+03 | 3.696 E-01 |

#### 3.3.1.2 Crack Initiation

For the purposes of this work, the crack initiation moment will be defined as the first one in which the value of SDEG, the status variable, achieve 0.90 or higher. With this consideration, we have that, for each one of the cases studies, the instant of crack initiation and the force applied on that moment was:

**Table 5:** Time of crack initiation per case

| Case | t (crack initiation) [s] | F (crack initiation) |
|---|---|---|
| A | 0.079603 | 1197.18 |
| A 2 | 0.084603 | 1128.04 |
| B | 0.3596 | 4918.63 |
| C 2 | 0.1496 | 1794.53 |
| D 2 | 0.2546 | 3373.73 |
| E 2 | 0.3196 | 4047.79 |
| F 2 | 0.3596 | 4918.63 |
| G 2 | 0.4746 | 6143.94 |
| H 2 | 0.2496 | 4108.27 |
| I 2 | 0.1896 | 3313.62 |

#### 3.3.1.3 Force x Displacement Curves

##### 3.3.1.3.1 Case A

Case A was the test for interlaminar fracture toughness. It was expected to have a behaviour similar to a brittle material, with rapid decrease of the force after the point of maximum force.

The maximum force achieved was 1201 N.

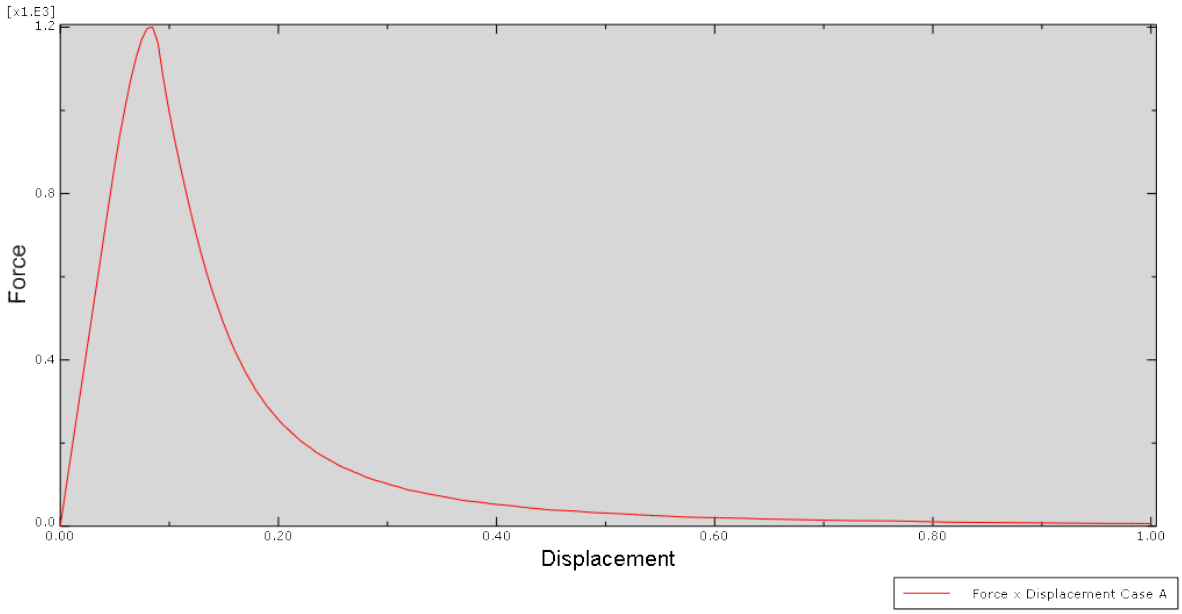


**Figure 67:** Force x Displacement curve: Case A

#### 3.3.1.3.2 Case B

Case B tested the translaminar fracture toughness, therefore a much superior maximum force was expected. A longer time until maximum force was also expected, and the same is true for a smoother, less abrupt slope of the force after the maximum until total separation.

The maximum force achieved was 4948 N.

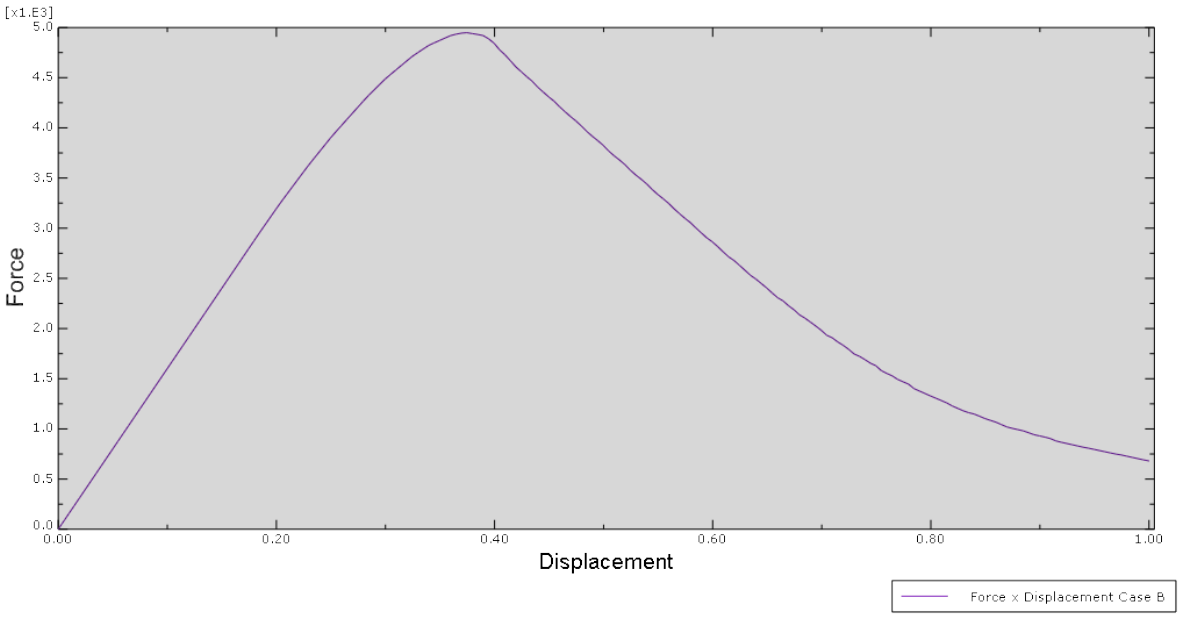


**Figure 68:** Force x Displacement curve: Case B

#### 3.3.1.3.3 Comparison: Case A - Case B

The comparison of case A and case B was performed to allow for a direct observation of the difference between the behaviour of the Force vs Displacement curve for interlaminar and translaminar fracture toughness tests.

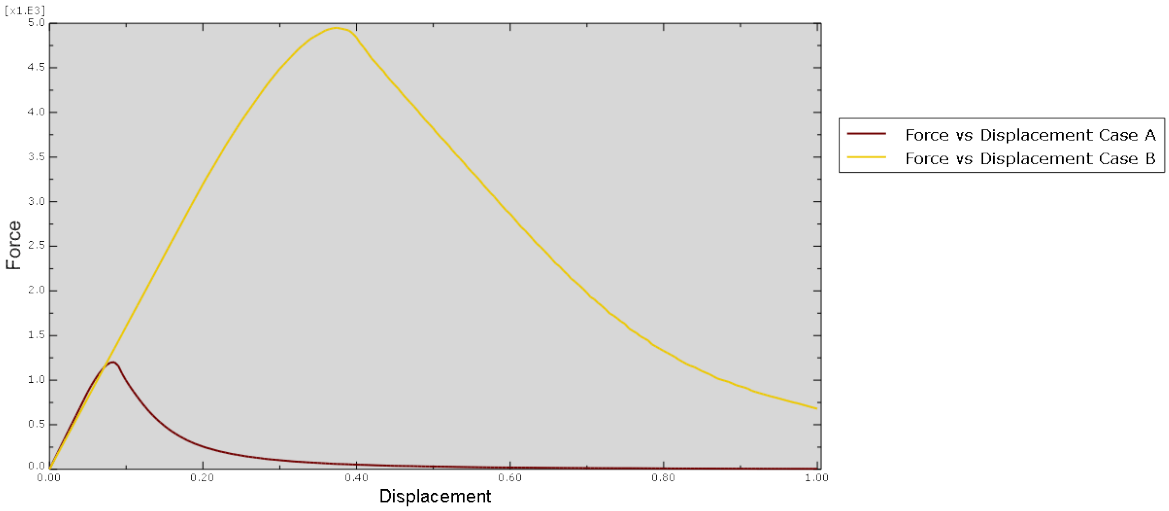


**Figure 69:** Force x Displacement curve comparison: Case A - Case B

#### 3.3.1.3.4 Comparison: Case A - Case A 2

Case A and Case A 2 differ on the Young and shear modulus applied on the solid (non-cohesive) parts. Case A 2 uses the modulus of case B.

This simulation was done to observe the effect of this properties in the final result.

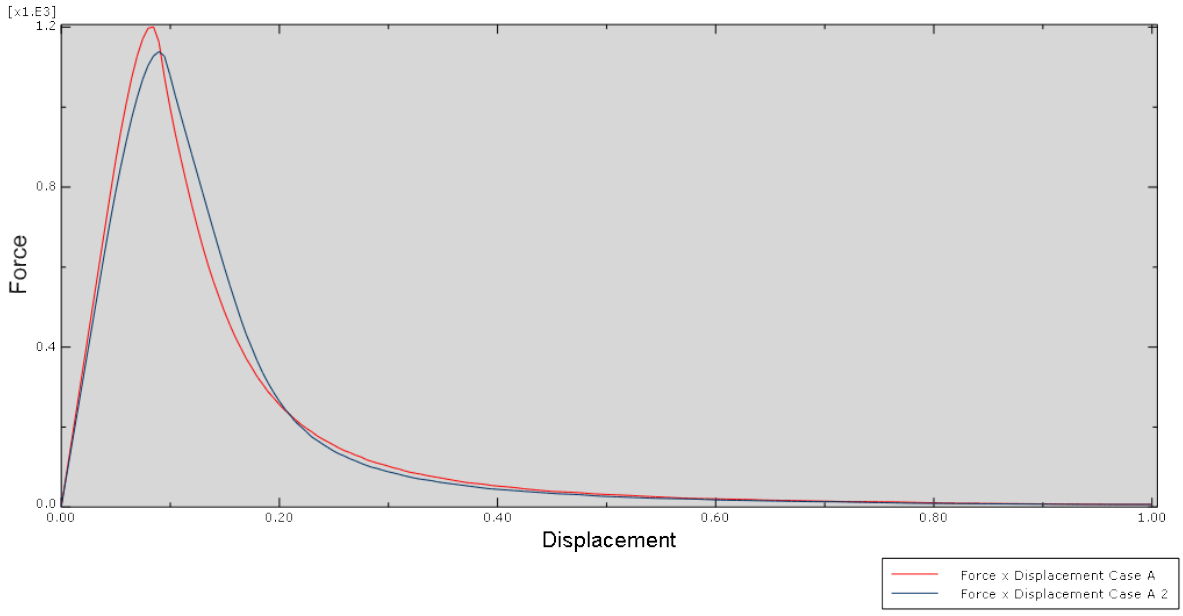


**Figure 70:** Force x Displacement curve comparison: Case A - Case A 2

#### 3.3.1.3.5 Comparison: Case F 2 - Case H 2 - Case I 2

Cases F 2, H 2 and I 2 differ on the modulus used on their cohesive elements. The simulation was done to understand the effect of those values on the simulation.

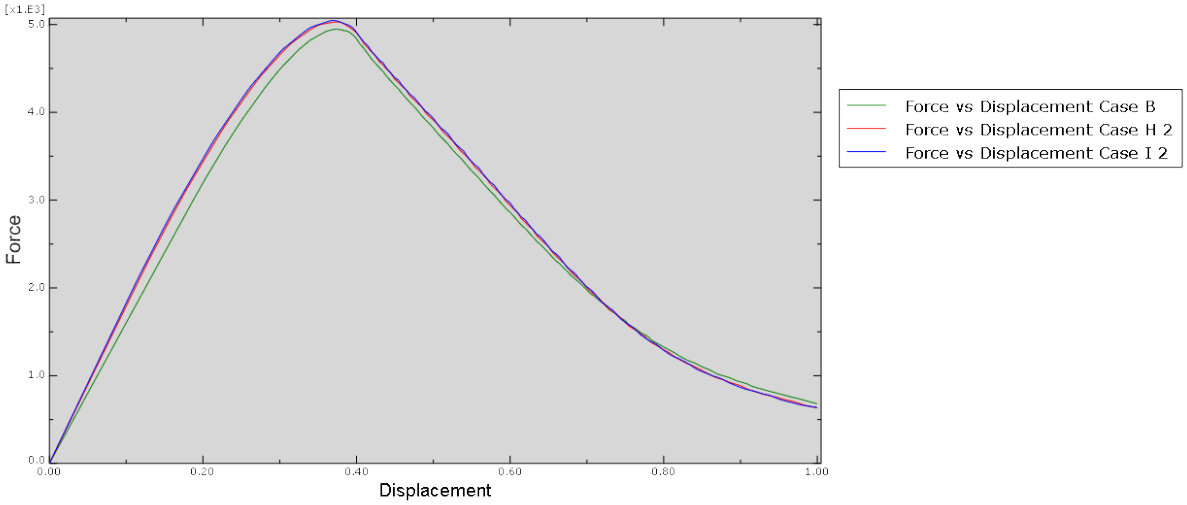


**Figure 71:** Force x Displacement curve comparison: Case F 2 - Case H 2 - Case I 2

#### 3.3.1.3.6 Comparison: Case A 2 - Case C 2 - Case D 2 - Case E 2 - Case F 2 - Case G 2

Finally, the direct comparison between those cases was done to understand the effects of both fracture energy and strength. A common simplification of this problem is to discard the influence of strength, therefore, ideally, the strength should not have effects on the result of the test, but a clear influence of strength is observed, this result will be further discussed later in this thesis.

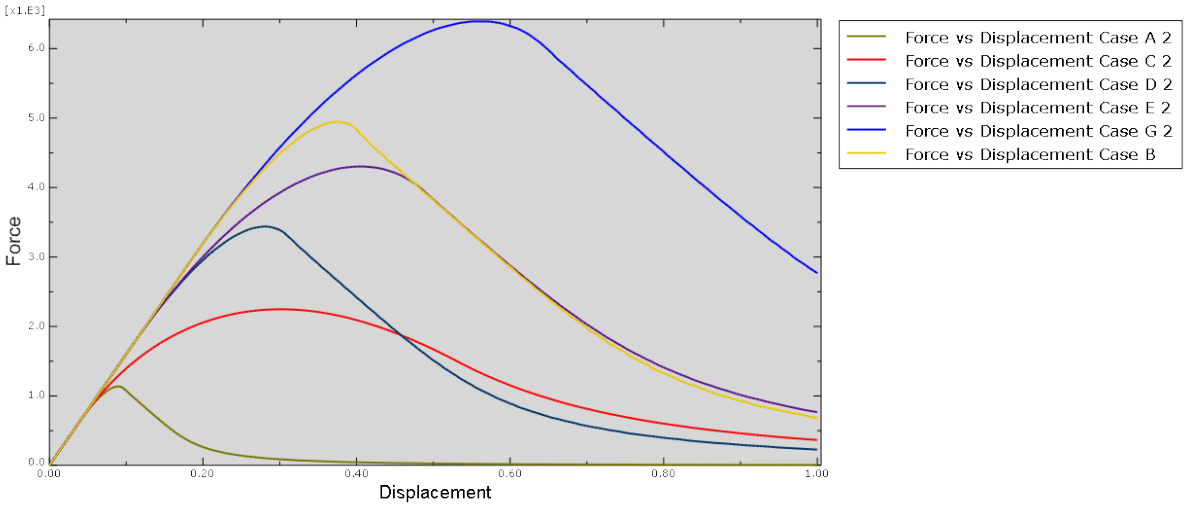


**Figure 72:** Force x Displacement curve comparison: Case A 2 - Case C 2 - Case D 2 - Case E 2 - Case F 2 - Case G 2

#### 3.3.1.4 Stress Fields

The Stresses will be here presented for the Case B/F 2 and Case G 2.

The stress fields are fundamental to understand if the test specimen design in fit for the test to be performed or if redesign is needed in other for the specimen to withstand the conditions of the test without undesirable failure modes.

##### 3.3.1.4.7 Stress Fields at t = 1

For the final time of the simulation, we can see that it was possible to obtain all the stresses on the specimen. The simulation could be carried throughout the entire displacement, without numerical problems. On Figures 73 we can see the final stress fields obtained.

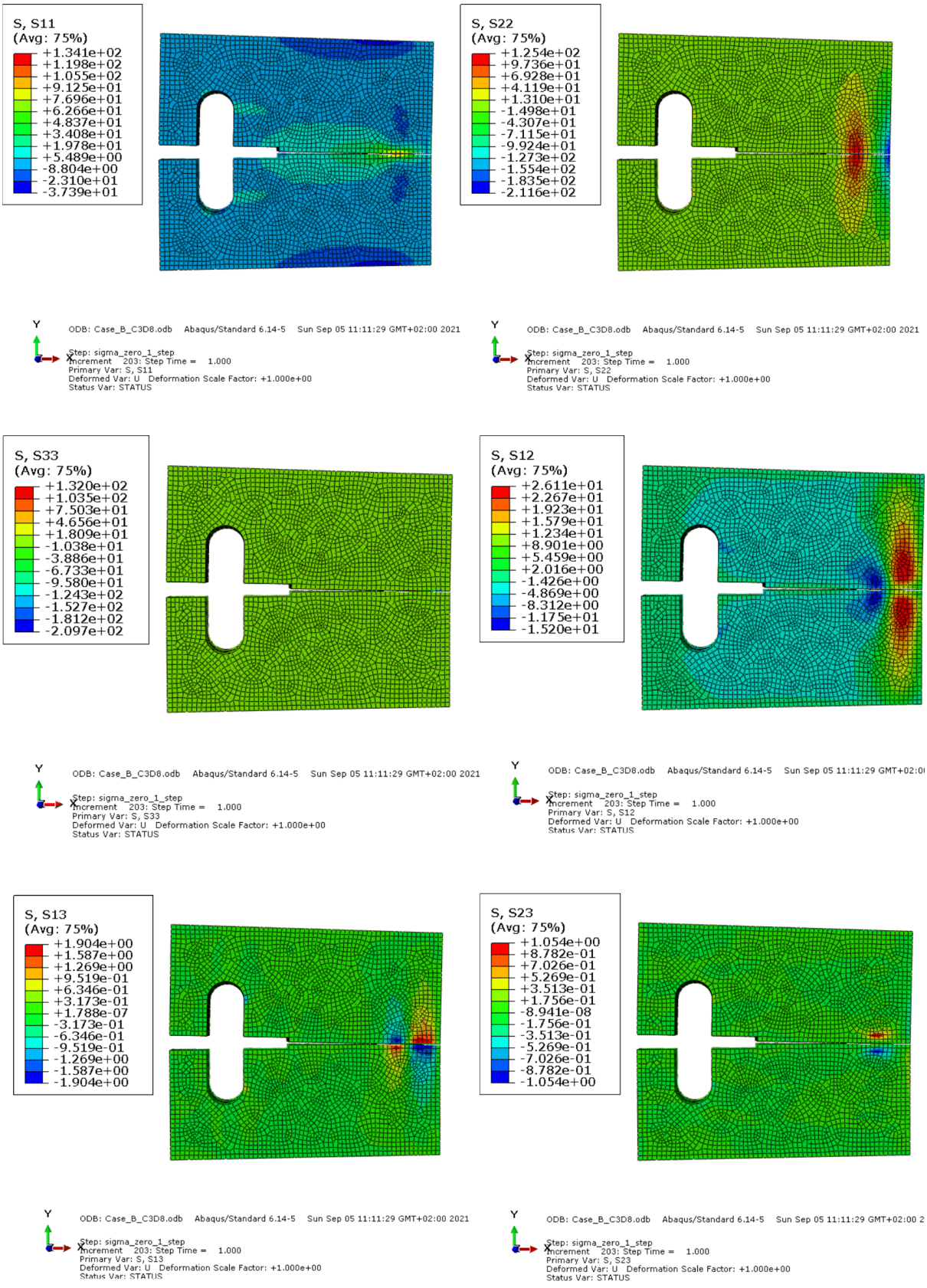


**Figure 73:** Case B - S11, S22, S33, S12, S13, S23 at T $\bar{1}$ [s]

#### 3.3.1.4.8 Stress Fields at t = t($F_{max}$)

The three important stresses for this study are the ones in the XY Plane; S11, S22 and S12, referring to the normal stress in X, normal stress in Y and Shear stress on XY. Due to the geometry of the specimen, some sections of the body will have higher stresses. Stress concentration happens on the notch itself, as it is its purpose and on the opening with which the body is fixated and the displacement is imposed.

In order to better understand what is happening on the specimen on the moment in which maximum force is applied on the test, the countour and the maximum stresses values and position can be seen for S11, S22 and S12 on Figures 74 to 79 .

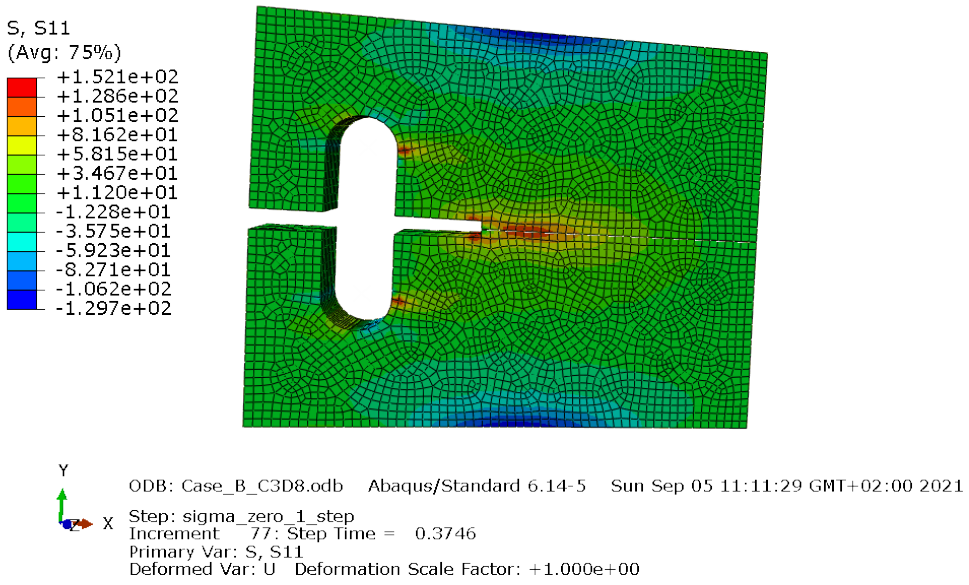


**Figure 74:** Case B - S11 t ($F_{max}$)

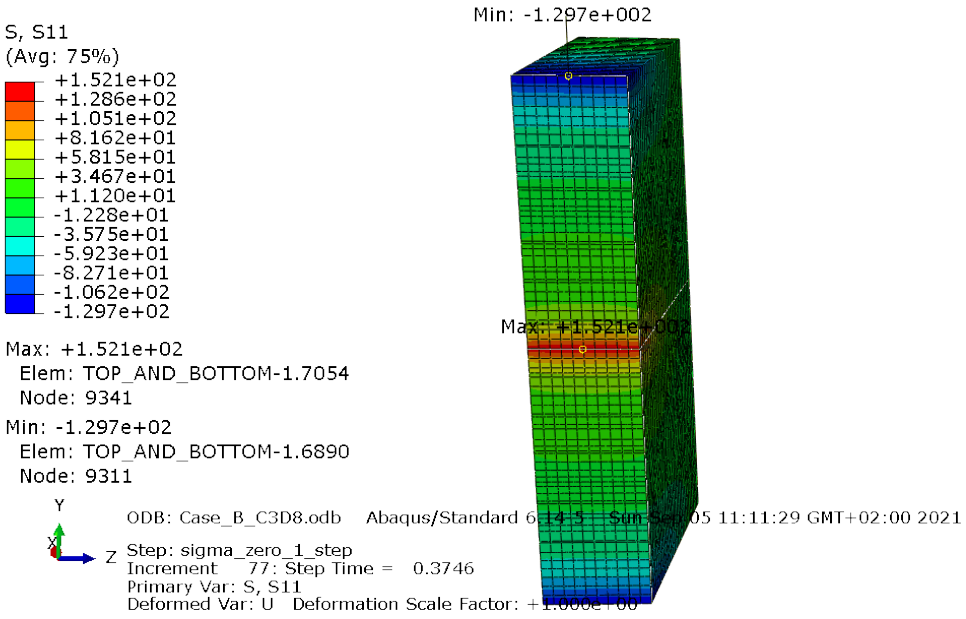


**Figure 75:** Case B - S11 t ($F_{max}$) - Maximum stresses

Three main zones can be identified as having high stresses for S11 on Figure 74,for traction the crack itself and the end of the circular section of the opening where the rigid body was created. The fact that a rigid body was used to apply boundary conditions instead of a contact interaction is the probable cause of this specific stress concentration. For compression, the top and bottom outer surfaces of the specimen are at risk.

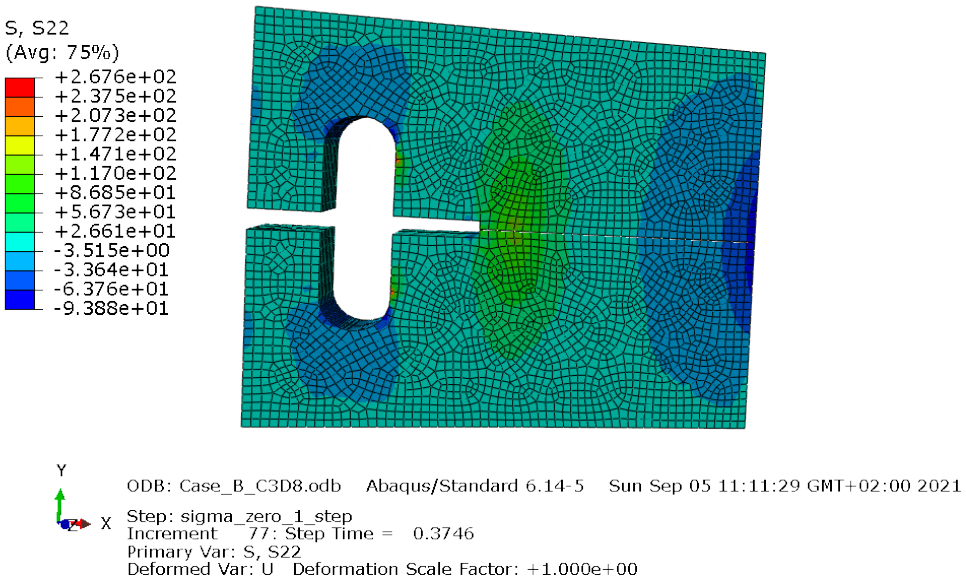


**Figure 76:** Case B - S22 t ($F_{max}$)

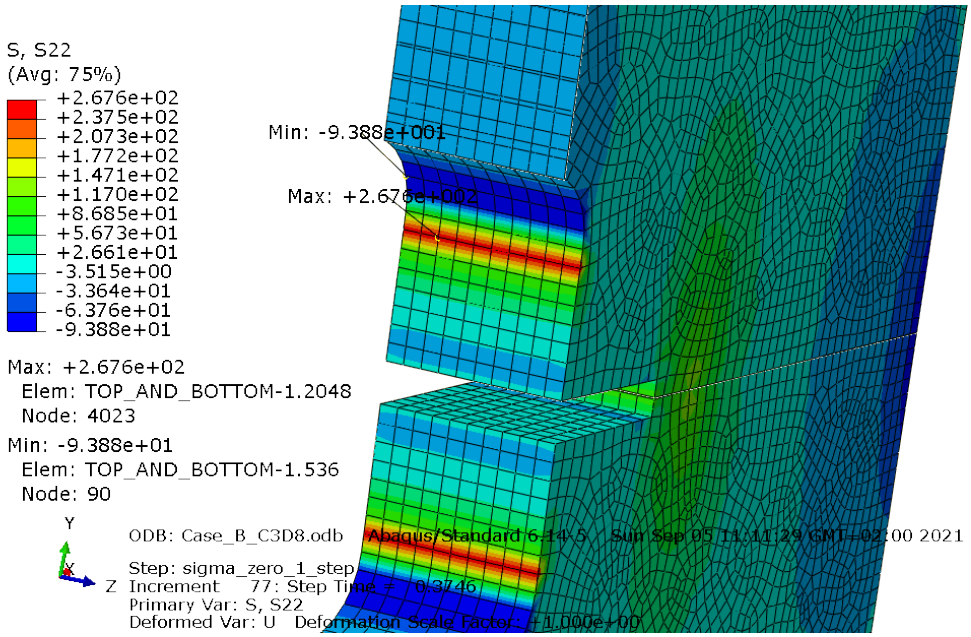


**Figure 77:** Case B - S22 t ($F_{max}$)- Maximum stresses

For S22, on Figure 76, the end of the crack plane is a point of stress concentration, but mainly, the circular section of the opening is again an interest. In this case, though, the stress concentration is not on the end of the circular section, indicating that this is not a stress concentration due to the rigid body usage, but an actual stress concentration that has to be monitored and take into account on the final design of the test specimen.

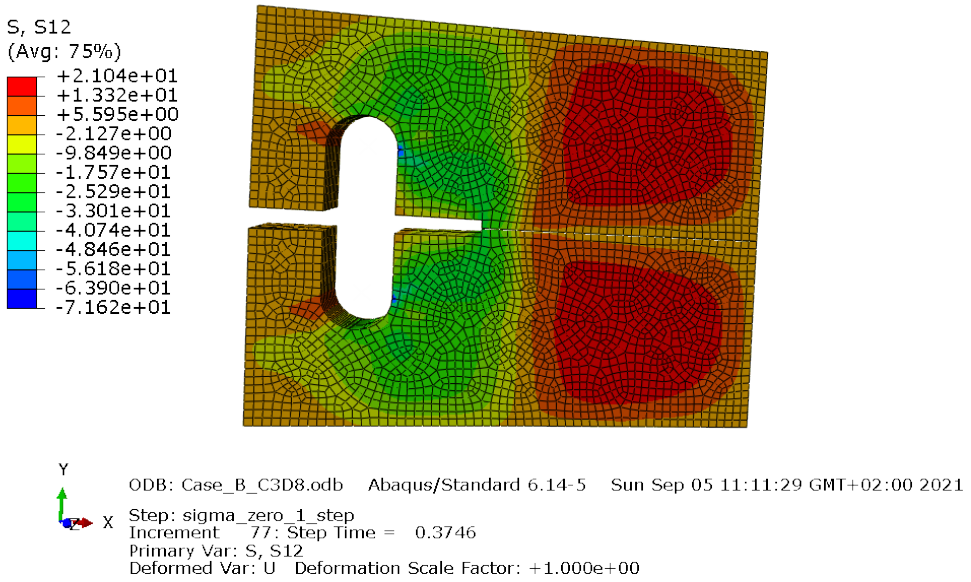


**Figure 78:** Case B - S12 t ($F_{max}$)

Finally, for the shear stress, we can see again the stress concentration at the

end of the circular session, indicating influence of the boundary conditions on the result. Other sections are not at risk.

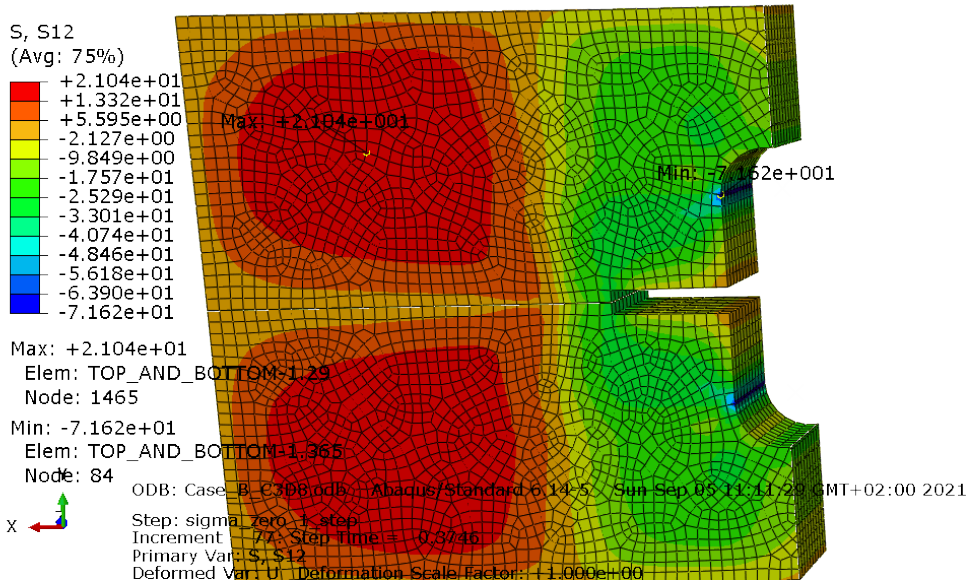


**Figure 79:** Case B - S12 t ($F_{max}$)- Maximum stresses

#### 3.3.1.4.9 Case G at t=t($F_{Max}$)

After observing the stress fields of Case B and the risks it presented, a further look on Case G was considered relevant to this thesis.

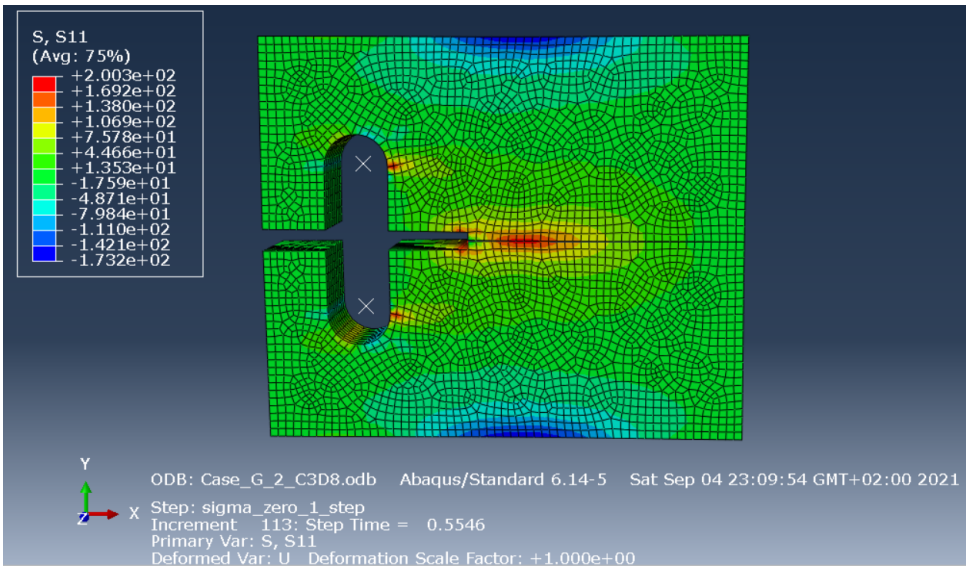


**Figure 80:** Case G 2 - S11 t ($F_{max}$)

The same critical regions can be identified in Case G 2 when compared to Case B, even higher stresses being present. The compression on the bottom and top faces are

very high and indicate that the specimen will present failure of the material in those regions.

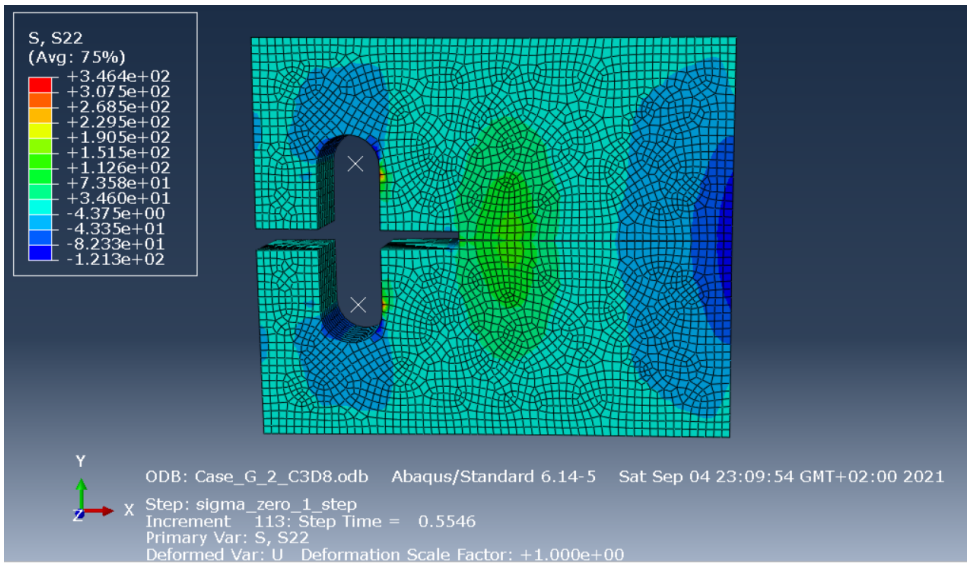


**Figure 81:** Case G 2 - S22 t ($F_{max}$)

On Case G 2 the main investigated area is the circular area for the stress field S22. The area presented a risk on Case B but was still bellow the limit value for compression. In Case G 2, in the other hand, we can see that the 120 MPa limit is surpassed, indicating that failure can occur when the pins impose the displacement on a specimen with higher fracture toughness. This will have to be taken into consideration in the final design of the specimen.

Finally, shear stress is also investigated, but does not seem to present risks of undesirable failures even at higher fracture energy.

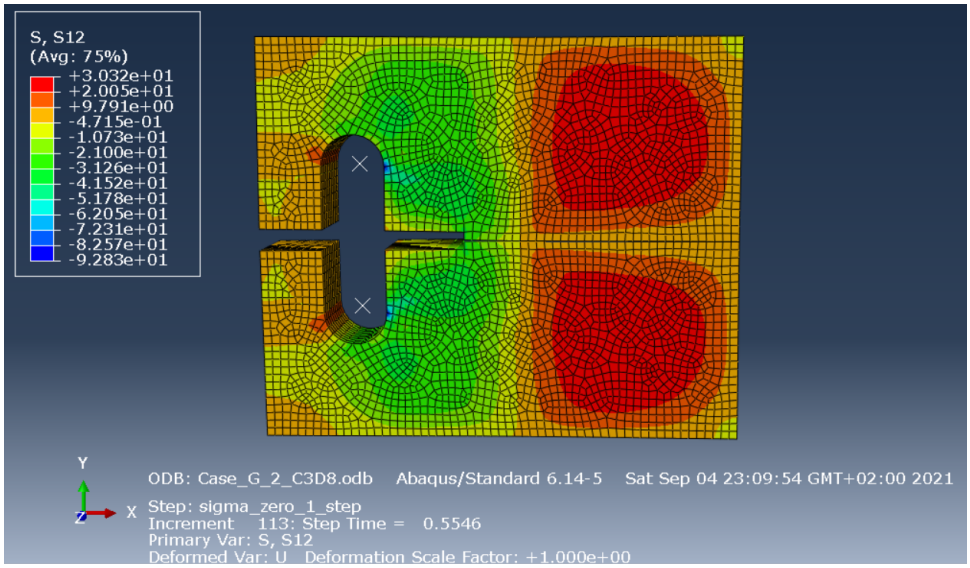


**Figure 82:** Case G 2 - S12 t ($F_{max}$)

#### 3.3.1.4.10 Maximum stresses on regions of interest

After identifying the regions where the stresses come close to their limit values on Cases B and G 2, the maximum stress values in those regions of interest were collected to allow a better analysis of the capacity of the specimen of withstand the test without undesirable failure modes, that is, failing only by crack initiation and propagation on the notch plane.

The regions of interest are presented on Figure 83 and the maximum stresses of interest on Figure 84.

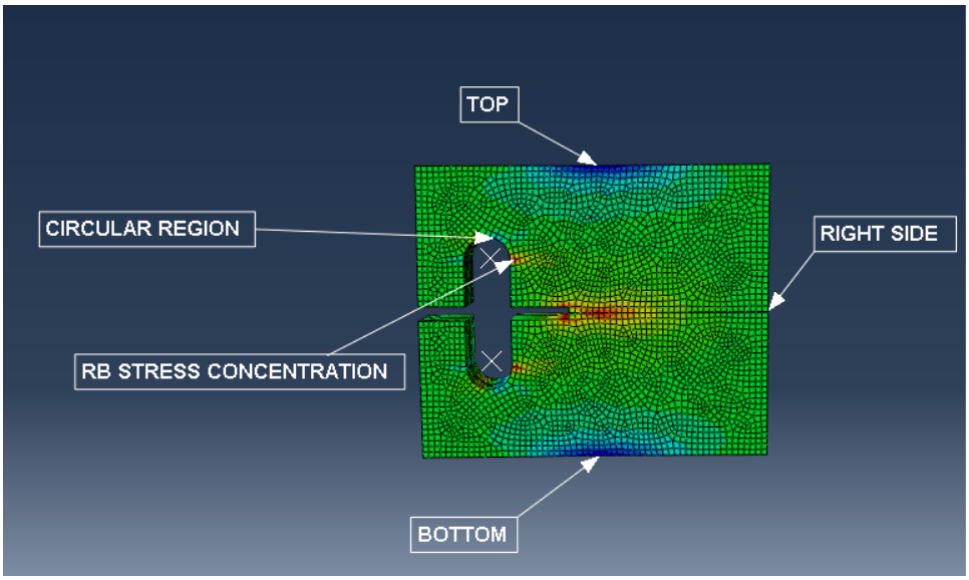


**Figure 83:** Regions of interest for stress investigation

| | Case B | | | Case G 2 | | |
|---|---|---|---|---|---|---|
| Regions of interest (Close to maximum stress values) | S11 | S22 | S12 | S11 | S22 | S12 |
| Crack | 152.1 | 120.6 | x | 200.3 | 139.6 | x |
| Circular region | x | -93.4 | x | x | -121.3 | x |
| Rigid body stress concentration | 127.8 | 267.6 | -71.6 | 196.2 | 346.4 | -92.38 |
| Top/Bottom | -129.7 | x | x | -173.2 | x | x |
| Right side surface | x | -80.9 | x | x | -121.3 | x |

**Figure 84:** Maximum values of stress in the areas of interest per case

## 3.4 Discussion

In this section the simulation results obtained in this work will be explored in order to derive conclusions and

| Regression Statistics | |
|---|---|
| Multiple R | 9.91E-01 |
| R Square | 9.83E-01 |
| Adjusted R Square | 3.04E-01 |
| Standard Error | 2.42E-02 |
| Observations | 6.00E+00 |

| *TIME* | Coefficients |
|---|---|
| Intercept | 0.051239193 |
| Nominal Stress - Normal only mode | 0.001480759 |
| Nominal Stress - First Direction | 0 |
| Nominal Stress - Second Direction | 0 |
| Fracture Energy | 0.012608273 |

| Regression Statistics | |
|---|---|
| Multiple R | 9.94E-01 |
| R Square | 9.89E-01 |
| Adjusted R Square | 3.15E-01 |
| Standard Error | 2.56E+02 |
| Observations | 6.00E+00 |

| *FORCE* | Coefficients |
|---|---|
| Intercept | 520.5695795 |
| X Variable 1 | 23.8771464 |
| X Variable 2 | 0 |
| X Variable 3 | 0 |
| X Variable 4 | 132.73691 |

**Figure 85:** Multivariate Multiple Regression Analysis - Crack initiation force and time

### 3.4.1 Crack initiation

The first point to be discussed is the influence of strength and toughness of the moment of crack initiation and force for crack initiation.

As we can see in Table 5, considering the properties of each case, presented in Table 1, we can see that Fracture Energy, as expected, has the biggest influence in both, the time of crack initiation and the Force necessary to start the crack.

The Strength also has an influence in the behaviour of crack initiation, causing significant variation of the values, but with a slower impact then the Fracture Energy. Analytically, that can be shown using an Multivariate Multiple Regression Analysis. Using the material properties to perform the regression is possible to observe a significant influence of strength and fracture energy. Note that, as the strength values were varied in the same proportion (Case A strength values, mid point between case A and B, Case B strength values), is natural that the regression points out a zero influence of the nominal stresses for first and second direction. In order to decouple those influences, simulations maintaining a fixed value of Nominal Stress (Normal Only) and varying the other two independently would need to be performed. This was not done in this case as this statistical analysis is used just as a way to have a quantitative view on the crack behaviour.

Note that the coefficient of determination for the regression is close to 1 for both force and time regressions, indicating that the regression fits reasonably with the actual behaviour of the crack initiation.

In order to better understand the influence of strength and fracture energy in

the force and time for crack initiation, the regressions were plotted on Figures 87 and **??** respectively.

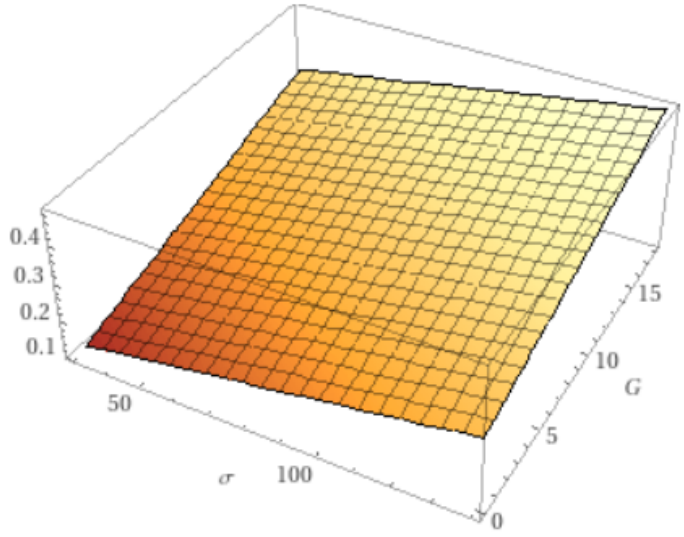


**Figure 86:** Multivariate Multiple Regression Analysis - Crack initiation time plot

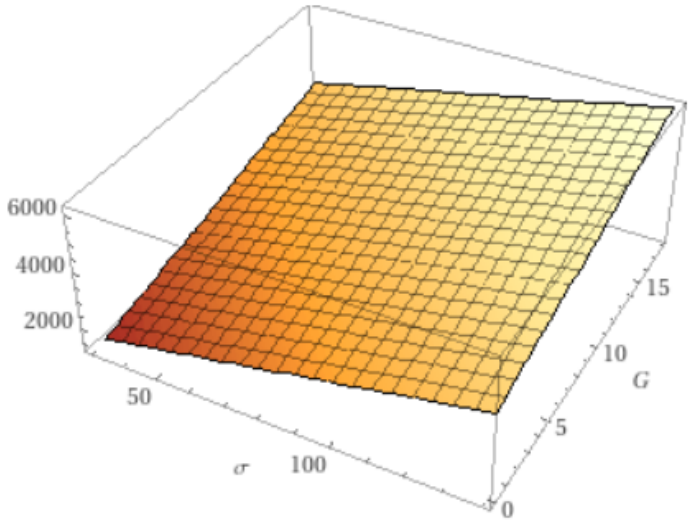


**Figure 87:** Multivariate Multiple Regression Analysis - Crack initiation force plot

### 3.4.2 Force x Displacement

The first point to be discussed in the Force x Displacement analysis is the fact that all simulations were able to arrive to the point of maximum stress and continue past that point until the end of the imposed displacement without any disruption of the test, without abrupt failure or numerical errors, indicating that , should the experiment be performed, no undesirable failure or behaviour in the CT specimen is expected and, that, therefore, the design of the CT specimen is adequate for testing. This will be better explored in the countour plot discussion.

Next, the curves presented previously will be discussed.

#### 3.4.2.0.1 Case A

In Case A, as the fibers are in the XZ plane, and, therefore, the energy dissipation mechanisms of the fibers are not in action, the curve represents a behaviour that is brittle-like, with a fast, steep ascension to the maximum value of force and also a steep decrease in the force, showing a fast propagation of the crack after the initiation.

The behaviour is not totally brittle, though, as the failure is not sudden or catastrophic.

It is important to compare this case with experimental data. Should the experimental test of the material demonstrate that the failure deviates the one predicted by the software, is important to modify the model to predict the actual behaviour of the material, making it reliable.

Different elements for the meshing, different damage evolution configuration or the imposition of safety factors on the materials properties for the model could be strategies studied to make the model more accurate if needed.

As this case involves smaller stresses when compared to the Case B, the design of the specimen will be mainly driven by Case B.

#### 3.4.2.0.2 Case B

In Case B we can clearly observe how the fact that the force application is aligned with the fibers influences the behaviour of the material. The energy dissipation mechanisms delay the start of the cracking,the resistance of the fibers greatly increase the maximum force value, and, in opposition to the Case A, the fracture is not brittle-like, in fact, the force decreases slowly, showing the desirable fracture behaviour from the material, that is, a gradual failure, avoiding catastrophic fracture, making the material of great interest to engineering applications.

Therefore, is important, that, during design phase, not only the correct manufacturing method and conditions, composition of the composite and fiber architecture are correctly selected, but also that during the orientation of the expected loads is know and the composite is oriented in such a way as to optimize load resistance and energy dissipation.

The curve behaviour is Case B is similar to what is expected for a CMC material when loaded in the same direction as its fiber. Comparison with experimental results is fundamental for validating the model, but we can already see that no strange behaviour on failure was identified that leads to believe that the model is not accurate.

#### 3.4.2.0.3 Case A - Case B

In this curve we can better appreciate the difference in maximum force, as well as the time for the crack to totally propagate in Cases A and B. It becomes even more apparently why the incorrect alignment of the fibers of the composite in relation to the loads of the structure can be detrimental to the integrity of the structure.

#### 3.4.2.0.4 Case A - Case A2

The comparison of this cases make it possible to appreciate the influence of the properties of the solid parts in the curve's behaviour. With the change in the direction of the properties, it's possible to observe a decrease on maximum force, but a delay in crack initiation and on the instant of maximum force.

#### 3.4.2.0.5 Case F 2 - Case H 2 - Case I 2

In the comparison of Case B (F 2),Case H 2 and Case I 2 the effect of the modulus can be seen. A increase in the modulus causes a decrease in the time instant for maximum force, but a increase in the maximum force value itself.

#### 3.4.2.0.6 Case A 2 - Case C 2 - Case D 2 - Case E 2 - Case F2 - Case G 2

This curves comparison is essential to better understand the influence of strength and fracture toughness. We can see how the increase in strength increases the value of maximum force and delays the moment to achieve the maximum force. Additionally, an increased value of strength, with no increase in fracture energy generates a less steep slope. The subsequent increasing on the fracture energy further increases the maximum force achieved, but also shortens the time to achieve the maximum force point and generates a steeper slope.

| Regression Statistics | |
|---|---|
| Multiple R | 9.92E-01 |
| R Square | 9.84E-01 |
| Adjusted R Square | 3.06E-01 |
| Standard Error | 3.12E+02 |
| Observations | 6.00E+00 |

| *MAX FORCE* | Coefficients |
|---|---|
| Intercept | 798.330725 |
| Nominal Stress - Normal only mode | 19.16646312 |
| Nominal Stress - First Direction | 0 |
| Nominal Stress - Second Direction | 0 |
| Fracture Energy | 171.8012925 |

| Regression Statistics | |
|---|---|
| Multiple R | 9.60E-01 |
| R Square | 9.21E-01 |
| Adjusted R Square | 2.02E-01 |
| Standard Error | 5.58E-02 |
| Observations | 6.00E+00 |

| *TIME (MAX FORCE)* | Coefficients |
|---|---|
| Intercept | 0.146360827 |
| Nominal Stress - Normal only mode | -4.57065E-05 |
| Nominal Stress - First Direction | 0 |
| Nominal Stress - Second Direction | 0 |
| Fracture Energy | 0.025059996 |

**Figure 88:** Multivariate Multiple Regression Analysis - Maximum Force and time for Maximum Force

### 3.4.3 Maximum Force

The maximum force is indicative of the fracture toughness of the material.

A common simplification applied to the CT test is to consider that only the fracture energy has influence over the test, this simulation shows that there is an influence also of the strength, that is usually discarded when the simplification is used, but that can be important to the final result.

The maximum force that the specimen can tolerates is influenced by both the strength and the toughness of the material.

A regression analysis is performed with cases A 2,B/F 2, C 2, D 2, E 2 and G 2 as can be seen in Figure 88, in order to understand quantitatively the influence of the different simulation parameters. Fracture energy plays the most important role influencing the maximum force value, but there is also a important influence of the strength.

With this coefficients we can obtain a plot to observe the effect of fracture energy (G) and strength($\sigma$) in the maximum force, this plot can be seen in Figure 89.

We can observe, on Figure 90 that the influence of strength is less important for the time in which maximum force is achieved then it is for the max force itself.

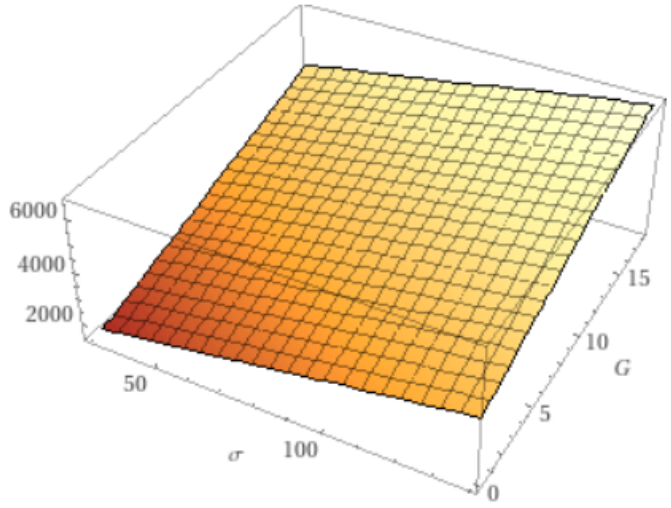


**Figure 89:** Multivariate Multiple Regression Analysis - Maximum Force Plot

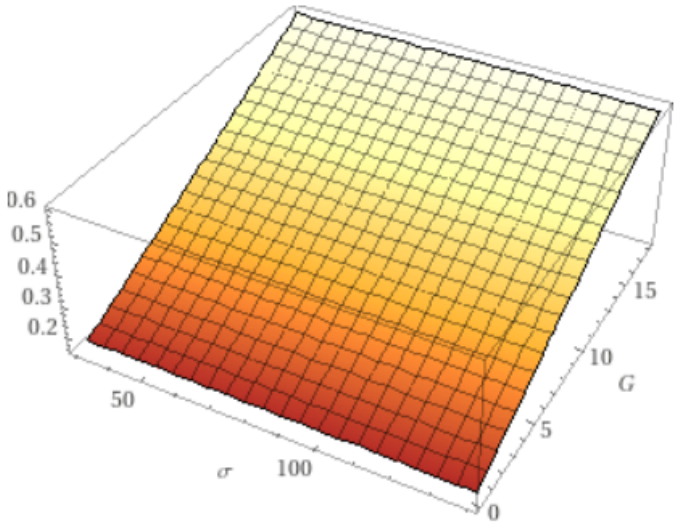


**Figure 90:** Multivariate Multiple Regression Analysis - Time for maximum force Plot

### 3.4.4 Stress Fields

The internal stresses for the moment of maximum force of Case B and Case G 2 were presented. Specifically, the countour for S11, S22 and S12.

Additionally, plots for the specific value and location of the maximum values of those stresses for Case B were also presented.

There are 3 critical regions for stresses, the first one being the notch and after the crack starts to propagates, the crack itself.

The second critical region is the circular holes, where the CT specimen will be fixated with pins. The pins apply the boundary conditions that we imposed on thi simulation. The region is specially critic for S22.

Finally, the top of the specimen is the critical region for compression. In figure 75 the compression on that region can be clearly observed.

The total maximum stresses observed on those regions allows us to draw some important conclusions about both the model itself and test specimen.

The use of the rigid body for application of the boundary condition simplified the model, when compared to the modelling of the fixation pin and the use of a contact interaction, resulting in an smaller computational cost and time needed to run each simulation. Had this choice not impacted on the simulation results, the rigid body could be used going forward. What was observed, though, was the rise of ambiguous stress concentration, that would probably not be observed on the real test.

This raises the need of modifying the model in the next steps of the project. The fixation pin must be modelled and a contact interaction must be used to fixate the pin in the test specimen. This will have a negative impact in the computational cost but will allow for more reliable results.

Furthermore, is important to analyze if the test specimen is adequate for this test and if not, to redesign the specimen in order to withstand the test conditions without failing in undesirable ways, that is, the failure must be in the crack plane and not in other points of the specimen.

On Figure 74 we can see that for tension the stress values surpass the maximum allowed by the material in two points, the crack and the end of the rigid body. Once the model is reworked with the contact interaction the second should not be a problem anymore, therefore, for tension the crack is propagating as it should, starting on the

notch and progressing on the plane of the cohesive elements.

For compression, in the other hand, we can see two areas where the stress is bigger then the maximum compression that the material can withstand (120 MPa). This means that those areas would be damaged as well.

For both the Case B and Case G 2, maximum compression stress was achieved even before the crack starts to develop, indicating that without modifications the specimen might failure by compression on those regions before the crack develops. To avoid this, modifications must be done on the test specimen, either to reinforce the area or to better distribute the stress.

For S22, not considering the stress concentration caused by the rigid body boundary condition, we observed the higher stresses on the circular region, on the crack region and on the right side of the specimen, but still within the limits of the material both for Case B and Case G 2, showing that undesirable failure is not predicted in this direction.

For shear stresses, S12, we observed again the stress concentration caused by the rigid body, other then that, for Case B the values are within the tolerated ones, indicating that the specimen can withstand the test without undesirable shear failure. The same is valid for Case G 2, indicating that no undesirable failure will happen for shear stress.

To fully confirm that not considering the stress concentrations caused by the rigid body is a reasonable assumption, the model using pins and contact interaction must be done to investigate the stress in that area.

### 3.4.5 Test specimen design modifications

In order to withstand the entire test and for the failure to occur only by crack initiation and development in the notch plane some strategies can be utilized. 3 different solutions are suggested:

1. Larger test specimen - a bigger test specimen allows for better distribution of the force, hopefully avoiding that the compression stresses cause premature failure in an undesirable manner. Multiplying the dimensions of the body by 1.25 and 1.5 and repeating the simulation for each value would help understand the size change needed.

2. Reinforcements - alternatively, on in parallel with the size modification, reinforce-

ments could be used to protect the specimen from failure by compression on the top and bottom surfaces. This solution does not avoid the high compression observed for S22 on the circular surface of Case G 2, though, and a risk of undesirable failure in that region remains for higher fracture energies.

3. Associate solution 1 and 2 - using both a change in size and a reinforcement can be used if only the change in size is not enough for the specimen to resist the test or to avoid excessive enlargement of the specimen and consequently excessive material usage, as a 50% increase in dimensions already means a 237.5% increase in volume of material for each specimen.

Therefore the approach suggested for the modification of the specimen is first investigating a change in the size of the specimen up to 1.5 times the initial dimensions and then, if needed, using a reinforcement to avoid excessive enlargement of the specimen while protecting against the compression on the top and bottom surfaces. The strategy for this reinforcements is to be defined by posterior work of the project.

# Conclusions

Ceramic Matrix Composites are a very promising class of materials. C/SiC composites have been achieving great results both in terms of mechanical properties and in preservation of such properties under ultra high temperature conditions.

The creation of a computational model to assist in engineering projects using such materials is fundamental.

In this thesis, a model was developed to help in the characterization campaign of IsiComp®, a C/SiC composite developed by Petroceramics in partnership with CIRA. Translaminar and interlaminar fracture toughness were tested.

The model demonstrated good compliance with the expected behaviour for translaminar fracture toughness. The cohesive elements proved to be promising in the simulation of crack initiation and propagation for ceramic matrix composites, as stated in previous articles and thesis studied in the bibliography.

To perfect the model and avoiding the stress concentration that the rigid body generated on the simulation it is necessary to model the fixation pins and apply a contact interaction between the pin and the specimen, instead

The energy dissipation micro mechanisms effects were very clear in the difference on the crack initiation and propagation from Case A (interlaminar fracture toughness) and Case B (translaminar fracture toughness).

The ratio between the force for crack initiation in case B and in Case A was of 4.1 . Which demonstrates not only the efficiency of the energy dissipation mechanism but also the importance of correct orientation of composites when using in engineering applications such as hot structures.

A very important conclusion of this thesis is that, contrary to common simplification, the strength does have an effect on the CT test, having a clear influence in the maximum force sustained by the specimen. Therefore, strength must be taken into consideration when testing and simulating tests for fracture toughness on CMC materials.

Furthermore, it was identified that the current design of the test specimen has a high risk of presenting undesirable failure modes and must be redesigned, by either modifying its dimensions or adding reinforcements.

In order to fully validate the model it is necessary to compare it's result with an

experimental campaign. This will provide fundamental data to calibrate the model with necessary parameters and to observe failure modes that were not identified by the model but that may happen due to wrong considerations or simplifications in the simulation parameters used.

# References


[1] F. W. ZOK A. G. EVANS. The physics and mechanics of fibre-reinforced brittle matrix composites. *JOURNAL OF MATERIALS SCIENCE 29 (1994)*, 1994.

[2] Oriol Gavalda Diaz; Gonzalo Garcia Luna; Zhirong Liao; Dragos Axinte. The new challenges of machining ceramic matrix composites (cmcs): Review of surface integrity. `https://www.sciencedirect.com/science/article/pii/S0890695518306084` accessed on 25-07-2021.

[3] Ehsan Bafekrpour. *Advanced Composite Materials: Properties and Applications*. Sciendo Migration, 2017.

[4] Stéphane Baste. Inelastic behaviour of ceramic-matrix composites. *Composites Science and Technology 61 (2001)*, 2000.

[5] Shengru Qiao Xuanwei Wang Jun zhang Chengyu Zhang, Jianjie Gou. Interlaminar shear strength of sic matrix composites reinforced by continuous fibers at 900°c in air. *Materials and Design 53 (2014) 93–98*, 2014.

[6] CIRA. Space rider, completata dal cira la realizzazione del primo flap in materiale ceramico isicomp®. https://www.cira.it/it/spazio/accesso-allo-spazio-satelliti-ed-esplorazione/pride/space-rider-completata-dal-cira-la-realizzazione-del-primo-flap-in-materiale-ceramico-isicomp® accessed on 02-09-2021.

[7] CIRA. Space rider, il body flap realizzato dal cira supera i test dinamici e dimostra la sua capacità di resistere ai carichi vibrazionali di lancio. https://www.cira.it/it/spazio/accesso-allo-spazio-satelliti-ed-esplorazione/pride/space-rider-il-body-flap-realizzato-dal-cira-supera-i-test-dinamici-dimostrando-la-sua-capacità-di-resistere-ai-carichi-vibrazionali-di-lancio accessed on 02-09-2021.

[8] CIRA. Space rider, the first flap in isicomp® material completed by cira. https://www.cira.it/en/space/accesso-allo-spazio-satelliti-ed-esplorazione/pride/space-rider-completata-dal-cira-la-realizzazione-del-primo-flap-in-materiale-ceramico-isicomp®/Space20Rider,20the20first20flap20in20ISiComp®20material20completed20by20CIRA accessed on 02-09-2021.

[9] CIRA. Tests on "isicomp", the new italian ceramic material, confirm its re-usability for further re-entry missions. https://webtest.cira.it/en/communication/news/test-in-pwt-su-

isicomp/Tests20on20"ISiComp",20the20new20Italian20ceramic20material,20confirm20its20re-usability20for20further20re-entry20missions accessed on 02-09-2021.

[10] ABAQUS documentation. About cohesive elements. https://abaqus-docs.mit.edu/2017/English/SIMACAEELMRefMap/simaelm-c-cohesiveoverview.htm accessed on 02-09-2021.

[11] ABAQUS documentation. Eight-node brick element with reduced integration (c3d8r and f3d8r). https://web.mit.edu/calculix_v2.7/CalculiX/ccx_2.7/doc/ccx/node27.html accessed on 02-09-2021.

[12] ABAQUS documentation. Understanding constraints. https://abaqus-docs.mit.edu/2017/English/SIMACAECAERefMap/simacae-c-itnconstraint.htm accessed on 02-09-2021.

[13] ESA. Hot structures for reentry vehicles. https://www.esa.int/Enabling_Support/Space_Transportation/Hot_structures_for_reentry_vehicles accessed on 27-04-2021.

[14] Roberta Farinelli. *"Characterization and Modelling of Fracture Response for Carbon-Carbon Composite Laminates"*. PhD thesis, Politecnico di Milano, 2017. unpublished thesis.

[15] American Society for Testing and Materials. Astm e399. http://web.eng.fiu.edu/LEVY/images/EGM6570/ASTM-E399.pdf accessed on 31-08-2021.

[16] GINGER GARDINER. Aeroengine composites, part 1: The cmc invasion. https://www.compositesworld.com/articles/aeroengine-composites-part-1-the-cmc-invasion accessed on 27-07-2021.

[17] David E. Glass. Ceramic matrix composite (cmc) thermal protection systems (tps) and hot structures for hypersonic vehicles. *15th AIAA Space Planes and Hypersonic Systems and Technologies Conference* , 2008.

[18] Hermann Hald. Return technology - hot structures and thermal protection systems. https://www.dlr.de/bt/en/desktopdefault.aspx/tabid-4303/3752_read-10083/ accessed on 27-04-2021.

[19] Mar-Bal Incorporated. History of composite materials. https://www.mar-bal.com/language/en/applications/history-of-composites/ accessed on 25-07-2021.

[20] José Maria Ferreira Dariusz M. Jarzabek Yongsheng Zhang Brahim Aissa Mohamed Bououdina Wojciech Dera Hengzhong Fan Yuan Fang J. Paulo Davim and Gilbert Fantozzi. *Ceramic Matrix Composites : Materials, Manufacturing and Engineering.* Walter de Gruyter GmbH, 2016.

[21] Todd Johnson. History of composites, the evolution of lightweight composite materials. https://www.thoughtco.com/history-of-composites-8204044 accessed on 25-07-2021.

[22] Jacques Lamon and Narottam P. Bansal. *Ceramic Matrix Composites : Materials, Modeling and Technology*. John Wiley Sons, Incorporated, 2014.

[23] James Lankford. The failure of fiber-reinforced ceramic-matrix composites under dynamic loading. *JOM 47, 64–68 (1995)*, 1995.

[24] Longbiao Li. Fatigue damage and lifetime of sic/sic ceramic-matrix composite under cyclic loading at elevated temperatures. *Materials 2017, 10, 371*, 2017.

[25] Drissi-Habti M. *Mechanical Behavior of Large Size Compact Tension Specimens of 2D Woven SiC-SiC Composite Materials*. Springer, Boston, MA, 1996.

[26] Joe Parrish California Institute of Technology Marcus Lobbia, Scott Perino. Hot-structure earth entry vehicle concept for robotic mars sample return. https://www.colorado.edu/event/ippw2018/sites/default/files/attached-files/aeroentrytech$_{3l}obbia_{p}resid630_{p}resslides_{d}ocid1152.pdfaccessedon02-09-2021$.

[27] M.J. LaffanS.T. PinhoP. RobinsonA.J. McMillan. Translaminar fracture toughness testing of composites: A review. *Polymer Testing 31 (2012) 481–489482*, 2012.

[28] NASA. Nasa armstrong fact sheet: X-38 prototype crew return vehicle. https://www.nasa.gov/centers/armstrong/news/FactSheets/FS-038-DFRC.html accessed on 27-08-2021.

[29] Peter G. Valentine Paul R. Gradl. Carbon-carbon nozzle extension development in support of in-space and upper-stage liquid rocket engines. *53rd AIAA/SAE/ASEE Joint Propulsion Conference, Atlanta, GA*, 2017.

[30] PETROCERAMICS. Petroceramics - markets - aerospace. http://www.petroceramics.com/index.php/markets/aerospace accessed on 02-09-2021.

[31] P.McMullen. Fibre/resin composites for aircraft primary structures: a short history, 1936–1984. https://www.sciencedirect.com/science/article/abs/pii/0010436184902799 accessed on 25-07-2021.

[32] R.Teti. Machining of composite materials. https://www.sciencedirect.com/science/article/pii/S000785060761703X accessed on 25-07-2021.

[33] Mandeep Singh Rayat; Simranpreet Singh Gill; Rupinder Singh ; Lochan Sharma. Fabrication and machining of ceramic composites — a review on current scenario. https://scholar.google.com/citations?view_op=view_citation&hl=en&user=

zVqbEB4AAAAJ&citation_for_view=zVqbEB4AAAAJ:u5HHmVD_uO8C accessed on 25-07-2021.

[34] NASA SBIR 2020 Program Solicitations. Hot structure technology for aerospace vehicles (sbir). https://www.sbir.gov/node/1657637 accessed on 31-08-2021.

[35] Yash Soni. The age of composite materials: History, classification applications. https://www.fabheads.in/blogs/the-age-of-composite-materials-history-classification-applications/ accessed on 25-07-2021.

[36] spazio news.it. Progetto prora: Completati con successo i test per sharp hot structures. http://spazio-news.it/progetto-prora-completati-con-successo-i-test-per-sharp-hot-structures accessed on 02-09-2021.

[37] Hua Liu W. Xiong, G. Jiao. Modeling the bundle bridging mechanism in 2d sic/c/sic composite materials. *Materials Science Composites Part A-applied Science and Manufacturing*, 1999.

[38] Hua Liu W. Xiong, G. Jiao. Fracture toughness of plain woven c/sic composites. *Kuei Suan Jen Hsueh Pao/ Journal of the Chinese Ceramic Society 36(8):1057-1061*, 2018.

[39] Sandra P. Walker, K. Daryabeigi, J. Samareh, R. Wagner, and W. Waters. A multifunctional hot structure heat shield concept for planetary entry. 2015.

[40] Yongsheng Liu Xiaoying Liu Bo Chen Yi Zhang, Litong Zhang. Oxidation effects on in-plane and interlaminar shear strengths of two-dimensional carbon fiber reinforced silicon carbide composites. *Carbon 98 (2016) 144-156*, 2016.